Department of Mechanical and Aerospace Engineering

Study on rain erosion: 3-D simulation of offshore

wind turbine blade structure

Author: Alexandros Giannakis

Supervisor: Professor David Nash

A thesis submitted in partial fulfilment for the requirement of the degree

Master of Science

Sustainable Engineering: Renewable Energy Systems and the Environment

2017

Copyright Declaration

This thesis is the result of the author's original research. It has been composed by the author and has not been previously submitted for examination which has led to the award of a degree.

The copyright of this thesis belongs to the author under the terms of the United Kingdom Copyright Acts as qualified by University of Strathclyde Regulation 3.50. Due acknowledgement must always be made of the use of any material contained in, or derived from, this thesis.

Signed: Alexandros Giannakis   Date: 25/08/2017

Abstract

Offshore wind energy has been proven to be a reliable power source for more than 25 years in the renewable energy sector. However, there are some drawbacks which can decelerate the increase of offshore wind farms. These issues concern mostly the installation and maintenance costs that are associated with the relatively limited lifetime of such offshore wind projects. One vital aspect of the maintenance costs is related to the erosion which can be a serious issue mainly at hostile environments (offshore). Erosion takes place mainly at the leading edge of the wind turbine blade due to the high velocity that this part experiences and can be attributed to sand, rain, UV sunlight, hail and extreme temperatures (Keegan, Nash and Stack, 2013). This phenomenon may lead to degradation of the aerodynamic wind performance and thus to unexpected expenses for repair and maintenance (Catapult, 2015). One of the proposed solutions is the use of coating protection materials resistant to erosion, along with woven fabrics beneath them in order to protect the structure (Keegan, 2014). Also, flexible tapes have been widely reported as a solution, despite their prerequisite for frequent replacement (3M, 2016). Alternatively, ACT Blade Ltd (2017) is trying to incorporate sail technology, not only to protect the blade from erosion but also to make the structure lighter so as to withstand the increasing length of the contemporary wind turbines (Ingenia, 2017). Therefore, the motivation for this research study derived from the erosion phenomena in offshore wind turbines and one aspect of erosion, in this case rain, was chosen for further investigation. This study is divided into five main parts. The first three parts cover the literature review of this phenomenon and work that has been published over this issue the last years. The fourth part concerns the creation of a 3mm rain droplet model impacting on a solid substrate, along with a validation model, to verify the accuracy of the results. The effect of changing coating thicknesses and the effect of changing boundary conditions were investigated in depth. The last part presents the results, which indicate some of the driving mechanisms of erosion. The study showed that gelcoat thicknesses of 0.2mm should be avoided and thicker layers should be applied, due to better stress field across the structure. Also, the damage threshold velocity was found to be steady at 61 m/s at any case, resulting in a value of fracture toughness at $0.77 \text{ MPa}\sqrt{m}$. The changing boundary conditions revealed the dominance of the nominal stresses over the shear ones in the cases of the gelcoat layer and the first ply of the composite.

Acknowledgements

First of all, I would like to thank my parents and my family for the support they have been providing me for all these years. Also, I would like to express my sincere gratefulness to my parents for their support and understanding during this year of my studies.

I would like to thank my colleagues and the University of Strathclyde for some valuable advice and support they provided on my thesis this year. Moreover, I would like to thank Dr. Mark Keegan for providing me with some valuable software advice. Last but not least, I would like to express my gratitude to Professor David Nash for the nice cooperation that we had and the support he provided me with throughout this dissertation.

Table of Contents

List of figures

List of tables

1. Introduction

Global warming, ice melting and air pollution have been identified as serious issues that our planet is facing and global efforts have been employed to mitigate or minimise such phenomena. In 1998 Kyoto Protocol had been the first global attempt in that direction which mainly focused on the identification of harmful gases named as 'greenhouse gases' and some limits had been set up by several committed countries in the reduction of emissions (United Nations, 1998). Another more recent effort had been the Paris agreement. The mission of that agreement concerned the global temperature to be restrained below the average of 2°C increase above pre-industrial levels (United Nations, 2015). Apart from the global efforts, Scottish Government has set some ambitious targets for 2020 and 2050 to reduce the greenhouse gases by 42% and 80% respectively from a baseline set distinctively for each greenhouse gas (The Scottish Government, 2009), (The Scottish Government, 2017).

Also, the European Union (2009) had published the EU targets, known as 20/20/20, to mitigate climate change, stating that greenhouse gas emissions should be reduced by 20%, renewables and energy efficiency should be increased both by 20% by 2020. In this context UK has set the target of 15% of the energy demand to be met by renewable sources by 2020. More specifically, Scotland is committed to provide 20% of the energy demand via renewable sources by 2020, whereas electricity demand should by met entirely by renewable sources by 2020 (The Scottish Government, 2011).

Offshore wind farms have recorded a substantial development, despite their relatively short history which had been not more than 30 years old (Environmental and Energy Study Institute, 2010). According to Global Wind Energy Council (2016) offshore wind features more than 14,000 MW capacity being installed globally, with UK being the leader in that market with a share of 36% in the global offshore wind energy market . Scotland has a potential of 25% of Europe's offshore wind energy (Offshore Wind Industry Group, 2010) with an estimated of 206 GW capacity (Marine Scotland, 2011).

However, there are many challenges associated with offshore wind farms which cover a wide spectrum in this field (The Scottish Government, 2011). These challenges are presented in the following table:

Challenges	Actions	Responsible Bodies
Reduce the costs for operation and maintenance	Need for increased market competition to bring the costs down	Private Companies active on this field
Grid access	Collaboration of the involved parties	Stakeholders and the Government
R&D	More research in this field	Institutions, Companies
High skilled personnel	More focused courses in colleges, universities	Universities, Colleges,
Regulation	Planning and consent process need to be accelerated	Crown Estate, Government, Legal Bodies

Table 1: Key Challenges of offshore wind energy (The Scottish Government, 2011)

The offshore wind farms in UK currently meet 5.4 % of the electricity demand and it is expected that this percentage will be increased by 2020 to 10% (The Crown Estate, 2016). The map below represents the offshore wind farms in the UK (UK Trade & Investment, 2015).

However, there are some obstacles in this increasing trend which need to be overtaken and they mainly concern the costs. The challenges associated with the costs are described in the literature as Levelised Cost of Energy (LCOE), which describes the cost of a project for every unit of electricity being produced during the lifetime of a wind turbine project (The Crown Estate, 2012). The former Department of Energy

and Climate Change (DECC) has set up the target of decreasing the LCOE below 100 £/MWh by 2020, meaning that innovations and design breakthroughs will be the cornerstone of that ambitious effort.
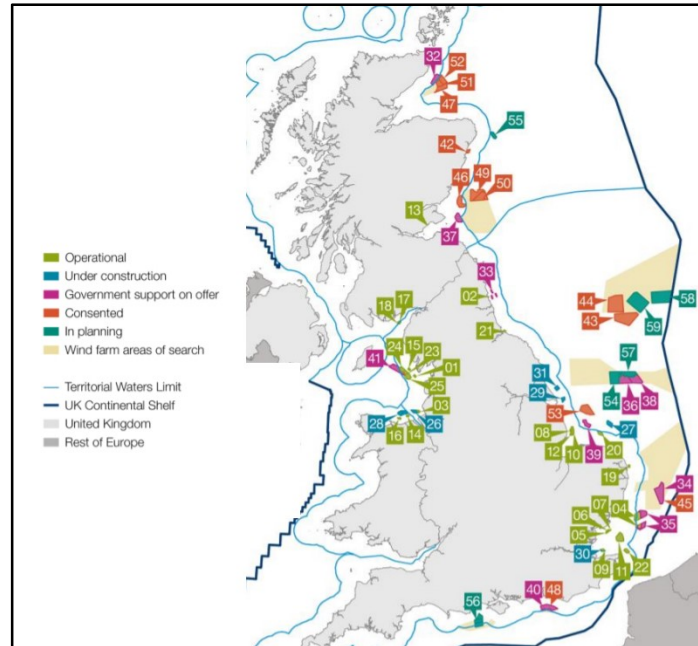
Figure 1: UK offshore wind farms (UK Trade & Investment, 2015)

1.1 Scope of work

This work focuses on the improvement and development of offshore wind turbines. The objectives of this research study are summarized in the following points:

- Study on erosion mechanisms associated with rain droplet impingement (limited studies on this area).
- Impact resistance of the wind turbine blade materials exposed at hostile environments.
- Examining the condition of the different layers of the structure when experiencing an impact of a rain droplet.
- Minimising the repair and maintenance costs of offshore wind energy which are considered to be difficult when being compared to onshore ones.
- Unplanned maintenance costs are considered high and do not contribute to achieving the 2020 target of LCOE < 100 £/MWh.

The deliverables of this project will intend to deal with the importance of gelcoats, the effect of boundary conditions and the condition of the rest of the structure that lies beneath the gelcoat. A consistent model will be created, which will describe the structure by using ANSYS/LS-DYNA (ANSYS Inc., 2017) and LS-PrePost (Livermore Software Technology Corporation, 2012). The model will simulate a 3 mm rain droplet impacting on a target. The results of the model will focus on the impact pressure, velocity dissipation, impact forces, plastic strain and stresses across the different layers of the structure.

The method that will be employed for this case is the Smooth Particle Hydrodynamics (SPH). A 3mm rain droplet will be used as a constant throughout this project along with one steady impact velocity at 100 m/s, which are both considered to be the worst case scenario during precipitation (Keegan, 2014), (Gohardani, 2011), (Amirzadeh, 2017). The variable factors which will be investigated are the thickness of the gelcoat material, which will range from 0.2 mm, 0.4 mm, 0.6 mm to 0.8 mm and the effect of different boundary conditions with a gradual degree of relaxation.

The challenges of this project are mainly focused on the limited information about the topic, the lack of mechanical properties for commercially used materials, the unfamiliarity with the software; the complexity of the simulations, the time restriction and the computational cost.

The erosive behavior of rain on solid substrates will be studied, in order to define the mechanisms of the phenomenon in such hostile environments. Condition monitoring techniques are excluded from the scope of work due to the extent of erosion results. However, condition monitoring plays an important role in the field and can contribute in encountering erosion.

1.2 Thesis structure

➢ Chapter 1: The aims, background and methodology are presented along with the limitations.

➢ Chapter 2: A review of the mathematical expressions and the materials used for offshore wind turbines are outlined together with the issue of erosion in the industry.

➢ Chapter 3: Erosion is analysed in depth not only by the use of analytical expressions but also by presenting relative publications which dealt with the phenomenon.

➢ Chapter 4: A trial model is created in order to verify the results and allow the creation and description of the realistic model which is described in this chapter as well.

➢ Chapter 5: The results of the model are presented in accordance to the changes in the gelcoat thickness and the boundary conditions.

➢ Chapter 6: This chapter includes the discussion, the future work, the limitations and the conclusions.

2. Background of offshore wind turbine blades

This chapter will present in depth the mathematical expressions about the operation of wind turbines, the commercial materials that are used and will provide a first awareness of erosion concerning the industry sector.

Wind energy is a very effective renewable energy source that has been commercially available for more than a century. In those years of evolution different types of wind turbines have been developed to harness wind energy. The different types of wind turbines are presented in the following table:

Type	Function
Horizontal Axis	Upwind rotor
	Downwind rotor
Vertical Axis	Using Drag forces
	Using Lift forces

Table 2: Different types of wind turbines (Clark and Kelly, 2016)

In Scotland wind energy attains a significant role in the electricity generation, producing more than a half of the energy compared to other renewable energy sources (The Scottish Government, 2017).

Figure 2: Renewable energy sources contribution to electricity production (The Scottish Government, 2017)

As it can be seen from the figure above, wind energy presents an upward trend and thus can be considered as a reliable source of energy, despite its intermittent nature. Onshore wind turbines contribute the most to this figure due to many advantages compared with the offshore wind turbines, with the most important being the LCOE. The LCOE can be described by the following equation (Thomson, Harrison, 2015):

$$LCOE = \frac{\Sigma_t^T \frac{F_t + D_t + O_t + C_t}{(1+r)^t}}{\Sigma_t^T \frac{E_t}{(1+r)^t}} \tag{1}$$

Where,

C = Capital Cost

O = Operations & Maintenance

D = Decommissioning Costs

F = Fuel Cost

E = Electricity Produced

R = Discount Rate

T = Lifetime of the project

In order for the LCOE to meet the goal of 2020, offshore wind turbines have been increased in size and power output. The following picture demonstrates this increasing trend (Sykes, 2016):
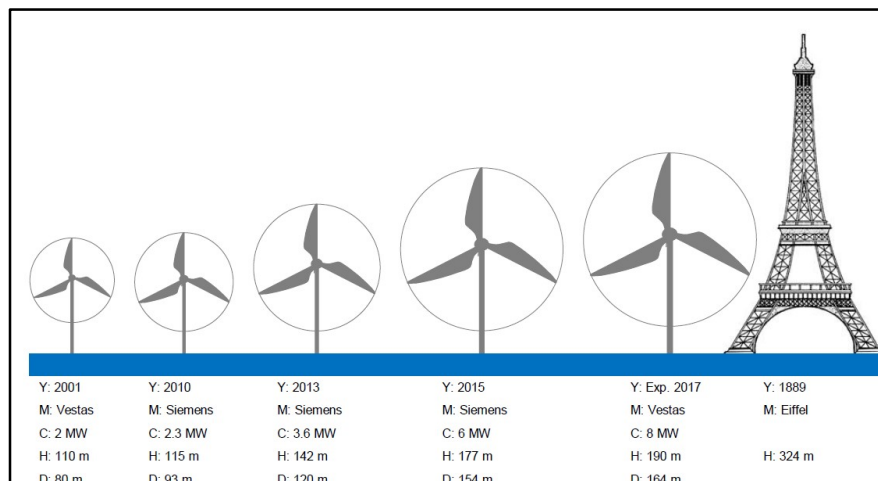
Figure 3: Up-scaling trend of offshore wind turbines (Sykes, 2016)

17

2.1 Operation of Wind Turbines

The determination of the location of a wind farm is dependent on the site wind set data and the consistency of wind at any times. Statistical data are broadly used to characterise and quantify the wind (Der Norske Veritas, 2014). Wind speed data are characterised by their relative height and therefore they can be described by the following equation at a height z above the sea level:

$$U(T,z) = U_{10} * (1 + 0.137 ln\frac{z}{h} - 0.047 * ln\frac{T}{T_{10}}) \tag{2}$$

Where h=10m, T_{10} = 10min and U_{10} is the 10-minutes mean wind speed velocity for that height. For modelling purposes of the wind a Weibull distribution is employed to record the wind in a long-term basis. A Weibull distribution is presented in the following equation for a 10-minute mean wind speed at a height H:

$$F_{U_{10}}(u) = 1 - e^{-(\frac{u}{A})^k} \tag{3}$$

Where k and A are parameters that are height and site dependent. After acquiring the Weibull distribution curve next step is to create a velocity exceedance curve, which represents the velocity of the wind in a typical year. The power production can now be calculated by the following equation (Energy Resources and Policy, 2016):

$$P = \frac{1}{2} * p * A * u^3 * C_p \tag{4}$$

Where,
p = air density
A = swept area
u = velocity
C_p = Power coefficient

The dependence of the velocity exceedance curve and the power production are depicted in the following figures.
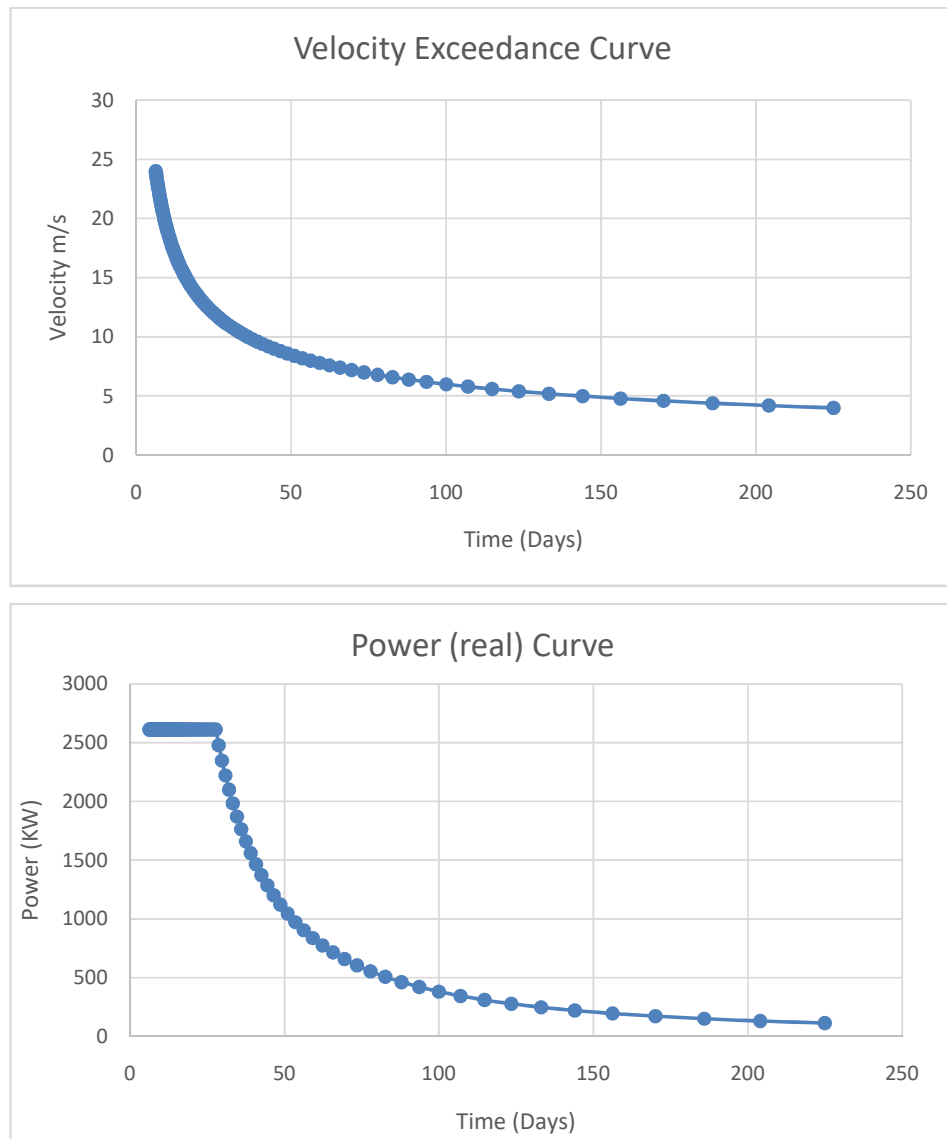
Figure 4: Relation between velocity exceedance curve and power output

From the power graph the annual power output can be calculated by calculating the area lying below the curve. The main components of a wind turbine are depicted in the following picture. At this point it should be highlighted that this project will focus on the wind turbine blades and thus more detailed theory will follow in this chapter.

Figure 5: Wind turbine components (Cao, Xie and Tan, 2012)

2.2 Key principles of wind turbine blades

The model that is used to simulate the aerodynamic loads in the blades is the Blade Element Momentum Theory (BEM). The loads developed in the blade are the drag, the lift, the angular velocity of the rotor and the wind velocity. These loads are depicted in the following figure (Greaves, 2016):
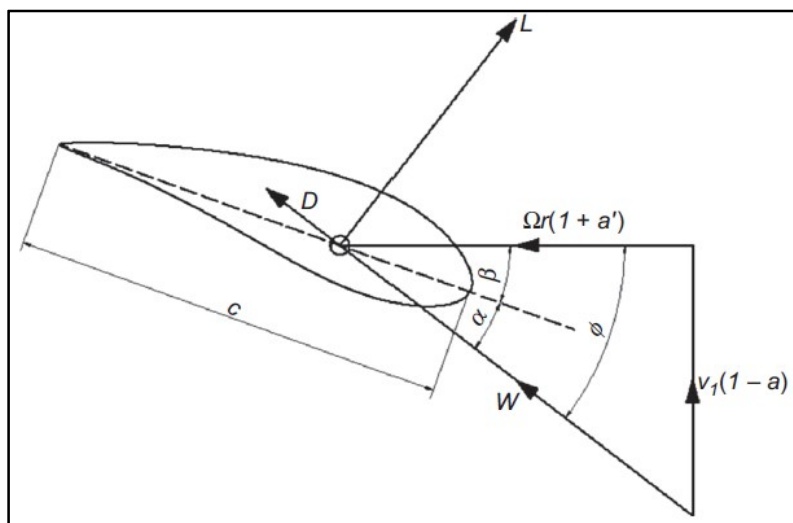
Figure 6: Blade Loads representation (Greaves, 2016)

The relative velocity W can be calculated by the following equation:

$$W = \sqrt{V_1^2 * (1 - a^2) + \Omega^2 * r^2(1 + a'^2)} \qquad (5)$$

Where

$$a = \frac{V_1 - V_2}{V_1} \qquad (6)$$

$$a' = \frac{\omega}{2 * \Omega} \qquad (7)$$

$$dL = \frac{1}{2} * p * C_L * W^2 * c * dr \qquad (8)$$

$$dD = \frac{1}{2} * p * C_D * W^2 * c * dr \qquad (9)$$

V_1 and V_2 represent the velocities of input and output respectively for a close volume system and dL and dD are the lift and drag force respectively. The final form of the axial force and the torque are given by the following equations:

$$dFx = \frac{1}{2} * p * W^2 * c * \beta * (C_L * cos\varphi + C_D * sin\varphi)dr \qquad (10)$$

$$dT = \frac{1}{2} * p * W^2 * c * \beta * (C_L * sin\varphi - C_D * cos\varphi)dr \qquad (11)$$

2.3 Manufacturing processes of wind turbine blades

The structural purpose of the wind turbine blades is multilateral and has to fulfill a number of standards according to the organisation Der Norske Veritas (2010). The blades should fulfill a number of structural criteria which are listed below:

- Buckling analysis (locally and globally)
- Fiber and Matrix failure analysis
- Inter-laminar and sandwich failure analysis
- Fatigue limit analysis
- Impact Damage analysis

The layout of the wind turbine blades can vary between different manufacturers, but the general structure can be described by the following picture. A variety of materials

21

are used to reinforce the structure, whereas at the same time the weight should be as low as possible and the stiffness as high as possible. The root is attached to the hub and the shell of the blade is comprised of different layers and materials which are attached to the shear web that provides internal structural stiffness. A thorough presentation of the cross section will be attempted in chapter 4.
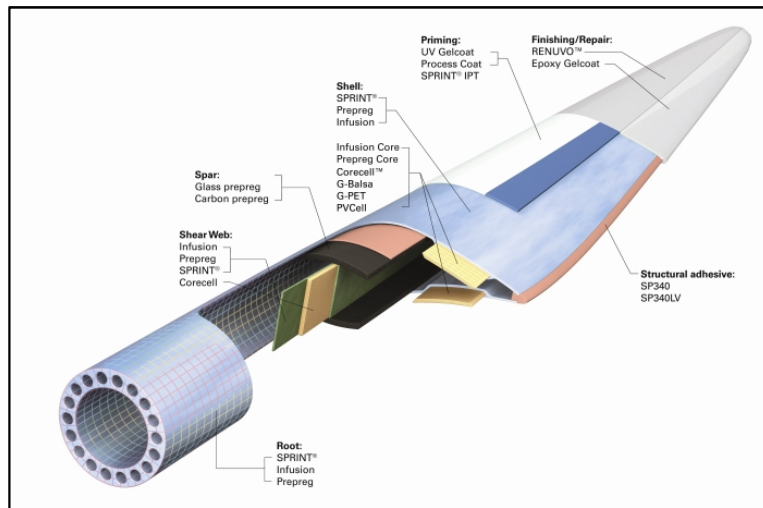
Figure 7: Wind Turbine Blade Layout (Bureau lesswatts, 2015)

In the literature various manufacturing techniques are described for the formation of the blades. The most prevalent techniques are described in the following table:

Name	Description
Wet lay-up	• Every layer of the fibrous material is poured into the mould • The resin and the hardener are mixed and poured into the same mould • Curing and assembly are the final stages • Labor-intensive process, voids and flaws can easily be created
Vacuum infusion	• The fibrous material is placed into the mould and it is being sealed • The hardener and the resin after being mixed, they are pumped into the sealed mould • Automated process, but careful selection of fiber fabrics is required
Filament winding	• Fibers are travelling through a resin bucket • Then they are attached into a rotating mandrel • Automated process, but there is difficulty in the alignment of the fibers
Prepreg	• The material is ready into layers of uncured • The prepreg is being put into the mould and sealed • Air is pumped out and then the material is cured • Automated process, high cost but better mechanical properties

Table 3: Manufacturing processes for wind turbine blades (Greaves, 2016), (Keegan, 2014), (Aymerich, 2012)

2.4 Materials used for wind turbine blades

As being discussed earlier, the material selection is done by fulfilling the structural criteria along with stiffness and strength while the weight of the structure is kept as low as possible (Nijssen and de Winkel, 2016). The materials that are mainly used for the wind turbine blades are mostly composites. The composites have the advantage of

attaining better mechanical properties per volume at a lower weight. The following picture highlights these key characteristics.
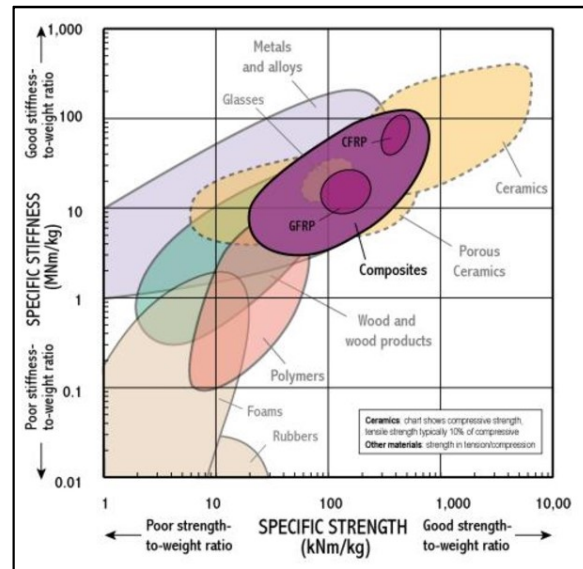
Figure 8: Comparative diagram of different materials (University of Cambridge, 2002)

Fibre re-inforced materials are mainly used to cover the majority of the volume of the blade. Composite materials are comprised of two parts, the matrix and the fibres. The so called matrix is usually a polymer thermosetting (epoxy, vinylester, polyester, urethane) resin and the reinforce material which is impregnated in the matrix (carbon, glass, Kevlar, boron) (Ninjssen and Brondsted, 2013). The fibres can be oriented in different directions in order to reinforce the structure in various mechanical loads that may occur throughout the lifetime. Different plies of either uni-directional, multi-directional or randomly-oriented materials are placed in the structure in the most efficient way. The result is a material with high specific strength and fatigue behaviour. The cross-section of a wind turbine with all the materials is depicted below.
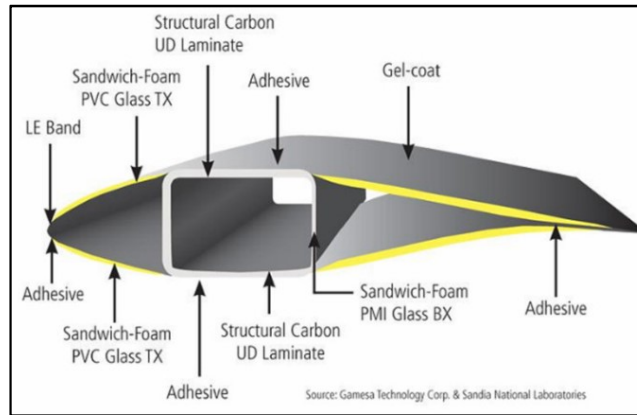
Figure 9: Wind turbine blade cross-section with all the materials (Rosato, Gamesa Corporation Technology and Sandia National Laboratories, n.d.)

Glass fibre composites are widely used by the industry in the sector of wind turbines, whereas carbon fibre composites are used rarely in longer wind turbine blades or for reinforcement purposes, due to their better mechanical properties (Greaves, 2016). The shape of the composites into the material can have the following forms:

- Particulate
- Flake
- Fibrous
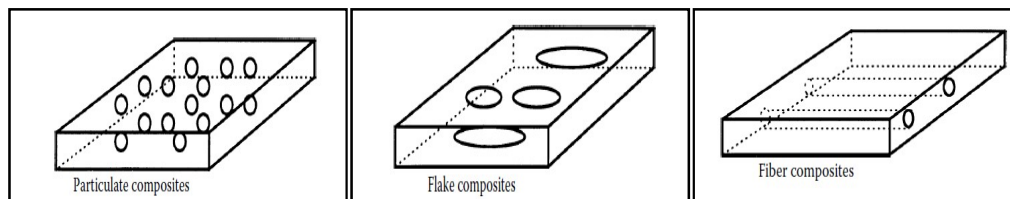
Figure 10: Different forms of reinforce materials (Kaw, 2006)

The particulate composites are consisted of randomly located particulates (alloys etc.) in the composite, with their purpose to be for reinforcement (Kaw, 2006). The flake composites are mainly made from flakes of matrices, such as glass and are mainly un-oriented. The fibrous composites are using fibrous materials such as glass, with different orientations in the structure in order to provide higher specific stiffness and better mechanical properties. Also, a structure can have different layers of fibrous material and with different fiber orientations as well (laminate material). The most

recent advance in this area is the so called prepreg materials which have been mentioned in the previous chapter.

There is another type of reinforced composite materials, which can have the form of plain weaves. Each ply of the material can have two axes of symmetry and the fibers are weaved inside the material in a way so as to add more stiffness to the material. In the following picture, a Kevlar weave is depicted.
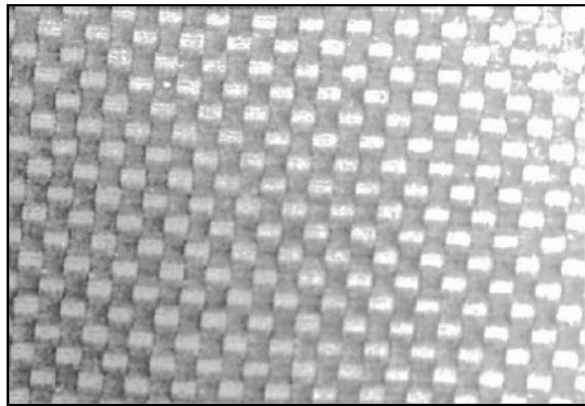
Figure 11: Kevlar plain weave material (Kaw, 2006)

The sandwich form uses a foam material between the different layers of material to increase the second moment of inertia and the buckling properties. The last layer of the materials is the coating protection which should have a thickness of 0.3-0.6 mm according to the organisation Der Norske Veritas (2010) for wind turbine blades. The gelcoat plays a key role in the construction not only because it dissipates and relieves the stresses across the material but it also refrains the composite from becoming wet and thus not degrade during time.

2.5 Erosion and coatings

Apart from the wind speed data and the structural side (load, aerodynamics, etc.) of the wind turbine blades, there is also the necessity to fulfil criteria of protection against environmental conditions (BS EN 61400-1:2005, BS EN 61400-3:2009). Some of them are humidity, air temperature, UV protection, rain, hail, snow, ice,

lightning, chemically active substances, impact resistance with different targets etc. Since, the coatings constitute the first material that is directly exposed to the environmental conditions; they should be carefully designed in order not only to withstand the harmful factors but also to take into account some other extreme factors that are not mentioned before.

According to Nijssen and Brondsted (2013), the gelcoats account only for 2% of the blade costs. Despite this low percentage they are proven to be vital components of the structure and thus attention should be drawn when they are applied to the last layer of the structure. Gelcoats and paints can be utilised for the coating protection, which are mainly comprised of thermoset polymer materials with a mix of different additives (Storm, 2013), (BVG Associates, 2011). The main materials are polyesters, epoxies, acrylates, vinylesters and polyurethanes. The most widely known applying techniques for gelcoat protection are the following (Keegan, Nash and Stack, 2013):

- In-mould application: A layer of coating material is added on top of the surface as part of the moulding process.
- Post-mould application: The coating material is painted or sprayed on top of the surface after the moulding process.

The company 3M proposes as protection either flexible coatings (two component polyurethane) or protection tapes (3M, 2016).
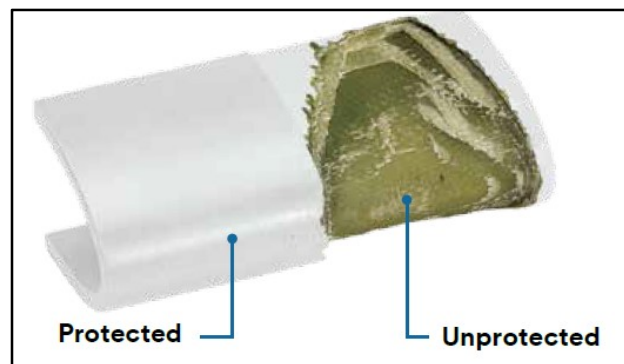
Figure 12: 3M coatings (3M, 2016)

Erosion has been recorded since the Second World War, which constituted an issue for military aircrafts (Gohardani, 2011). In that publication the author described the complexity of erosion mechanism in accordance to aircrafts. The importance of both analytical and experimental documentation was highlighted as well. Also, erosion has been experimentally investigated in the field of steam turbine blades (Azevedo, Sinatora, 2009), (Ahmad, Casey and Sürken, 2009). With the ever increasing length and height of offshore wind turbine and the higher tip speeds (due to tolerance from tip noise), erosion has been reported as an issue that required investigation, especially offshore wind turbines (Keegan, Nash and Stack, 2012), (Nijssen and de Winkel, 2016). All the factors mentioned above, affect the erosion and in some cases they accelerate this wearing mechanism. Megavind (2016) and International Renewable Energy Agency (2016) have both stated that erosion is one of the common failures that take place among others, which should be addressed. Windtrust (2013) and Troedsson (n.d.) have both highlighted the importance of leading edge erosion and the high costs that are associated with the phenomenon. Also, they state that the degradation starts periodically, even at early stages of the lifetime, by mass loss of the material which in turns leads to reduced aerodynamic performance and thus less power production. The U.S. Department of Energy (2014) has reported extensively on erosion issues that are classified in the operational and maintenance costs (O&M), highlighting at the same time the importance of modelling, material improvements and testing. The following pictures depict the phenomenon.

Figures 13, 14: Wind turbine blades and the erosion being present (Rempel, 2012), (Hetcel, 2014)

Erosion is possible to take place even in the first 2 years of operation (Wood, 2011), (Keegan, Nash and Stack, 2013), (Rempel, 2012). It is reported in the literature that the erosion invokes increased drag with decreased lift coefficient, which in turns may result in up to 25% decreased annual energy production (Sareen, Sapre and Selig, 2013).

At this point, it should be clarified that extensive reports from companies have not been found; therefore the financial figures from erosion and the results in the O&M costs have not been recorded. However, the effort of creating databases with that phenomenon has been reported in the available literature (Keegan, 2014) by big companies, such as Global Energy Service and LM Wind Power.

2.6 Maintenance

The maintenance and repair required in an unlike event of incident, such as erosion, demands a good organisation among the different parties. The offshore environment is very hostile and thus a good coordination of human resources is vital. The main

parties that are involved with this operation are the following (The Crown Estate, 2013):

- Onshore logistics
- Offshore logistics
- Administration and operation
- The activity itself

One big challenge is the transportation of the technicians and the equipment to the area of service. The technicians will access the wind turbine either by workboats or by helicopter. Fixed-based workboats can be employed as well, depending on the amount of time needed for maintenance. The maintenance activities can either be scheduled or not. Moreover, efforts are focused to deliver a risk management analysis that can predict and minimise costs. The damages are classified depending on the rate of occurrence and have a failure and repair rate respectively. The following equations represent these terms respectively (Tavner, 2012).

$$\lambda = \frac{1}{MTBF} \tag{12}$$

$$\mu = \frac{1}{MTTR} \tag{13}$$

MTBF = mean time between failure
MTTR = mean time to repair

The following equation describes these quantities

$$MTBF = MTTF + MTTR = \frac{1}{\lambda} + \frac{1}{\mu} \tag{14}$$

So the (commercial) availability (time that the wind turbine is operative and produces power) of the wind turbine can be described by the following equation:

$$A = \frac{MTBF - MTTR}{MTBF} = 1 - \frac{\lambda}{\mu} \tag{15}$$

In the path of mitigating the risks of downtime and reducing the O&M costs Tavner (2012) published the failures that have been researched for the period of 1991-2004. Among the failures the rotor blades have a significant contribution to this area with an average downtime per failure of 9 days and an annual failure frequency of around 30%. Given the complexity of maintenance in offshore wind turbines, erosion can be an issue that seems to be increasing issue among various manufacturers (ACT Blade Ltd).
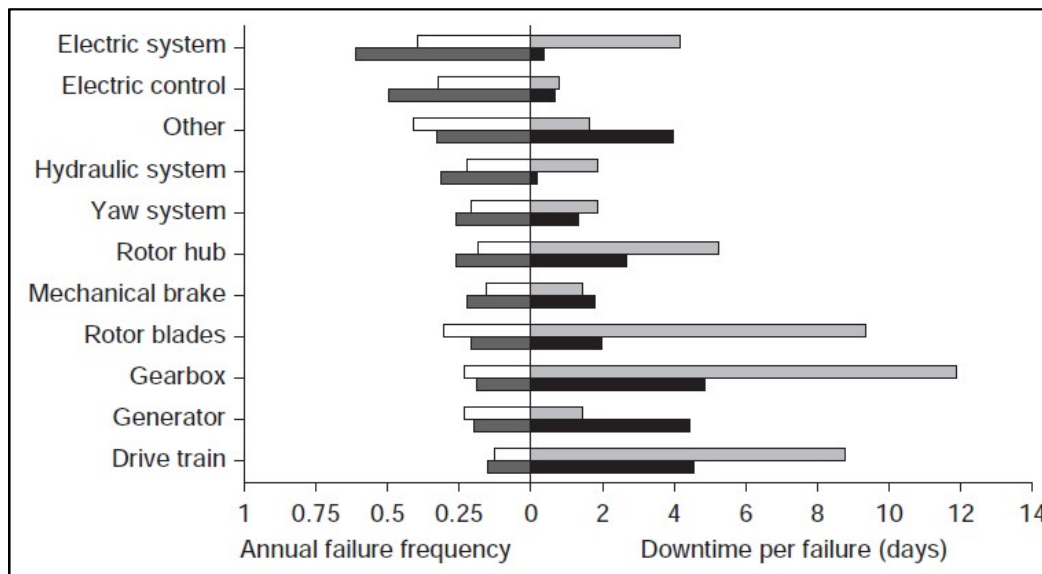
Figure 15: Wind turbine servicing components monitored from 1991-2004 (Tavner, 2012)

2.7 Overview

This chapter presented the background of wind turbines in general together with the materials that are mainly used in this sector. A link of erosion with the maintenance costs and the LCOE was attempted as well. Also, industry reviews concerning the phenomenon were summarised. The next chapter of this work will present erosion in depth by mathematical expressions and publications in this field.

3. Literature review

The aim of this chapter is to present a literature review in chronological order, aiming to establish a solid background on the erosion and the various mechanisms that are associated with this phenomenon. Furthermore, this attempt will be complemented by some experimental and analytical background, in order to maintain a smooth transition across the project and a solid scientific base.

3.1 On rain erosion phenomena

The investigation of rain erosion should start from the physical phenomenon of rain. Precipitation levels can vary from place to place and from region to region. The following map depicts the annual precipitation levels in the UK through historical data. It is obvious from the figure that the west coast of the UK is more exposed and thus it receives higher levels of rain. The lack of offshore precipitation maps with historical data makes it difficult for safe conclusions concerned the precipitation levels in the coasts of UK and thus about the wind farms.
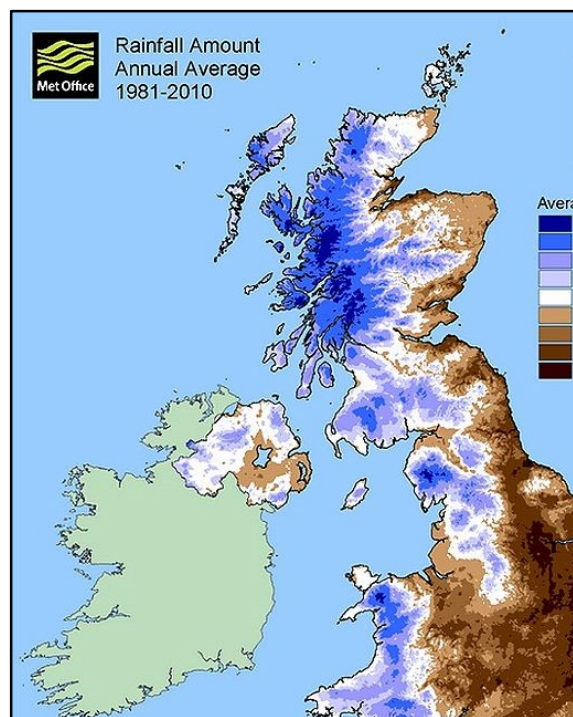
Figure 16: Annual precipitation levels 1981-2010 (Met Office, 2015)

Many efforts have been recorded with the purpose to quantify rain drops. Best (1950) has proposed the following equation (reproduced from Amirzadeh, 2016) to be used in terms of describing the droplet size distribution:

$$F = 1 - e^{-(\frac{d}{1.3*I^{0.232}})^{2.25}} \tag{16}$$

Where, d is the droplet diameter in mm and I the rain intensity in mm/h. The rain intensity can be described by the following equation:

$$W = 67 * I^{0.846} \tag{17}$$

Where, W is the volume of water in the air. The following figure represents the rain droplet size density curve by making use of both equations (16), (17) (Kubilay, et al., 2013).
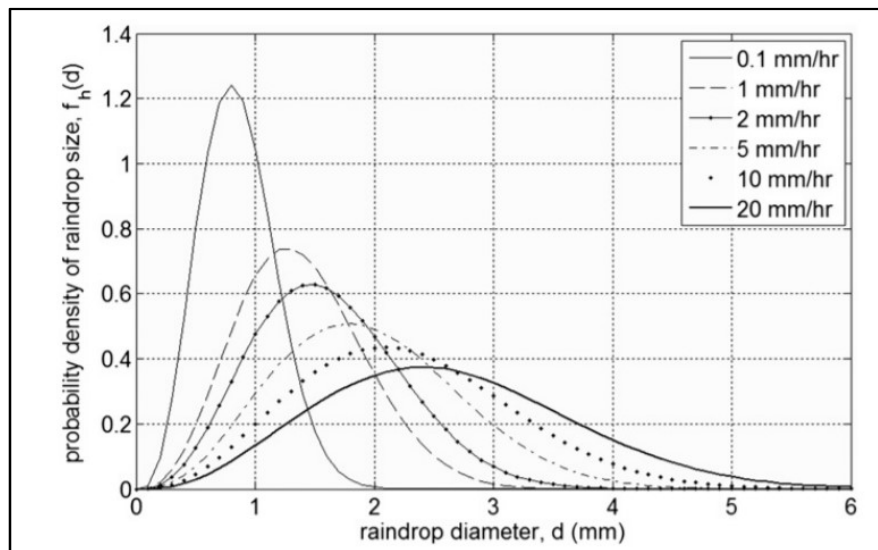
Figure 17: Probability density curve of the mean rain drop size (Kubilay, et al., 2013)

The figure above suggests that the raindrop diameter varies accordingly with the intensity of rain induced. The most common sizes of rain drops are those between 0.5 and 3 mm according to the figure. According to Keegan (2014), the impact velocity

is dependent on the angle of the blade and varies accordingly. The figure below shows that the impact velocity can be at least 90 m/s with a maximum of 100 m/s.
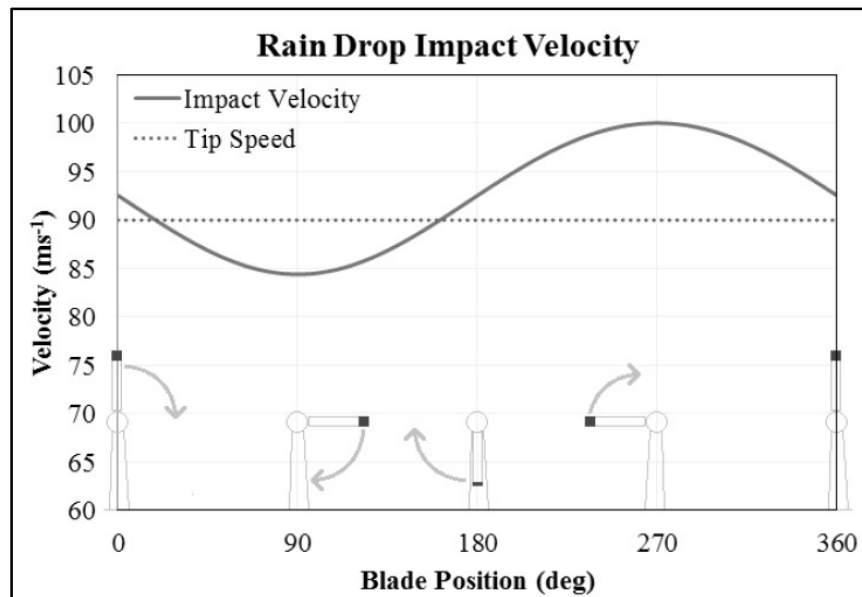
Figure 18: Terminal Impact velocity on a wind turbine blade (Keegan, 2014)

In an attempt to explore the nature of rain, the phenomenon should be examined microscopically as well. The next picture illustrates the phenomena which take place at the moment that the rain impacts on any solid surface. Gohardani (2011) depicted the mechanisms dominating at that time.
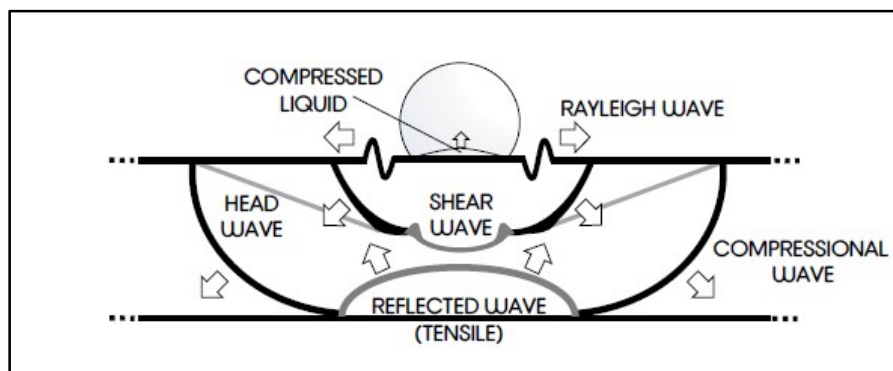
Figure 19: Rain droplet impingement (Gohardani, 2011)

The pressure being induced in the surface of the rigid material is known as waterhammer pressure and has the following mathematical equation:

$$P = p_0 C_0 V_0 \tag{18}$$

Where, p_0 is the density of the liquid, C_0 the speed of sound in the liquid and V_0 is the velocity impact. The first stage of the wave is the compression and the second stage is the incompressible wave, which reduces after the first propagation of the compression wave. The equation that describes this dissipation is the following:

$$P = \frac{p_0 * V^2}{2} \tag{19}$$

A modified waterhammer pressure equation has been recorded by Dear and Field (1988) which takes into account the target body and calculates the pressure on the surface:

$$P = \frac{P * p_l C_l p_s C_s}{p_l C_l + p_s C_s} \tag{20}$$

The term l stands for the liquid and the term s stands for the solid surface which is being impacted by the droplet. The damage which is generated in the target has been investigated in terms of velocity. The damage is proportional to the impact velocity, to the surface toughness and to the droplet size; described below through Evans, Gulden and Rosenblatt, (1976):

$$V_{dt} = 1.41 * \left(\frac{K_{IC}^2 * C_R}{p_w^2 C_w^2 d_w}\right)^{0.333} \tag{21}$$

Where, K_{IC} is the target's fracture toughness, C_R and C_w are the wave velocities, p_w is the density of the water and d_w is the droplet's diameter. The Rayleigh-velocity is given by the following equation according to Achenbach (1973):

$$C_R = \left(\frac{0.862 + 1.14 * v}{1 + v}\right) * \left(\frac{E}{2 * (1 + v)p}\right)^{0.5} \tag{22}$$

35

Where, E is the Young's modulus of the material and v is the Poisson's ratio of the material. The force which is being exercised on the surface of the solid can be described by the following equation (Nearing, Bradford and Holtz, 1986), (Imeson, Vis and de Water, 1981):

$$F = \frac{m*V^2}{d} \tag{23}$$

Lateral jetting is the second stage of that phenomenon, which is characterised by a spread of water jets to the solid surface (Valaker, Armada and Wilson, 2015), (Zhang, Dam-Johansen and Bernad Jr., 2014). The contact edge velocity which is depicted below is higher than the impact velocity. This means that uneven surfaces can be affected by the erosion mechanism.

Figure 20: Lateral Jetting phenomenon (Zhang, Dam-Johansen and Bernad Jr., 2014)

3.2 Research on rain erosion phenomena in wind turbines

In the paper of Adler (1995) DYNA3D (origin of LS-DYNA) had been used to simulate a waterdrop of 2mm impacting on a zinc sulphide surface at 305m/s. No clear conclusions had been drawn from this work but the behaviour of the rain droplet was captured successfully. Also, the propagation of the stress wave through the thickness of the material had been captured as well. The next picture depicts this phenomenon.
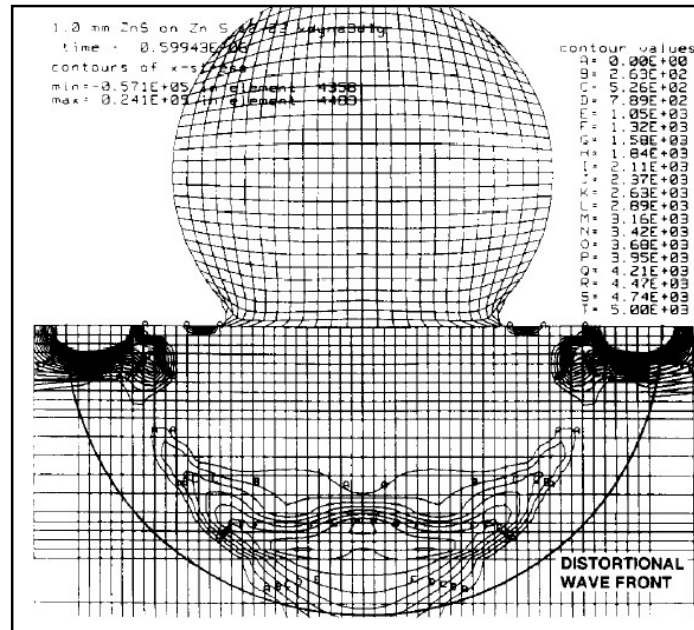
Figure 21: Generation of compression wave (Adler, 1995)

Dalili, Edrisy and Carriveau (2007) had tried to investigate the factors which affect the performance of wind turbine blades. Erosion had been identified as one of those factors that can lead to unplanned shutdowns and unpredicted power losses. As a proposal, the authors identified the advances in the coating materials as being crucial to confront the issue effectively.

Karmouch and Ross (2010) had tested a new coating made of epoxy reinforced material with silica nanoparticles. This coating system attained improved hydrophobic properties in heavy rain climates and in high UV exposure climates as well.

Li, Ninokata and Mori (2011) had performed a 2-D simulation with respect to rain droplet impacting onto a rigid wall. A CFD analysis had been used for the purposes of rain droplet modeling and valuable conclusions had been made. The compressibility of the liquid has a vital role in the evolution of the phenomenon and the pressure is at its highest in the edges and not in the center of impact.

A silica float glass brittle material was examined by Salman and Yildirim (2011) in accordance with rain erosion by using LS-DYNA as a simulation tool. A water jet is

37

impinged to a plate and different types of failure modes are investigated. The thickness of the plate is the most important factor which drives all the simulations. The following figure represents the penetration of a water jet into the plate.
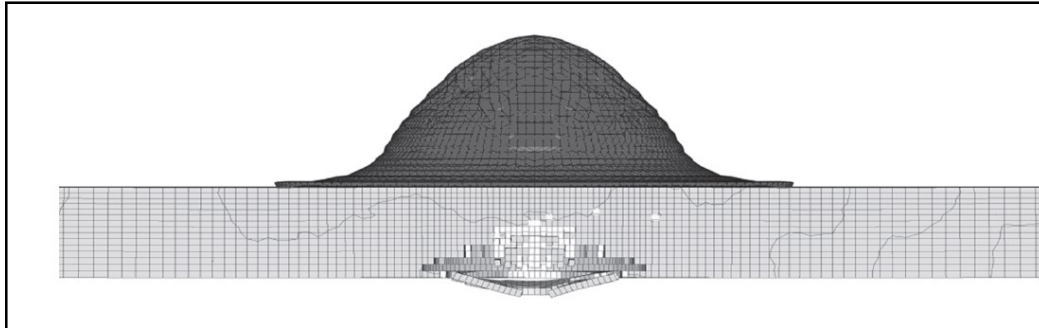
Figure 22: Water jet perforating a plate made of brittle material (Salman and Yildirim 2011)

Keegan, Nash and Stack (2012) have simulated a rain droplet impacting on a wind turbine blade. ANSYS explicit dynamics was employed to simulate a 3mm rain droplet that impacts a surface in a range of impact velocities 30-140 m/s. Pressures and stresses had been calculated, presenting a consistency with the theoretical models that describe the impact. In the following figure the correlation between the analytical and the ANSYS-results based model is depicted.
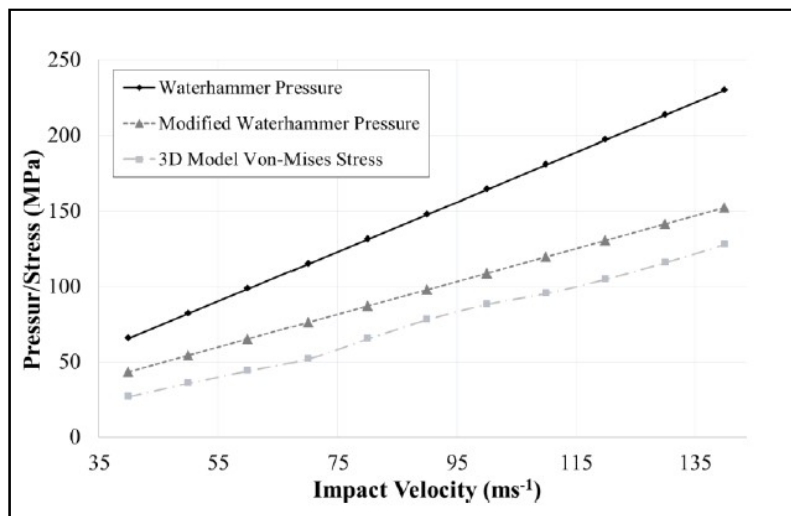
Figure 23: Comparison between analytical and computational results (Keegan, Nash and Stack, 2012)

The paper of Sayer, et al. (2012) had revealed the results and mechanical properties after 18 years in service life of a DEBRA-25 wind turbine blade. The results showed a good overall performance of the wind turbine blade without any remarkable changes in the behavior. However, it was proposed that rain erosion should be tested in the tip of the blade in an attempt for further understanding of the phenomenon.

In the paper of Sareen, Sapre and Selig (2013), an experimental investigation had been performed in order to evaluate the effect on the overall performance of the wind turbine blade that erosion has. A DU 96-W-180 wind turbine airfoil had been tested in various Reynolds numbers and angles of attack. The conclusion for the specific airfoil had shown a 5% energy production loss in the annual performance.

The paper of Keegan, Nash and Stack (2013) had demonstrated a theoretical background of the leading edge erosion in wind turbine blades induced by rain and hailstone. A review of the models that describe rain and hailstone had been thoroughly discussed. A numerical model of the leading edge of the wind turbine blade had been developed. The impact of hailstone in the structure of the blade is obvious in the following figure.
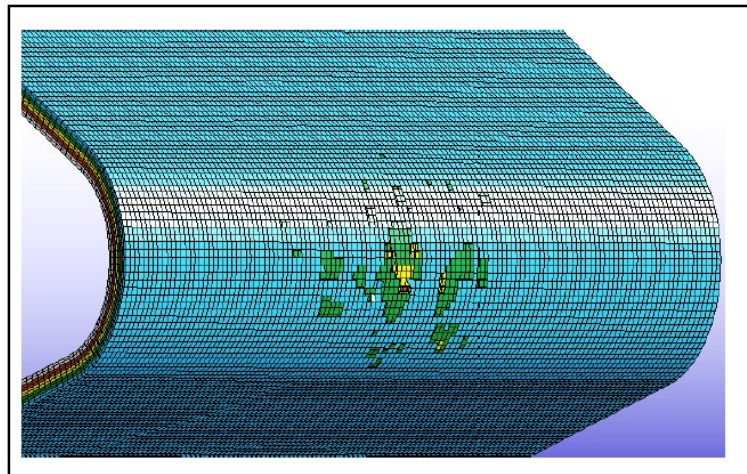
Figure 24: Hailstone damage to the leading edge of the blade (Keegan, Nash and Stack, 2013)

Zhang, et al.(2014), had investigated rain erosion on wind turbine blades with experimental set ups, by exposing various coating systems to rain and measured erosion in terms of material loss. The specimens had been exposed to different rainfall intensities, different droplet sizes and at different velocities. The following figure represents the results, which indicate that even after 1.5 hours of rainfall exposure the coating is eroded.
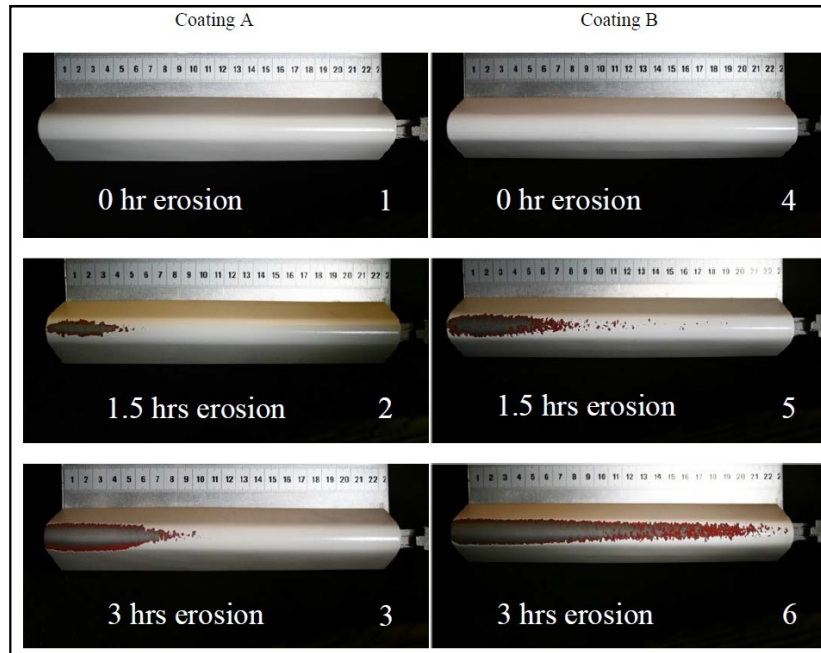
Figure 25: Erosion extent compared in two different coatings (Zhang, et al., 2014)

Water jet velocity has been proven to be the most vital factor in the initiation of erosion. Finally, abrasion resistance has been found to be one property that can be attributed to erosion (Zhang, et al., 2014).

Valaker, Armada and Wilson (2015) used four different types of coating materials which had been tested according to their erosion-resistance intended for offshore wind turbines blades. The four coatings employed for the experimental set up had been made from 100% PU, FN reinforcement, SiC reinforcement and an industrial one. The outcome of this experiment revealed that the industrial coating attained the highest material loss and suffered mainly from cohesive failure. SiC reinforced

coating had performed in the best way, whereas the pure PU coating had the best distribution between cohesive and adhesive failure mechanisms.

Slot, et al. (2015) studied erosion patterns in an experimental basis and through a surface fatigue approach. The presence of Rayleigh waves has been highlighted along with tensile stresses behind the Rayleigh wave front. Also, coating life has been correlated to the droplet size, rain intensity and the fatigue properties. Moreover, according to their findings, since erosion derives from fatigue, preventative measures such as enlargement of the safe area or reduction of water pressure should be considered as well.

Castorini, et al. (2016) in their paper they employed mathematical models to simulate the pressure field across a wind turbine blade, finite element model for particle-cloud trajectories and an erosion model. The erosion patterns had been simulated in order to be confirmed with the actual observed ones. A good correlation between the actual observed phenomena and the analytical model had been concluded.

Cortes, et al. (2017) had investigated the performance of a cohesive zone between the coating and the material and the affection on the performance. Specimens have been tested and simulated numerically in order to investigate the material interface interactions. The interface between the gelcoat and the laminate using a cohesive zone, contributed to the effort of understanding erosion mechanisms.

In the first part of Amirzadeh, et al. (2017) paper, a rain simulation is performed and a novel model describing the stochasticity of rain is being used. Through this frame rain erosion had been investigated in wind turbines. A stochastic model was created in order to represent rain intensity and rain volume in air volume. Impact pressure as a means of different rain droplet sizes had been created and sensitivity studies had been performed so as to create the most efficient model at the least computational cost. The next figure represents the propagation of pressure when fending off the node of impact.
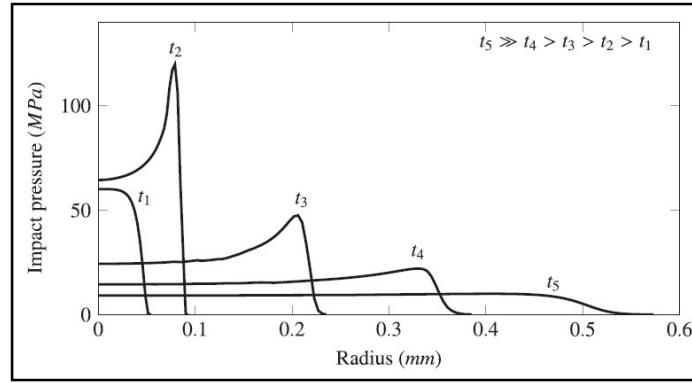
Figure 26: Pressure distribution propagating into a surface (Amirzadeh, et al., 2017)

The second part of the paper describes the computational model that had been employed and the fatigue life model that had been developed. Abaqus had been chosen as a software tool to simulate the rain drop impacting a solid surface. The rain droplet had been created in the form of tall columns which differ in height according to the rain intensity. The blade layup utilized is depicted in the following picture. Through this analysis, fatigue life models had been created in order to recognise patterns according to the size of the rain droplet and rain intensity and as a result a fatigue life equation had been proposed.
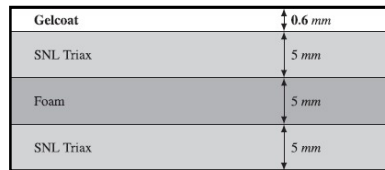
Figure 27: Material layup (Amirzadeh, et al., 2017)

The expected damage per year can be calculated by the following equation:

$$E\left[a_{year}\right] = \Sigma_I(a_I * \frac{1}{second} * t_r \frac{hour}{year} * 3600 \frac{second}{hour})P_I \qquad (24)$$

Where, a_I is the damage accumulation rate, t_r are the average total hours per year with rain days and P_I is the probability of mass related to rain intensity. Therefore, the expectation of the fatigue life is given by the following equation:

$$t_f = \frac{1}{E\left[a_{year}\right]} \qquad (25)$$

42

3.3 Rain erosion and experimental standardisation

The first experimental setup being recorded for rain erosion investigation purposes had been the one from the Air Force Wright Aeronautical Laboratories Materials Laboratory (Zahavi, Nadiv and Schmitt Jr., 1981). The figure below represents this experimental set up.

This experimental laboratory equipment was able to reach impact velocities of up to 400 m/s. Since then many similar experimental layouts have been employed to investigate on erosion issues. Not many papers have been published so far which include experimental investigation of rain droplet erosion, with Zhang, et al. (2015) and Siddons, et al. (2015) being among some of the most important. At this point, it is worth mentioning the standard ASTM G73-10 which investigates the resistance of various materials towards erosion and cavitation (ASTM International, 2010). Patterns of both mechanisms are investigated, by the response of the solid substrate to drops or jets. The most significant pattern is the incubation period and the maximum erosion rate for bulk materials. These data are used to predict the long-term exposure behaviour through empirical laws (ASTM International, 2010). The impact velocities range from 60 m/s to 600 m/s.
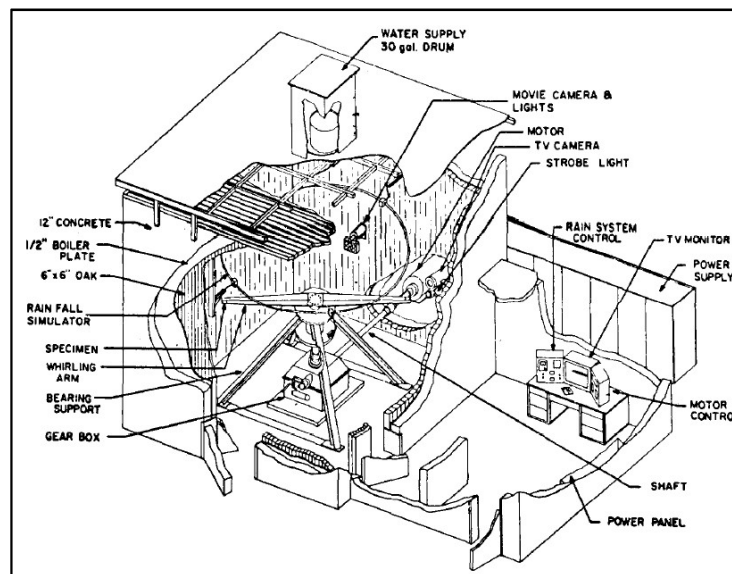

Figure 28: Rain erosion experimental set up (Zahavi, Nadiv and Schmitt Jr., 1981)

3.4 Numerical approach

In the field of erosion, a computational approach is considered as necessary in order to simulate the phenomenon with the highest possible resolution. The advances in computational capabilities allowed the research to progress further and theories have been established and verified. As presented in chapter 3.2 ANSYS had been utilised in many cases of modelling erosion. In this project ANSYS LS-DYNA is being used as a solver and LS-PrePost as a pre and post-processing software tool which supports fully the LS-DYNA keyword files. Therefore, the model will be created in LS-PrePost, the analysis will be performed by ANSYS LS-DYNA and the results acquisition through LS-PrePost (Livemore Software Technology Corporation, 2012).

LS-DYNA features both implicit and explicit solvers in their non-linear dynamic finite element code (Predictive engineering, 2017). Implicit analysis is used for both static and dynamic loading and explicit dynamics at acceleration problems. The problems that require a dynamic analysis make use of the following equation:

$$ma^n + cv^n + kd^n = f^n \qquad (26)$$

Where, n is the known time step. The difference between the implicit and explicit dynamics is located in the way of determining the displacement d^{n+1} in the time step t^{n+1}. Explicit dynamics is mainly used in purely non-linear problems where the time step is required to be as low as possible and the simulation time is increased dramatically, whereas in cases of small non-linearities higher time steps are employed and thus implicit dynamic analysis may be used. The difference between those two methods is presented in the following table.

Solver Approach	Equation
Explicit	$d^{n+1} = f(d^n, v^n, a^n, d^{n-1}, v^{n-1}, \ldots)$
Implicit	$d^{n+1} = f(v^{n+1}, a^n, d^n, v^n, \ldots)$

Table 4: Implicit and explicit dynamic analysis (Predictive engineering, 2017)

There are three main finite element methods that can be employed for the analysis of short time and high speed contacts. Those methods are summarised in the following table:

Finite Element method	Description of the method
Lagrangian	In this method an element is assigned to a given geometry. An element may different number of nodes. The main characteristic of this method is that the nodes follow interaction rules between them and the body is deformed accordingly. In general the method keeps track on every property changing.
Eulerian	In this method a volume is used to mesh a defined geometry in the Euler called domain. It is a very useful method for impact and ballistic modelling but the geometry is not deformed from its original shape. The main difference between this method and the Lagrangian is that in this method can be characterised as stationery whereas in the Lagrangian a time history of all the properties is kept.
SPH (Smooth Particle Hydrodynamics)	This method had been developed in the 1970's for astrophysics applications. SPH is a CFD (Computational Fluid Dynamics) approach with a Lagrangian mesh-less approach. It is very useful for engineering problems that experience large deformations, moving interfaces and crack initiation. Also, the system is consists of particles which have a set certain properties and the interaction between them can be described by a weight or smoothing function and the particle acceleration through the pressure gradient and density (Liu and Liu, 2010).

Table 5: Finite element methods (Keegan, Nash and Stack, 2012), (Predictive engineering, 2017), (Shadloo, Oger and Le Touze, 2016)

SPH method with an implicit dynamics solver will be used throughout this project, for the following reasons:

- It captures the phenomenon and depicts the changes in volume and in the material.
- The literature proposes this method for rain droplet simulations since it seems to attain better simulation times and resolutions.
- In high velocity impacts where shock waves propagate, the equations of motion and state are capable to describe such motions in a medium (Liu and Liu, 2010).
- Keeps record of the material particles and can determine any changes in position (Liu and Liu, 2010).

3.5 Summary

A description of erosion and more specifically the aspect of rain were presented through mathematical equations, which some of them will be used later. An overview of relevant publications in the field of erosion was attempted in order to present the limited work in this area. A description of the available simulation methods for the phenomenon was made, for a smooth transition to the next chapter which will describe the software and the model.

4. Model Description

This chapter will describe the model which will be simulated for the purposes of this erosion study. The complex model of a wind turbine blade will be described and then a simplified model of the realistic one will be extensively described and simulated. Also, a trial model will be presented in order to validate the results.

4.1 Description of the Initial Model and the Simplified

A wind turbine blade is consisted of seven structural parts with different material layup. These parts are presented below in the following picture.
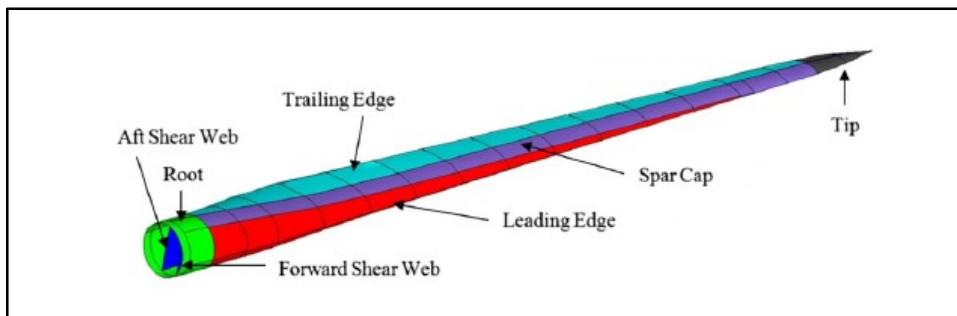

Figure 29: Wind turbine blade components (Hu, et al., 2016)

The leading edge and the tip of the blade suffer from erosion, since they experience higher velocities (Keegan, Nash and Stack, 2013), (Rempel, 2012). The leading edge of the wind turbine blade will be simulated in this thesis, since the vast majority of information about the layup of the structure concerns this part of the structure. The materials and the exact structure of a wind turbine blade are not widely and commercially available and can vary between manufacturers. Therefore, the model which will be developed will be based on the previous literature projects. According to Hu, et al. (2016), Amirzadeh, et al. (2017) and Keegan, Nash and Stack (2012) the structure of the leading edge may have three different potential cross-sections. These three models are summarised in the following table:

Author(s)	Wind Turbine Blade Type	Layup from the leading edge from top to bottom of the structure
Hu et al.(2016)	5 MW of National Renewable Energy Laboratory (Jonkmann et al.,2009)	-Fiber Glass material (QQ1 at $[\pm45]_2$ at 8 mm -Foam (Corecell^{TM} M-Foam M200 at 36 mm) - Fiber Glass material (QQ1 at [-45/+45] at 8 mm
Amirzadeh et al.(2017)	SNL 100-00 Sandia (Griffith and Ashwill, 2011)	-Gelcoat(0/6 mm) -SNL 100-00 Triax ($[\pm45]_2/[0]_2$ at 5 mm) -Foam (5 mm) - SNL 100-00 Triax ($[\pm45]_2/[0]_2$ at 5 mm)
Keegan (2012)	Upwind WMC5MW (Nijssen,2007),(Bir and Migliore, 2004)	-Gelcoat (0.4 mm) -Chopped Strand Mat (0.51 mm) -Bi-Axial Glass Fiber Composite (0.53 mm at [0/45/0])

Table 6: Different layups across multiple layers of wind turbine blades (Hu, et al., 2016), (Amirzadeh, et al., 2017) and (Keegan, 2012)

In the present thesis the chosen layup includes the first layer of the material being a gelcoat epoxy resin and two plies of composite material (E-Glass) with the fibers being oriented at +45° and -45° respectively. This layup is a combination of all three structures described above and a simplified model which has been proposed by Hu, et al. (2016). The pictures below present the initial model and the simplified one as being generated in Ls-PrePost. The simplified one neglects the existence of foam and the two composite plies of material below the foam. This simplification assists on decreasing the computational cost by the use of proper boundary conditions. Moreover, this research intends to identify the effects of erosion in lower layers lying beneath the gelcoat. Furthermore, the mesh can be denser and thus more accurate results can be drawn by that simplification of the model.
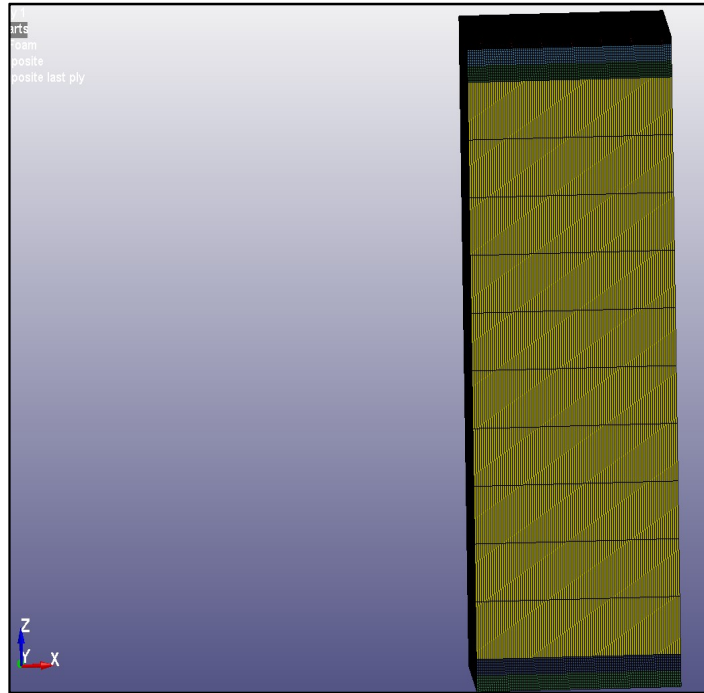
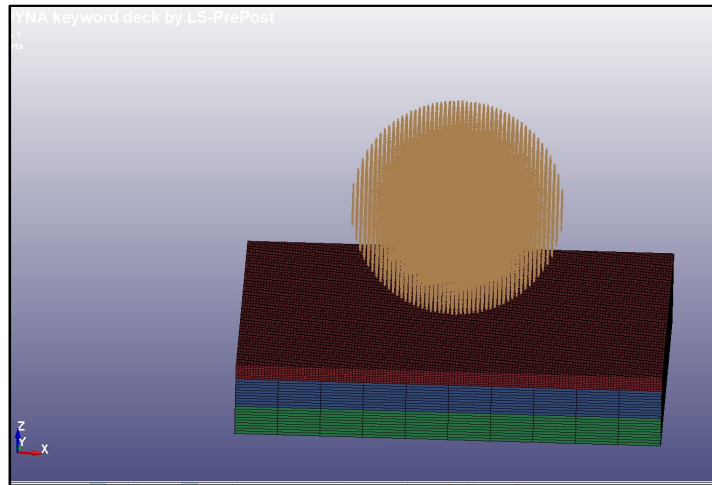**Figure 30:** Realistic Model structure of the leading edge

Figure 31: Simplified model of gelcoat, two plies of composite and a rain droplet

The size of the structure has been defined to be at 6x6 mm for two main reasons. The first reason concerns the computational cost, since the time of simulation increases dramatically when the size of the structure increases in size. The other reason covers the aspect of surface wave reflections that are created after the impact of the rain droplet and they might affect the results.

49

4.2 Calibration of the Model

In this sub-chapter of the thesis a description of the model will be presented and the inputs, assumptions will be discussed in this part. The challenge of the simulations includes the definition of the parameters which can affect the model and the results. A sufficient number of trial models have been performed in order to define the key parameters and properties that can influence the results. A verification of the results has been performed in order to build the complex model with the composite material and to define the key results that can describe the aspect of erosion.

One of the most important steps in modelling includes the verification and justification of the results in a very simple model. This simple model includes a 1mm and a 3mm rain droplet and an impact target which is made of an isotropic material, in this case aluminium 6061. The kinetic energy, the impact force and the waterhammer pressure had been identified as the indicating results in this direction of validation. The kinetic energy is distinctive for the different rain droplet sizes and the different impact velocities according to the following equation:

$$K = \frac{1}{2} * m * v^2 \tag{27}$$

Where m is the mass of the rain droplet and v is the impact velocity. The following figure represents the values of the kinetic energy according to the different rain droplet sizes and the different impact velocities.
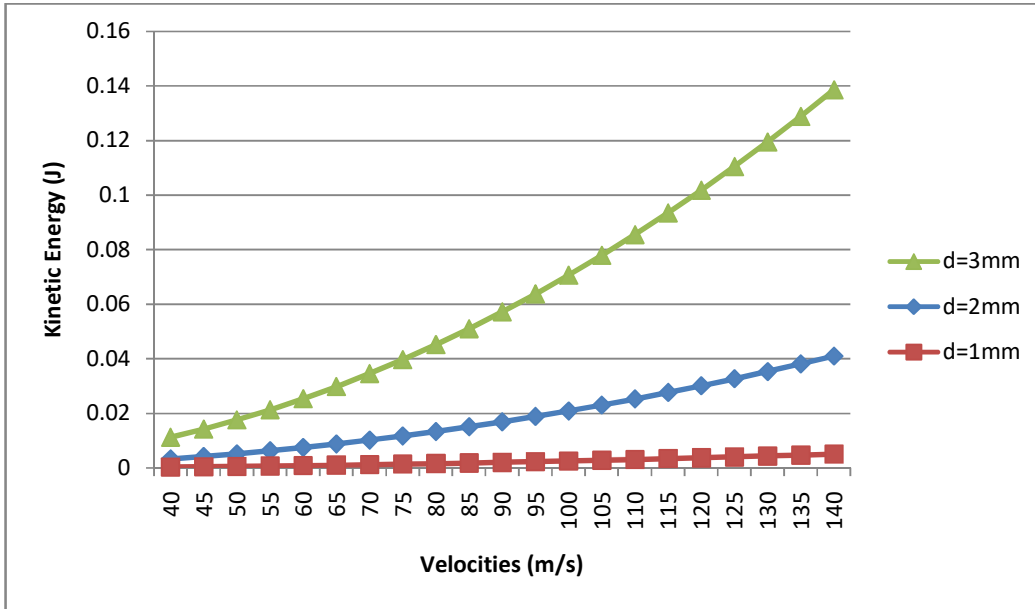
Figure 32: Kinetic Energy in a wide range of velocities and droplet diameters

As far as the impact force concerned the equation (23) has been used and the following figure represents the impact force in the same range of values.
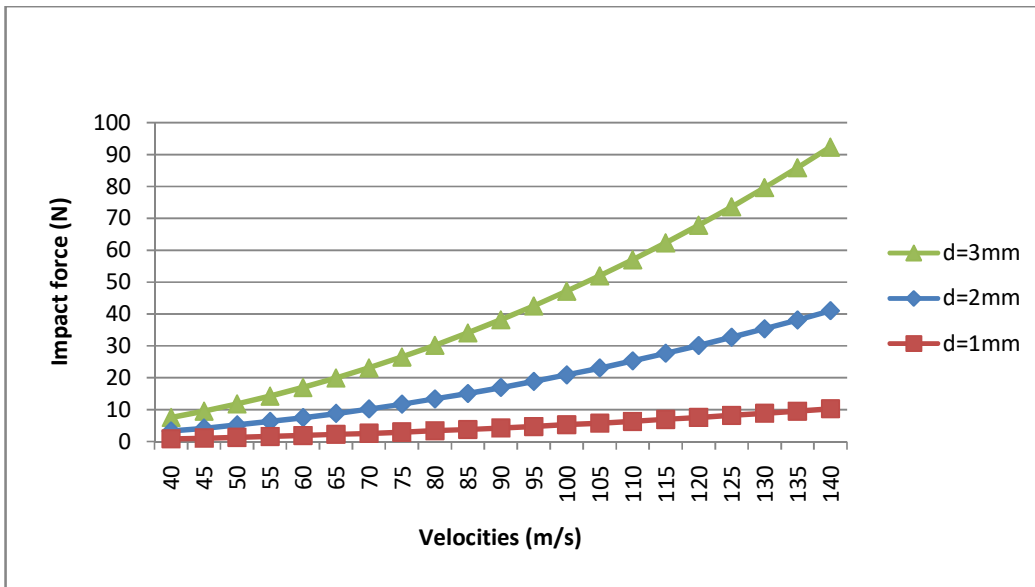

Figure 33: Impact Force in a wide range of velocities and droplet diameters

As far as the waterhammer pressure concerned the equations (18) and (20) have been used. The equation (20) required the density of the aluminium and the speed of sound in the aluminium. The density of the aluminium has been found to be at 2700 kg/m^3

(ASM Aerospace Specification Metals Inc., 2000). The speed of sound in the aluminium had been defined by the following equation (Nayfeh, 1995):

$$C_S = \sqrt{\frac{K}{p}} \tag{28}$$

Where, K is the bulk modulus of the material and ρ the density of the material. The Young's modulus had been found to be 38.1 GPa by Khlystov, et al. (2013). The bulk modulus had been defined by the following equation (Bower, 2008) at 3719 m/s with a poisson's ratio of 0.33:
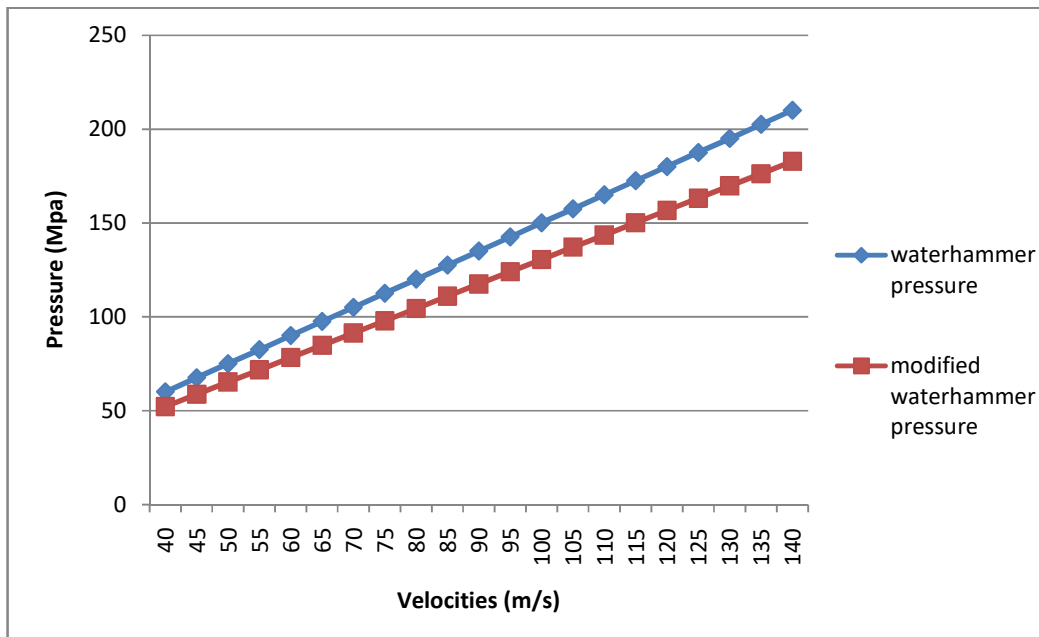
$$K = \frac{E}{3(1-2*v)} \tag{29}$$

Figure 34: **Waterhammer pressure in a range of different velocities**

According to these analytical values the model had to be created and the results had to match with a certain level of reasonable error.

The geometry of the aluminum plate was created through the shape mesher tool, where the dimensions had been assigned and the finite elements mesh had been

created with 337500 elements in total for the best accuracy of results (Keegan, 2014). The properties of the aluminum material are summarized in the following table. The keyword PLASTICITY_COMPRESSION_TENSION (Livermore Software Technology Corporation, 2014) had been used for this purpose and the following table represents the input values (Khlystov, et al. 2013):

Young's modulus	2700 kg/m^3
Density	38.1 GPa
Poisson's ratio	0.33
Tensile Yield stress	275 Mpa
Tensile strain at break	0.08
Compressive Yield stress	3 GPa
Compressive stress at break	4 Gpa
Compressive strain at break	0.14

Table 7: Aluminium 6061 mechanical properties

The ADD_EROSION material keyword had been added on top with a compressive strain at failure to be at 0.14 as referred above, in order to simulate the erosion state. Solid elements had been used to simulate the aluminum material. The boundary conditions in this case of problems required the bottom of the target to be fixed from all rotations and translations (Yarrapareddy and Kovacevic, 2007), (EITobgy, Ng and Elbestawi, 2005), (Amirzadeh, et al., 2017) and (Keegan, 2014). Two curves had been defined to describe the compressive and tensile behavior of the material with the DEFINE_CURVE keyword manager. The two curves had been assigned into the keyword PLASTICITY_COMPRESSION_TENSION in card option 2.

As far as the droplet concerned the SPH generation tool was used to create the geometry of the sphere of 1mm droplet and 50 nodes in x,y and z direction were used. This number of nodes was considered to induce less computational cost but a good accuracy of results (Keegan, 2014). The material MAT_NULL had been used to assign the density of the rain droplet at 1000 kg/m^3 and had a dynamic viscosity of 0.001 Pa s at 5°C. The equation of state had been defined by the keyword EOS_Gruneisen and the properties of water used were the speed of sound at 1647 m/s

and the S1 unitless coefficient of the Gruneisen equation to be 1.921. The equation of state is important for the calculation of the fluid pressure (Liu and Liu, 2010). These properties have been assigned to the material. The contact keyword which was chosen was the NODES_TO_SURFACE_SMOOTH. The slave was the droplet and the impact surface was the master with the soft constrained formulation card option activated. The material and the section were then assigned to the created parts.

Next step was the simulation of a 1mm and 3mm rain droplet with the same characteristics as described above, at 50 m/s. The following picture represents the geometry of that simple model of a 1mm rain droplet.
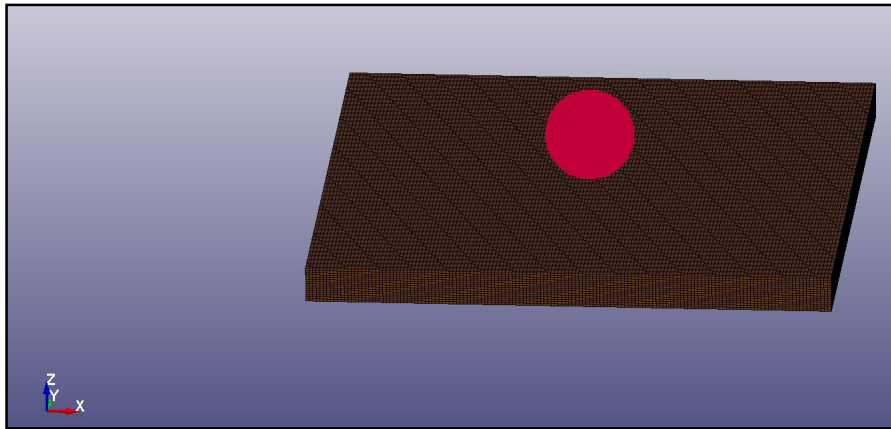
Figure 35: Geometry of the model

The following figures represent the results of the 1mm rain droplet simulation. The first graph depicts the kinetic energy, which presents a small error of 3% compared to the equation (27).
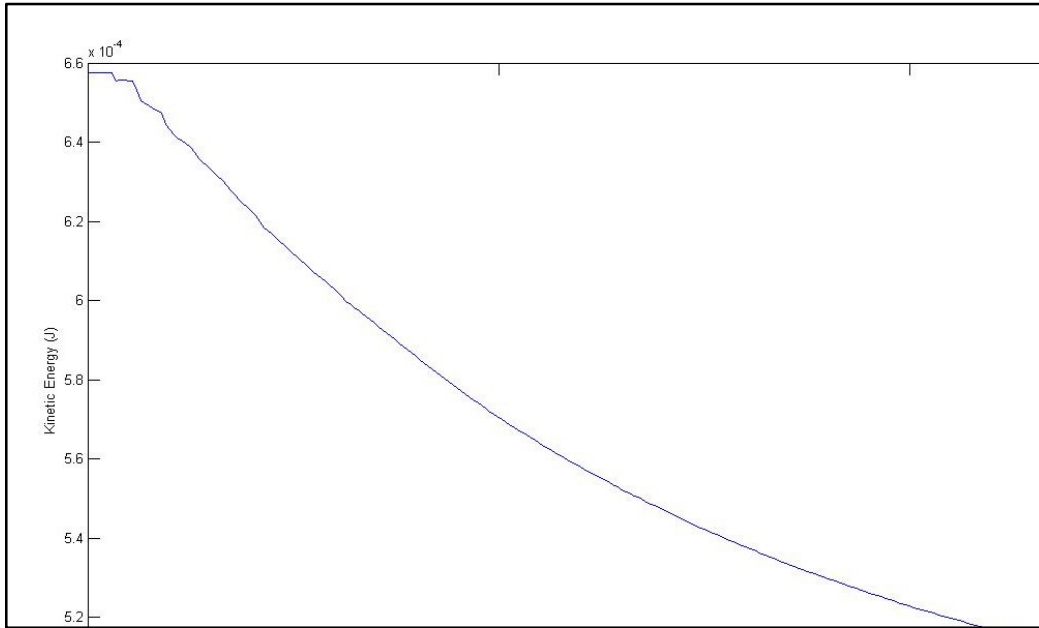
Figure 36: Kinetic Energy of a 1 mm rain droplet

The next set of graphs included the impact force and the waterhammer pressure with 35% and 20% error compared to equations (23) and (18) respectively.
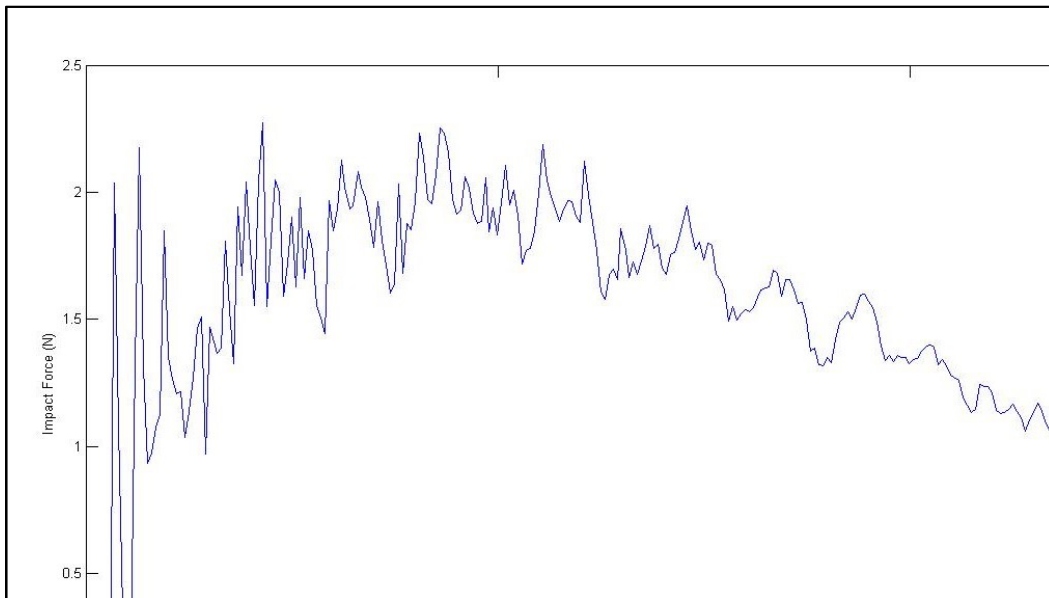

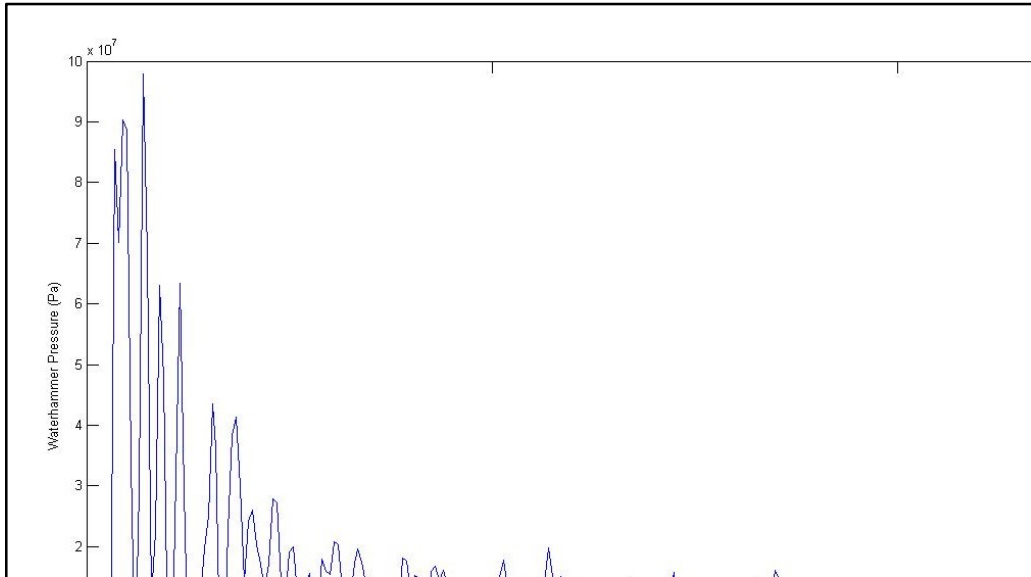**Figure 37: Impact Force vs Time of a 1 mm rain droplet**

Figure 38: **Waterhammer Pressure vs Time of a 1 mm rain droplet**

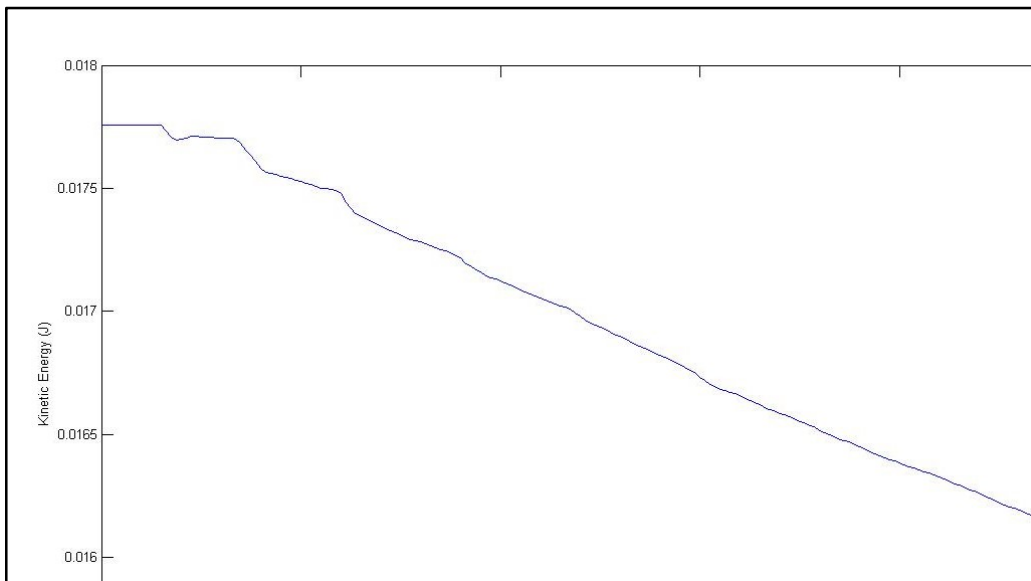The following graph depicts the kinetic energy of a 3 mm rain droplet and the error is around 1%.

Figure 39: **Kinetic Energy of a 3 mm rain droplet**

The last set of graphs for this sub-chapter include the impact force and the waterhammer pressure with 36% and 25% error compared to equations (23) and (18)

respectively. This error might be a result of mesh sensitivity study, damping phenomena or the behaviour of the solid substrate (Keegan, 2014).
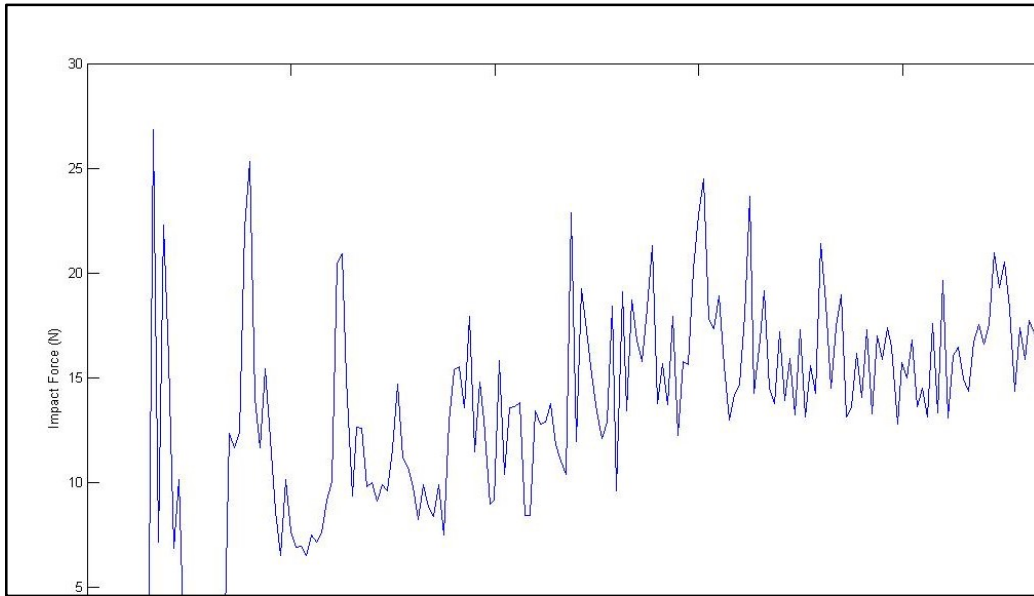
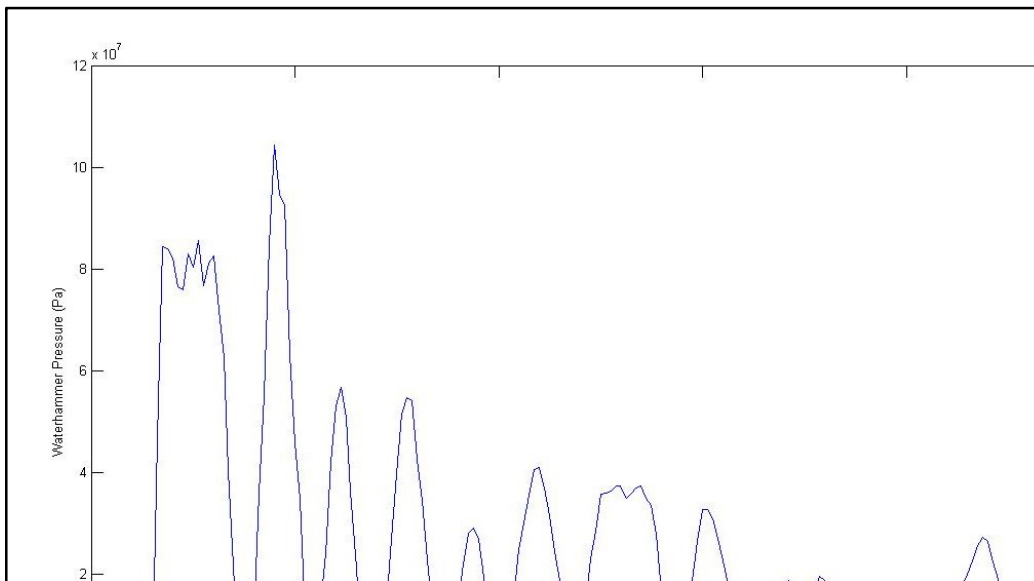**Figure 40: Impact Force vs Time of a 3 mm rain droplet**

Figure 41: Waterhammer Pressure vs Time of a 3 mm rain droplet

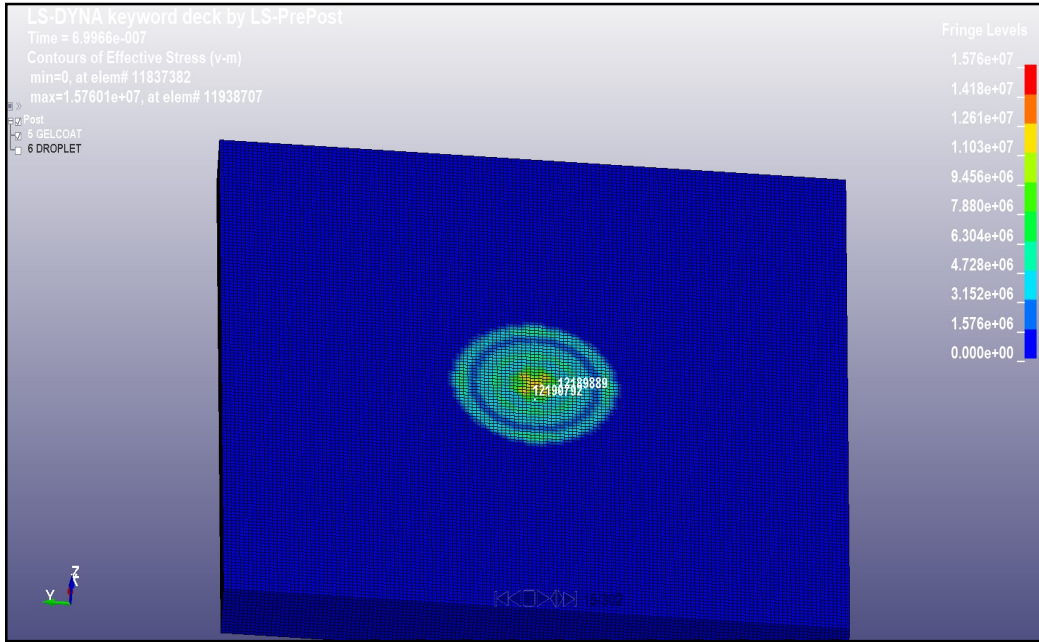The following figures depict some snapshots from the rain droplet and the solid surface.
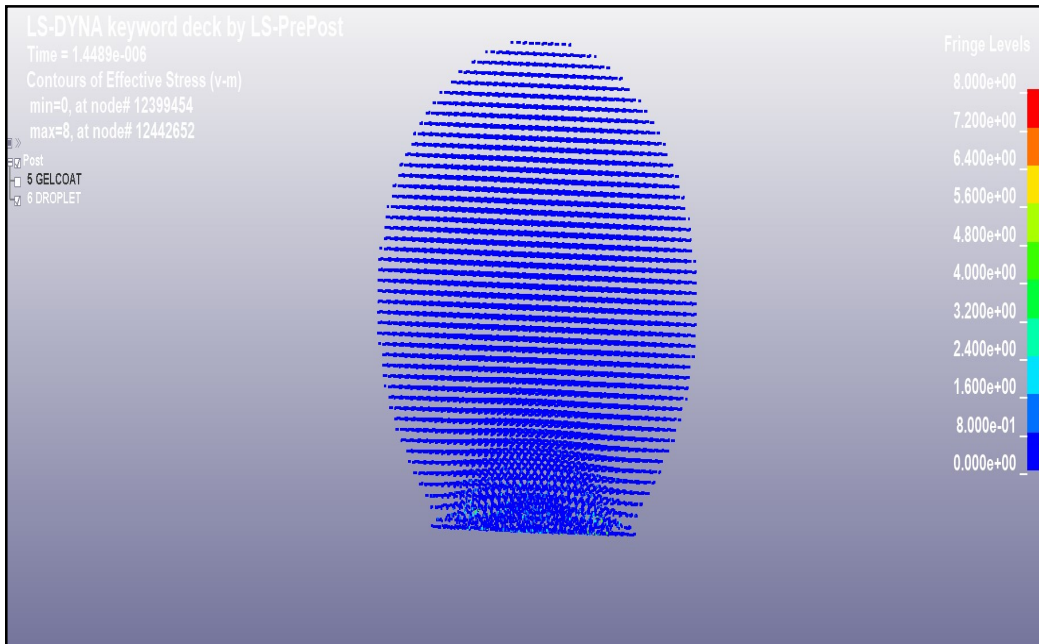
Figure 42: **Stress generated on the surface**

Figure 43: **Stress generated on a 1 mm rain droplet**

4.3 Simulation model description

After the validation of the simplified model with the isotropic material, the creation of the more complex state follows. The model is consisted of three different layers, firstly the gelcoat and then the two layers of composite material at +45 and -45 degrees respectively. This choice was made according to table 6 in an attempt to minimise the shear stresses anticipated in this case and simulate a realistic structure layup. The following picture depicts this layup.
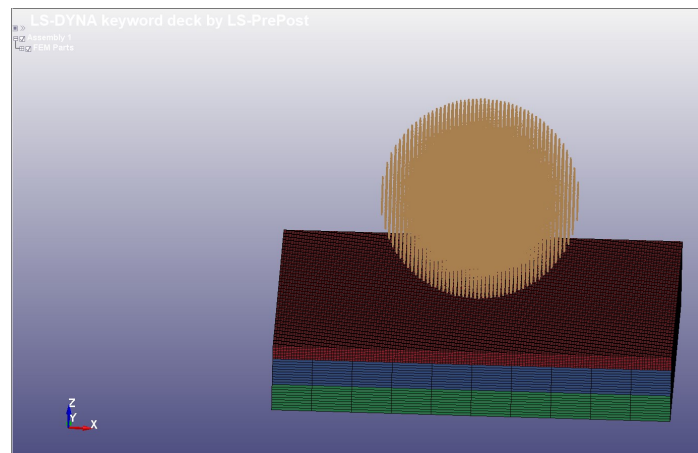

Figure 44: Layup of the model

The geometry of the gelcoat layer was created through the shape mesher tool, where the dimensions had been assigned and the finite elements mesh had been created with 337500 elements in total for the best accuracy of results (Keegan, 2014). As far as the droplet concerned the SPH generation tool was used to create the geometry of the sphere of 1mm droplet and 50 nodes in x,y and z direction were used. This number of nodes was considered to induce less computational cost but a good accuracy of results (Keegan, 2014).

Next stage of this procedure is the creation of boundary and initial conditions through the create entity tool. Boundary conditions have been applied to the bottom of the plate fixing both rotations and translations in all the possible directions. Also, the impact velocity is created through the initial keyword with a value 100 m/s in the z-direction.

The crucial stage of this process concerned the meticulous input of the mechanical properties through the MAT keyword. For the gelcoat the keywords of ADD_EROSION and MAT_PLASTICITY_COMPRESSION_TENSION (Livermore Software Technology Corporation, 2014) have been used. The properties of the epoxy are presented in the following table (Littel, et al. (2008) :

Epoxy Epon E 862	
Poisson's ratio	0.4
Young's Modulus (Gpa)	2.5
Density (kg/m^3)	1150
Tensile Yield stress (Mpa)	90
Tensile strain at break	0.25
Compressive Yield stress (Mpa)	120
Compressive stress @ break (Mpa)	180
Compressive strain @ break	0.3

Table 8: Properties of Epoxy Epon E 862

Two curves had been defined to describe the compressive and tensile behavior of the material in the DEFINE_CURVE keyword manager. The MAT_ADD_EROSION material keyword had been added on top with a compressive strain at failure to be at 0.3 as presented in the table above, in order to simulate the erosion state (Livermore Software Technology Corporation, 2014).

The material MAT_NULL had been used to assign the density of the rain droplet at 1000 kg/m^3 and had a dynamic viscosity of 0.001 Pa s at 5°C. The equation of state had to be defined by the keyword EOS_Gruneisen and the properties of water used

were the speed of sound at 1647 m/s and the S1 unitless coefficient of the Gruneisen equation to be 1.921.

As far as the two composite plies concerned, the keyword MAT_COMPOSITE_FAILURE_SOLID_MODEL (Livermore Software Technology Corporation, 2014) had been used in order to simulate the behavior of the composite E-Glass material. The properties of this material are presented in the following table (Menna, et al., 2011):

E-Glass Composite	
Density (kg/m^3)	1500
$E_1 = E_2$ (Gpa)	26
E_3 (Gpa)	8
G_{12} (Gpa)	3.8
$G_{23} = G_{13}$ (Gpa)	2.8
v_{12}	0.1
$v_{23} = v_{13}$	0.25
XT =YT (Mpa)	414
ZT (Mpa)	120
XC =YC (Mpa)	458
ZC (Mpa)	500
S_{12} (Mpa)	105
$S_{23} = S_{13}$ (Mpa)	65

Table 9: Properties of E-Glass composite material

To change the orientation of the fibres the element editing tool had been used for this purpose. After the definition of the materials, the definition of sections was the next step. The composite and the gelcoat used the SECTION_SOLID keyword with the default constant stress elements and the rain droplet the SECTION_SPH with the default values. After the proper assignment of the section and the material properties, the assignment of both keywords to the created parts was achieved through PART keyword (Livermore Software Technology Corporation, 2014).

The last part of the creation of the model concerned the choice of contact type between three different materials. The first type of contact is between the rain droplet and the gelcoat. For this type of contact, the keyword CONTACT_NODES_TO_SURFACE_SMOOTH was chosen for its accuracy of results (Keegan, 2014). The slave was the rain droplet and the master the gelcoat layer. Also, the option card 9 was used for the simulation with the default values. For the contact type not only between the gelcoat and the first ply but also for the contact between the composite plies, CONTACT_AUTOMATIC_SURFACE_TO_SURFACE_TIEBREAK was used having as master the surface that is lower in the structure.

Last step, included the set up of some controls through the CONTROL keyword. The keywords of CONTROL_ENERGY, CONTROL_HOURGLASS, CONTROL_CONTACT and CONTROL_SPH were used. The termination time was defined by CONTROL_TERMINATION and a time step reduction factor of 0.4 was used through CONTROL_TIMESTEP as a best practice for these simulations (Keegan, 2014), (Livermore Software Technology Corporation, 2014).

After the description of the model, the next chapter will present the results of it along with some discussion points of every figure.

5. Results

This chapter is divided into two parts. The first part concerns the approach of changing gelcoat thicknesses from 0.2 mm to 0.8 mm with a 0.2 mm step. A set of results will be presented with a purpose of establishing erosion patterns in changing gelcoat thicknesses. The second part of this chapter takes into account the effect of boundary conditions in the case of 0.2 mm of gelcoat which is the most susceptible case to changes. Two appendixes have been created one for each approach, in an attempt for clarity and homogeneity with the main body of this dissertation. Matlab (The Mathworks Inc., 2017) has been used for the acquisition of results in raw x,y data.

5.1 Effect of changing gelcoat thickness

The first physical property that will be presented is the effective plastic strain. This property can display the initiation of damage in the solid substrate. A threshold should be defined at this point in order to indicate the initiation of damage in the gelcoat. Therefore, a threshold of 1% strain will be used to describe the initiation of erosion in the gelcoat, according to Littel, et al. (2008). Above this threshold damage will be considered as significant enough for damage to be created to the epoxy. The following graph is a comparison between the different coating thicknesses.
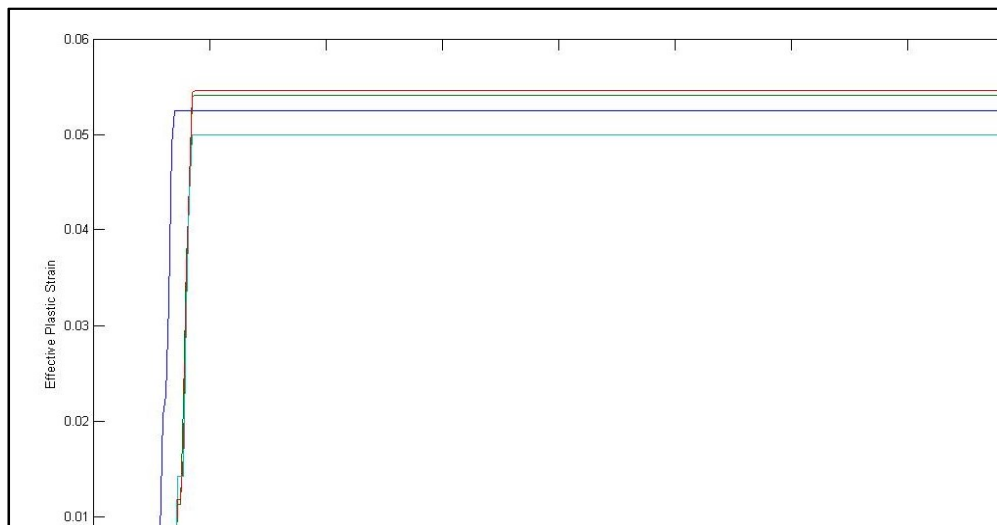
Figure 45: Effective plastic strain rate

The plastic strain occurs after 1µs in the cases of 0.4 mm, 0.6 mm and 0.8 mm compared to the case of 0.2 mm. This means that erosion takes place earlier in the case of 0.2 mm compared to the other cases. The individual graphs of effective plastic strain rate are located in Appendix 1.

Another aspect that is worth mentioning concerns location of the effective plastic strain. The next diagram presents this distance in accordance with the centre of impact.
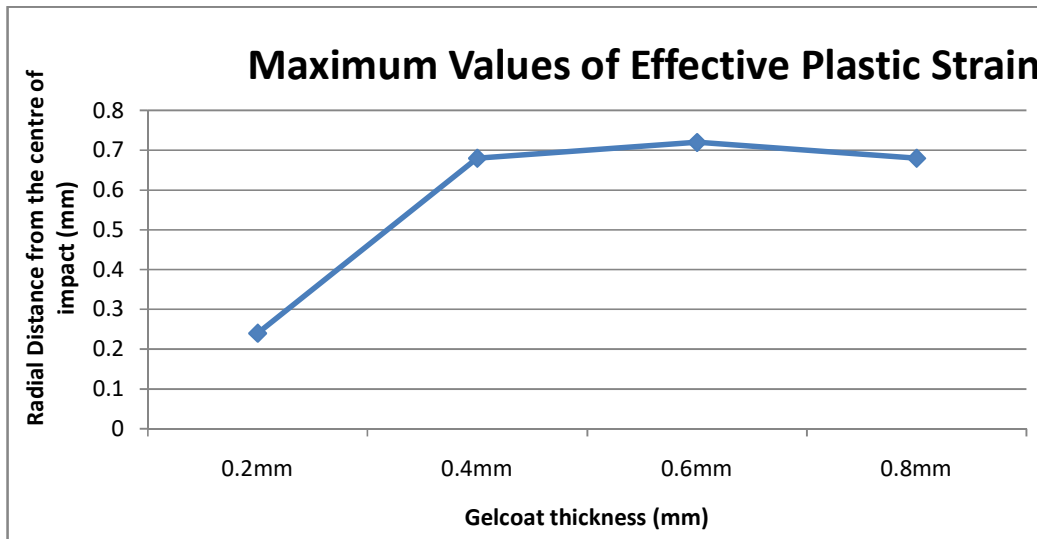

Figure 46: Location of effective plastic strain

It is obvious from this graph that the case of 0.2 mm has a different behaviour pattern that the other cases. In this case the effective plastic strain is located closer to the centre of the impact at a distance of 0.25 mm. It is also worth mentioning that in the case of 0.6 mm the maximum value of effective plastic strain is located 0.4 mm further compared to the cases of 0.4 mm and 0.8 mm coating thickness.

The following picture depicts the case of 0.2 mm and shows the magnitude of effective plastic strain. The element having the peak value of effective plastic strain is depicted.
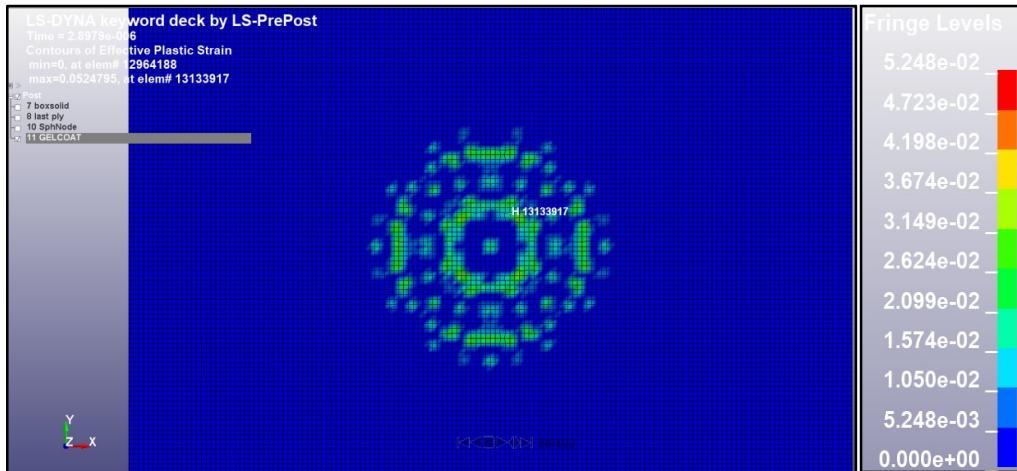
Figure 47: Magnitude of effective plastic strain at 0.2 mm

The effective plastic strain can be linked with the following effective Von-Mises stresses comparative diagram as well. The time of maximum effective plastic strain can be used to conclude about the time of lateral jetting effect.

The interpretation of this comparative diagram reveals that the effective plastic strain happens during the onset of lateral jetting in the cases of 0.2 mm, 0.4 mm and 0.6 mm, whereas in the case of 0.8 mm this happens after the onset of lateral jetting. Another observation is that in the case of 0.2 mm there are three peak values almost equal, creating higher stress field in the coating layer. The individual diagrams are placed in appendix 1.
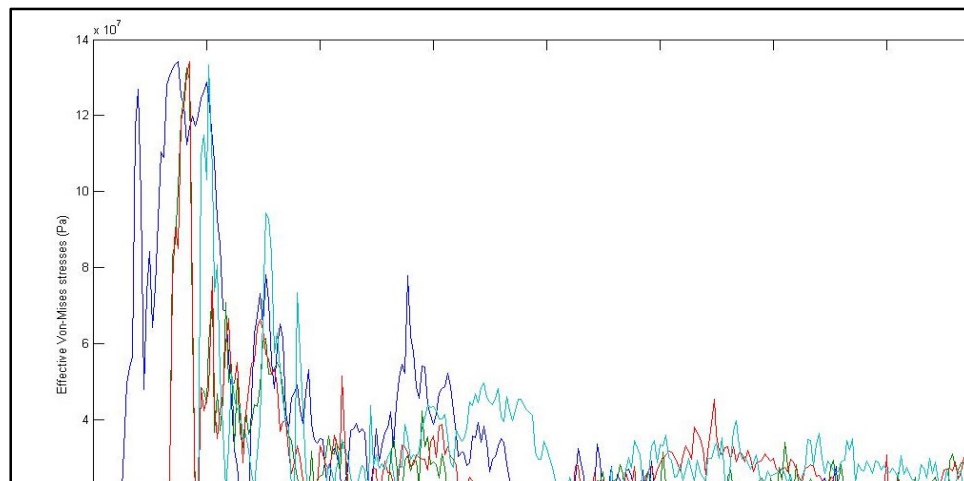
Figure 48: Effective Von-Mises stresses vs time

65

The figures below represent the propagation of the Rayleigh wave for the case of 0.2 mm in various snapshots. Rayleigh wave propagation has been described in chapter 3, as being surface waves which are propagating in solid mediums.

| 0.34 µs | 0.55 µs |
| 0.75 µs | 0.95 µs |
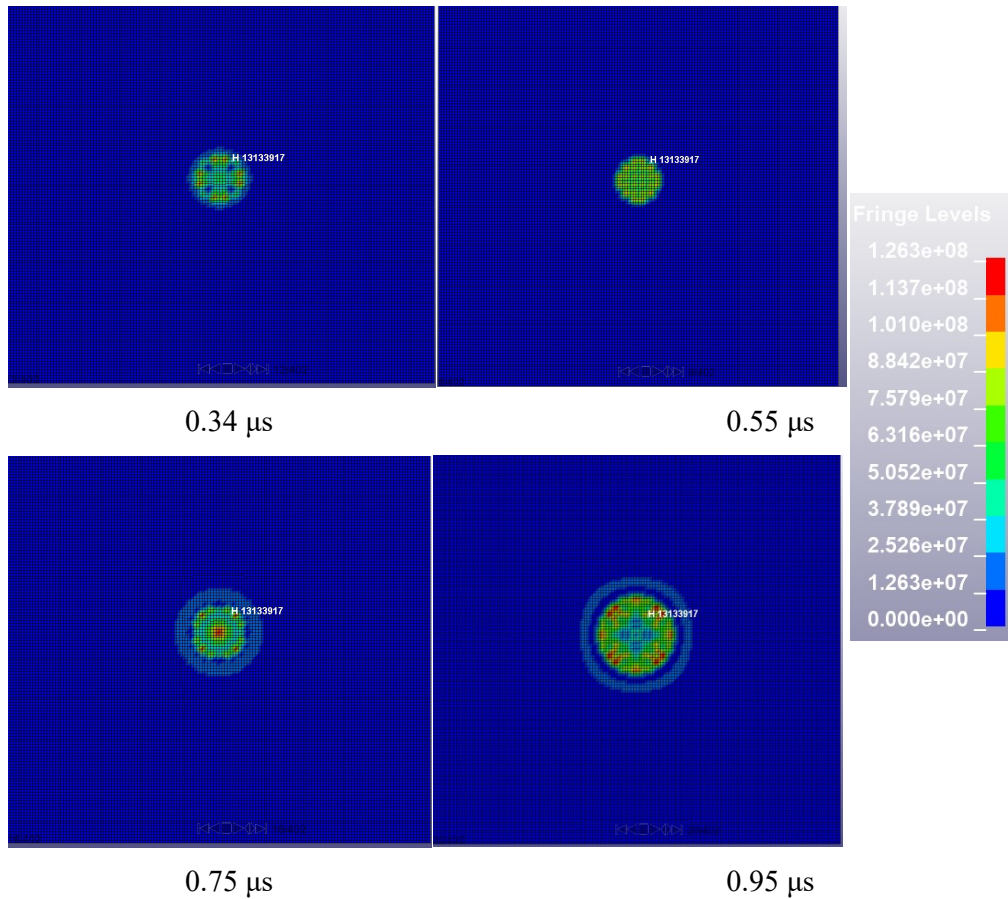
Figure 49: Snapshots of Rayleigh wave propagation

The next comparative diagram represents the waterhammer pressure for the different cases. The case of 0.2 mm shows 11.8% higher peak value when compared to the other cases. Generally, this case represents a higher pressure field across the rain droplet. The individual diagrams are placed in appendix 1. Below the comparative figure a snapshot of waterhammer pressure is presented in order to indicate the compression wave generated in the droplet due to the local compression of the liquid at the moment of impact.
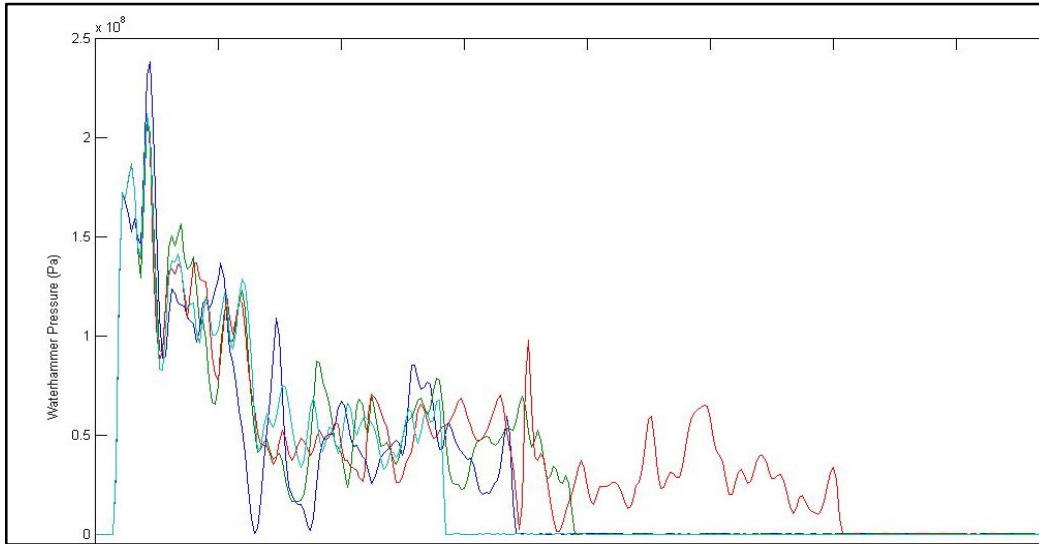
Figure 50: Waterhammer Pressure vs time

35μs   55μs

95μs   1.3μs
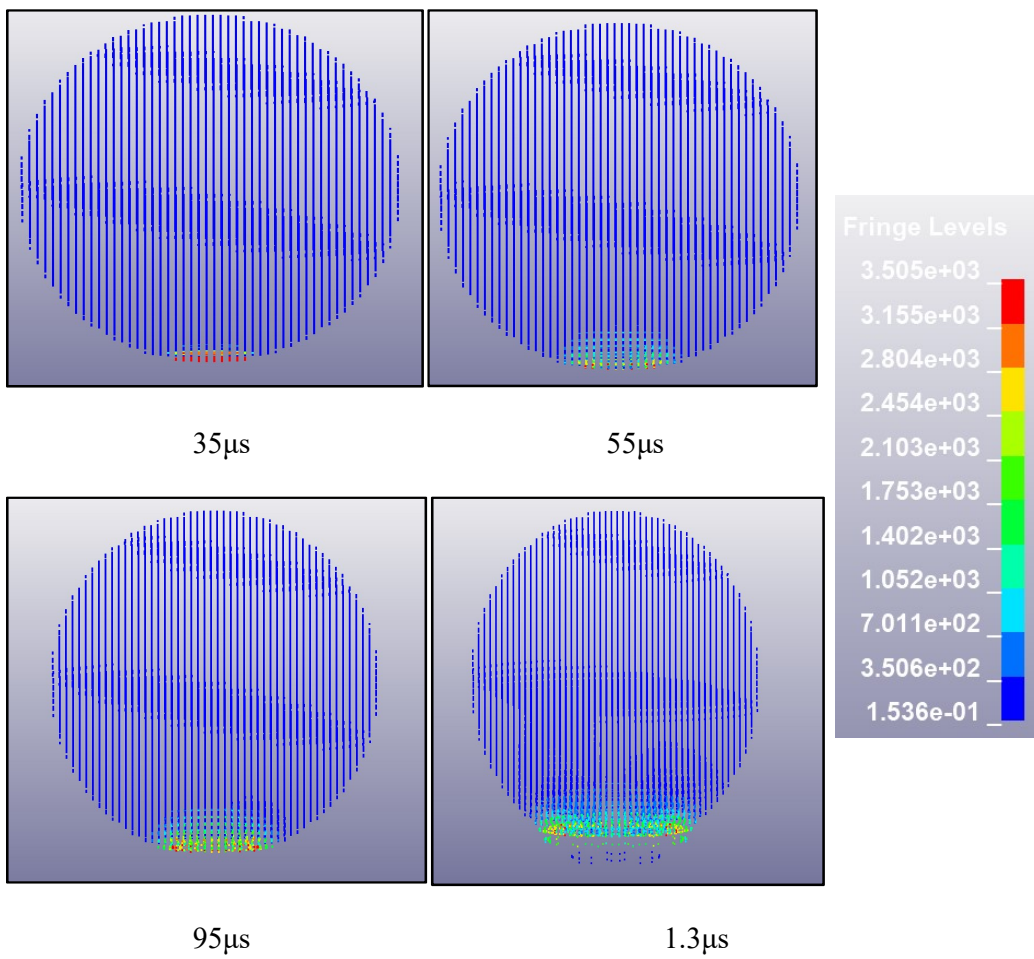
Figure 51: Snapshots of waterhammer pressure

The next comparative diagram shows the impact force that is being generated in the solid substrate during the impact with the rain droplet. The values seem to be fluctuating around 85 N, with a divergence of 1-4%. Therefore, no clear conclusions can be drawn through this diagram. The individual diagrams are placed in appendix 1.
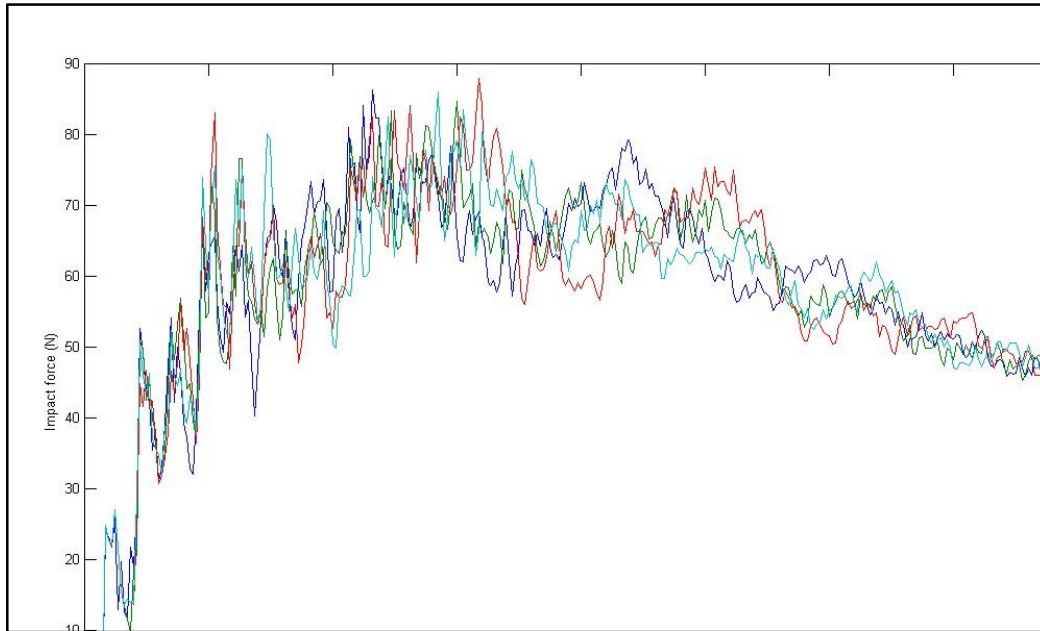

Figure 52: Impact force vs time

The kinetic energy was not depicted, since it is independent of changes in the gelcoat thickness and has the form of figure 39.

The next set of comparative diagrams will be comparing the stresses being developed through the thickness in an attempt to study the composite material layers which are placed below the gelcoat. The next diagram shows the Maximum Von-Mises stresses created in the three layers.

The trend in the following graph shows that the cases of 0.6mm and 0.8mm indicate a similar behavior with 30% lower Von-Mises stresses in the first ply of the composite material. The differences are almost eradicated in the last ply and this might be affected due to the boundary conditions which are applied for these cases.
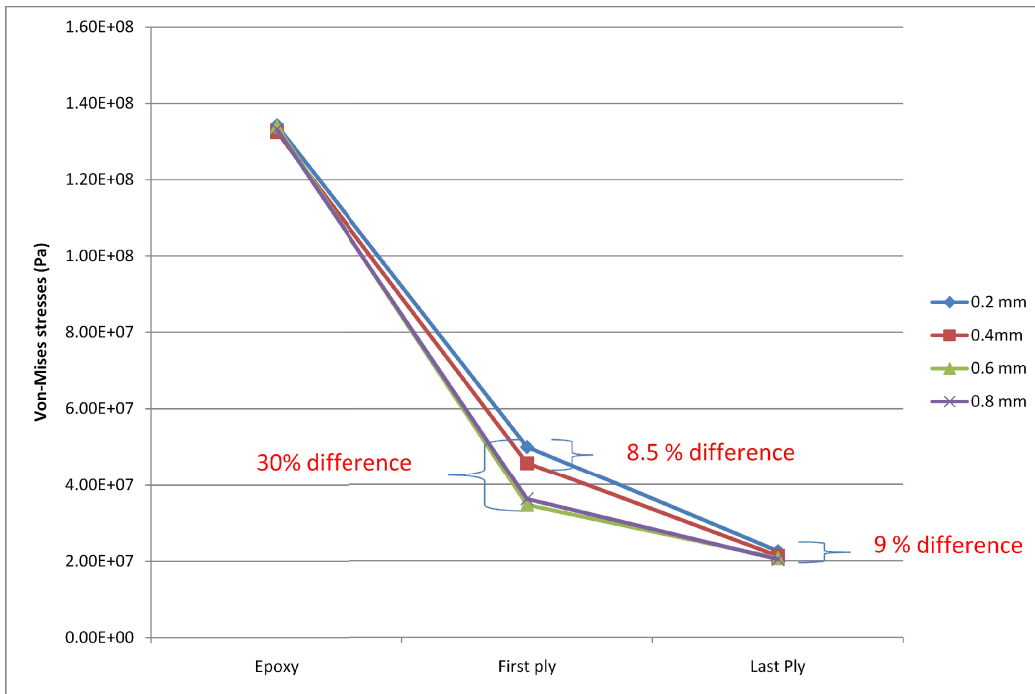
Figure 53: Peak values of effective Von-Mises stresses

The following graph shows the maximum shear stresses created according to the Tresca criterion. The behavior is anticipated to be close to the one of the previous graph. The only minor difference is found in the last layer with a difference of 2% compared to the previous graph.
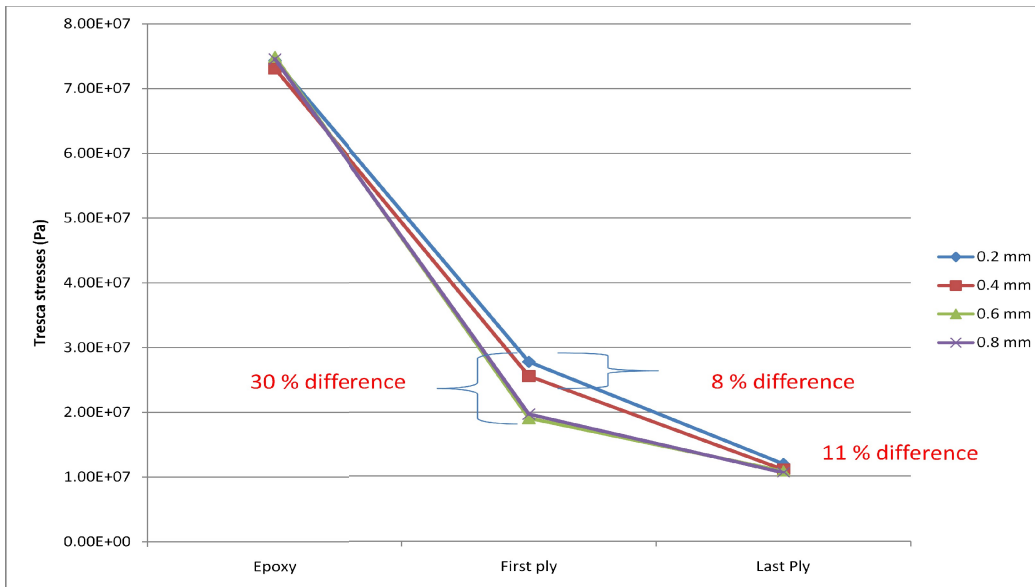

Figure 54: Peak values of Tresca stresses

The following comparative chart presents the kinetic energy dissipation across the different layers of the structure. As expected, the thickness of the gelcoat layer affects the kinetic energy relief throughout the structure as we proceed deeper in the core of the structure. The case of 0.2 mm behaves in a different way making the structure more susceptible to impacts.
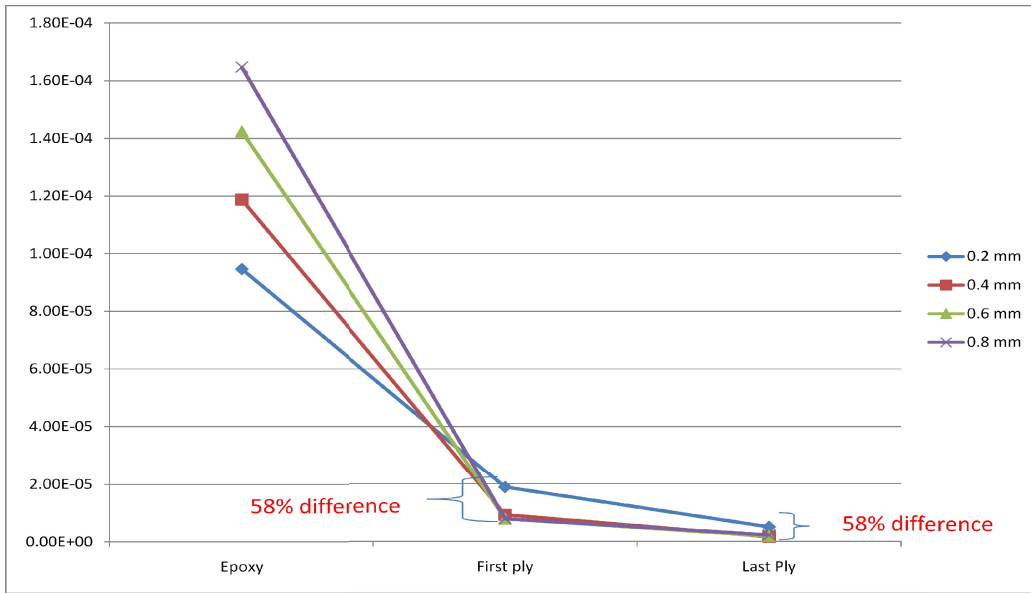
Figure 55: Kinetic energy dissipation across the different layers

The following diagram shows the displacement of the rigid bodies (gelcoat, first ply and second ply) in the z-direction.
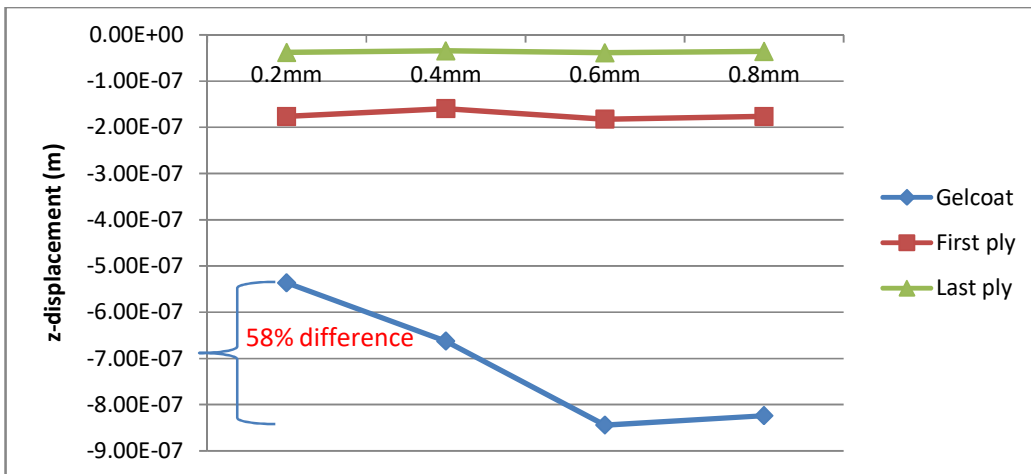
Figure 56: z-displacement through the thickness

The above diagram shows that the composite layers that lie beneath the gelcoat are preserved in a steady state and do not seem to be affected by the impact independently of the thickness of the gelcoat. However, in the case of the gelcoat the thickness affects significantly the displacement in the z-axis, with the thicker gelcoat absorbing most of the energy of the impact.

The next set of diagrams shows the distribution of the maximum values of nominal stesses σx, σz and the shear ones σzx, σxy.
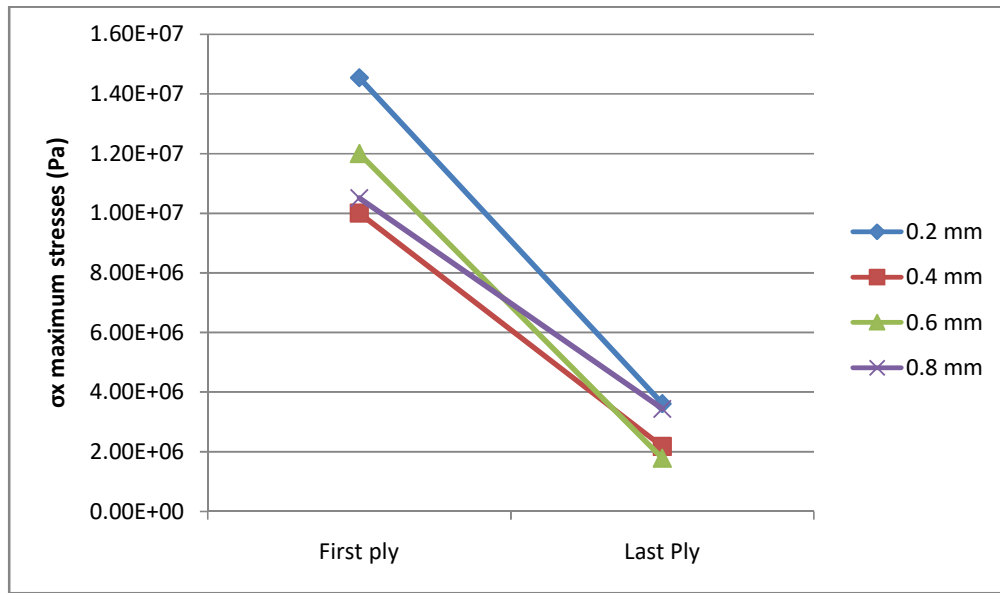
Figure 57: maximum σ_x stresses across the composite plies

This comparative diagram shows the maximum values of σ_x stresses between the layers of the composite. The case of 0.2 mm has the highest stresses exercised along the structure, whereas the cases of 0.4 and 0.6 mm attain more stable behaviors. In the case of 0.8mm the stress differentiates and decreases with the smallest rate in the last layer of the structure. The stresses σ_y will not be presented since the material behaves as orthotropic and $\sigma_x = \sigma_y$. Therefore, the next diagram which will be presented concerns the σ_z stresses. This diagram shows an expected behavior with the thickness of the gelcoat driving the stresses along the z-axis.
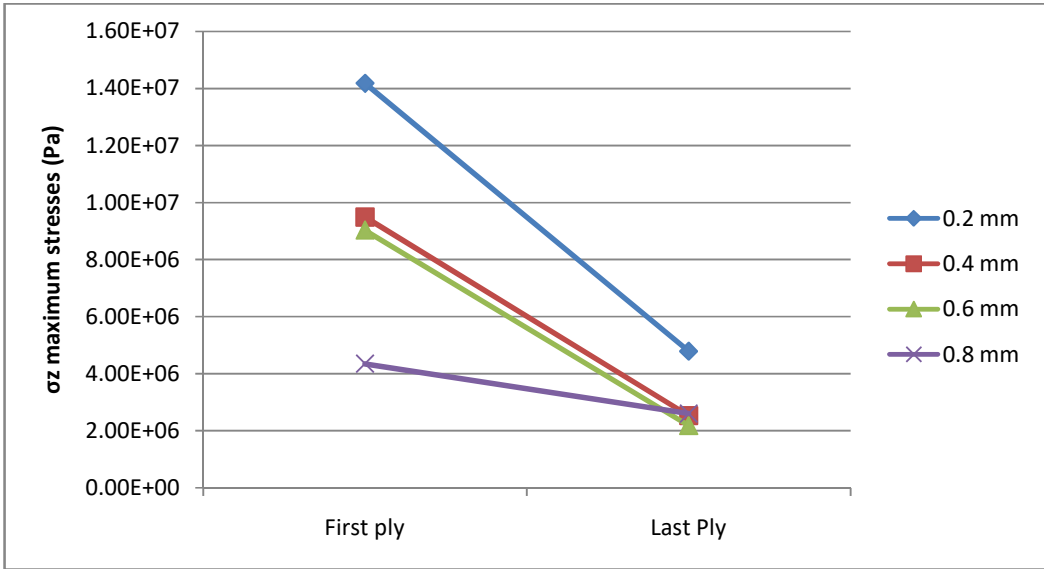
Figure 58: maximum σ_z stresses across the composite plies

The next set of diagrams will present the shear stresses that are exercised in the xy and zx directions. It is obvious through the xy stresses that the cases of 0.6 mm and 0.8 mm present a smoother stress field in that direction.
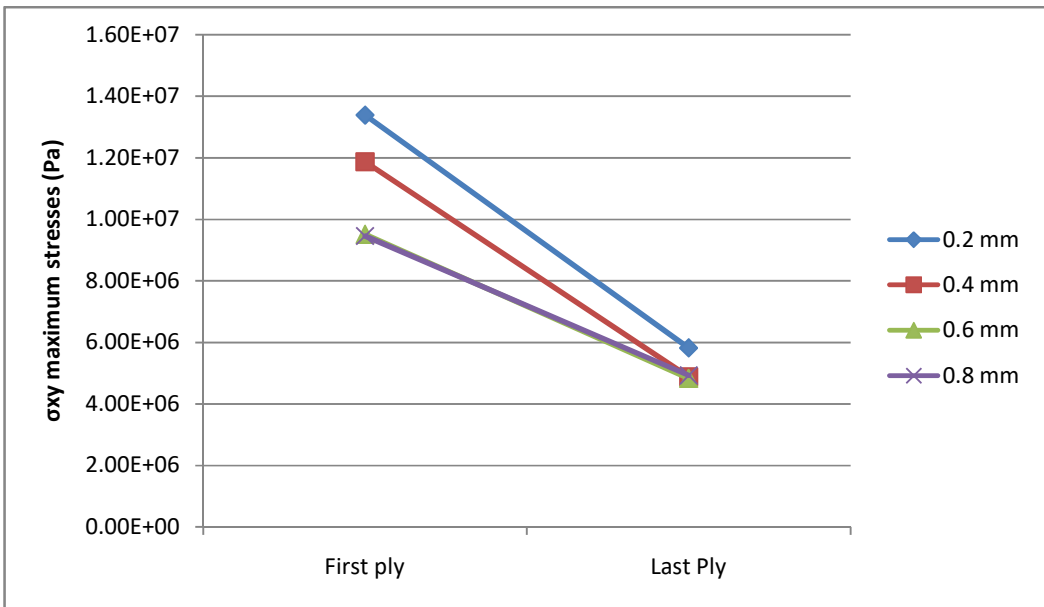

Figure 59: maximum σ_{xy} stresses across the composite plies

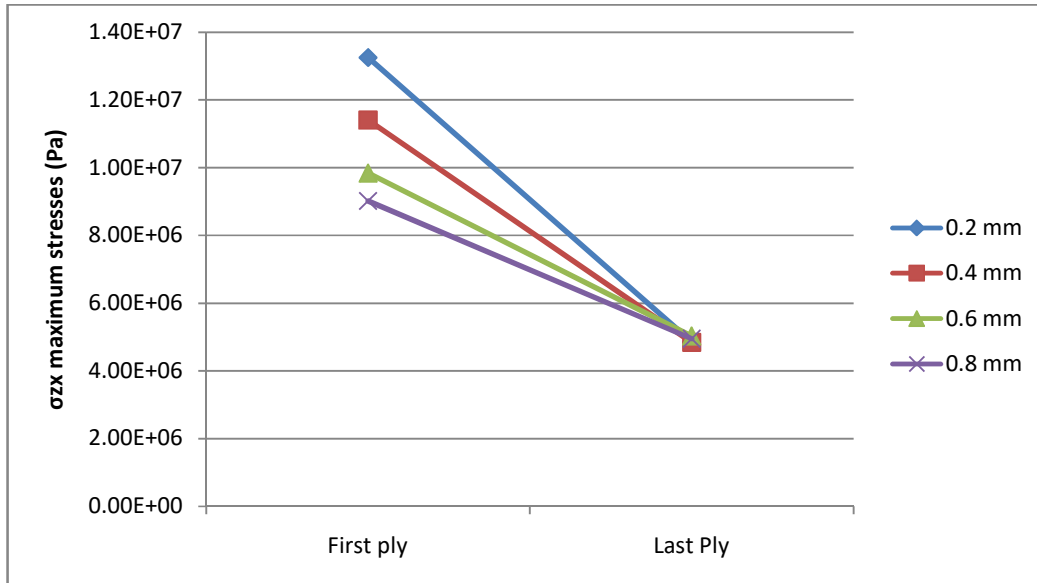The shear stresses in the zx direction presented an expected behaviour as in the case of nominal stresses in the z axis.

Figure 60: maximum σ_{zx} stresses across the composite plies

The radial distance from the center of impact in different stresses is placed in Appendix 1. Also, the individual diagrams can be found in the Appendix 1.

As far as the nominal stresses concerned, the case 0.6 mm shows a steadier and smoother response in the stresses. The case of 0.6 mm shows the best behavior in the last layer of the composite, whereas the case of 0.8 mm shows the best performance in the first layer. As far as the shear stresses concerned, the behavior in the last ply is the same for all the cases.

5.2 Effect of changing boundary conditions

In this investigation approach, 5 different boundary conditions have been tested with progressive relaxation techniques for the case of 0.2 mm gelcoat thickness. This case seems to have the worst behavior as far as the stresses concerned as presented in the previous analysis, thus it was chosen for further investigation. At first, the bottom is fully fixed and the four peripheral edges of the plate are fixed as well. This is supposed to be the most cumbersome type of boundary condition and will be referred

as case B in the following figures. The second stage is the simulation which has been described above with the bottom of the plate fixed and will be described as case A. The third, stage is the allowance of the rotational degrees of freedom in the x and y axis, which is case C. The fourth one, includes the third case and allows the freedom to translate in the x and y axis as well, which is case D. The final stage is more complex. This case uses the degrees of freedom in the bottom and the edges facing the x-axis are allowed to translate in the x-axis and rotate in the x and z axis and the edges facing the y-axis are allowed to translate in the y-axis and rotate in the x and z axis Amirzadeh, et al (2017), which will be referred as case E. The comparative results are presented in the following graphs.

The effective plastic strain and the maximum impact force show some level of small fluctuation. The waterhammer pressure does not present any differences.
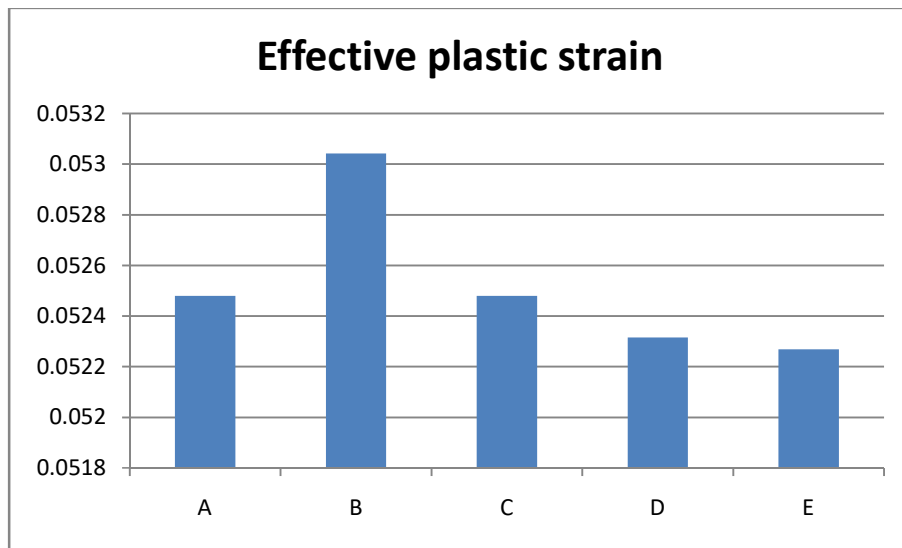
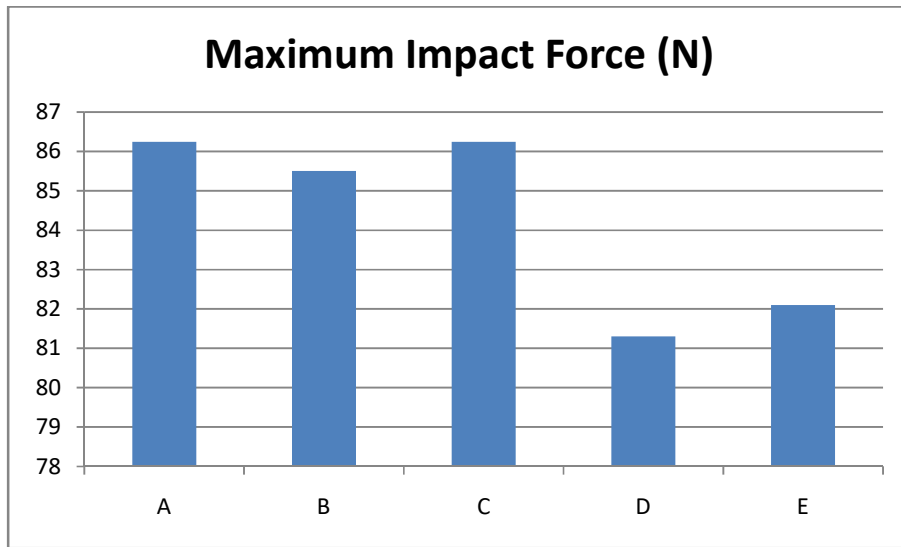**Figure 61:** Maximum effective plastic strain

Figure 62: Maximum impact force

The effective Von-Mises stresses and Tresca stresses are depicted in the following figures. Some differences can be found in the last ply of the composite, but in general they can be considered negligible.
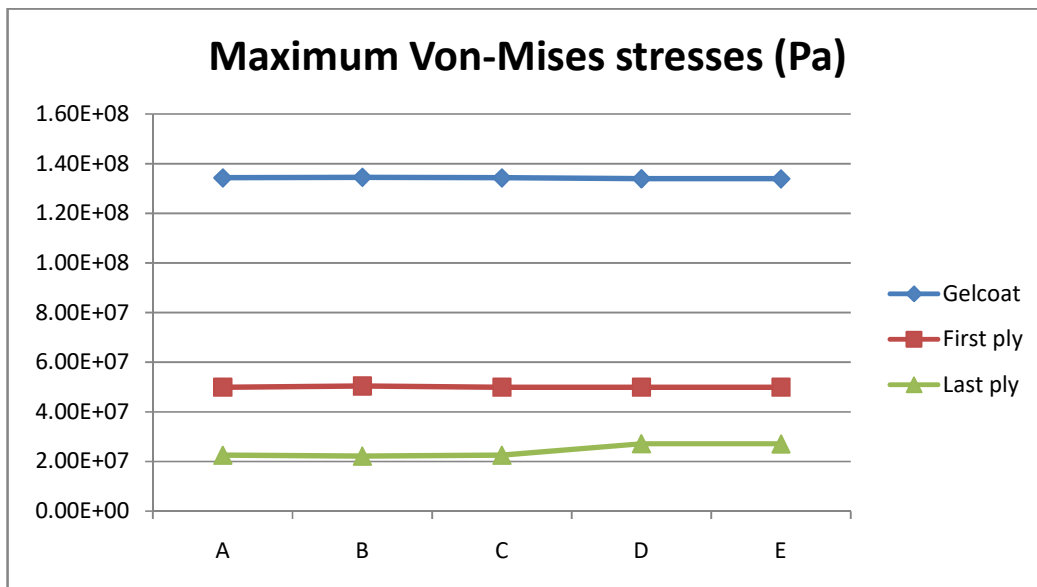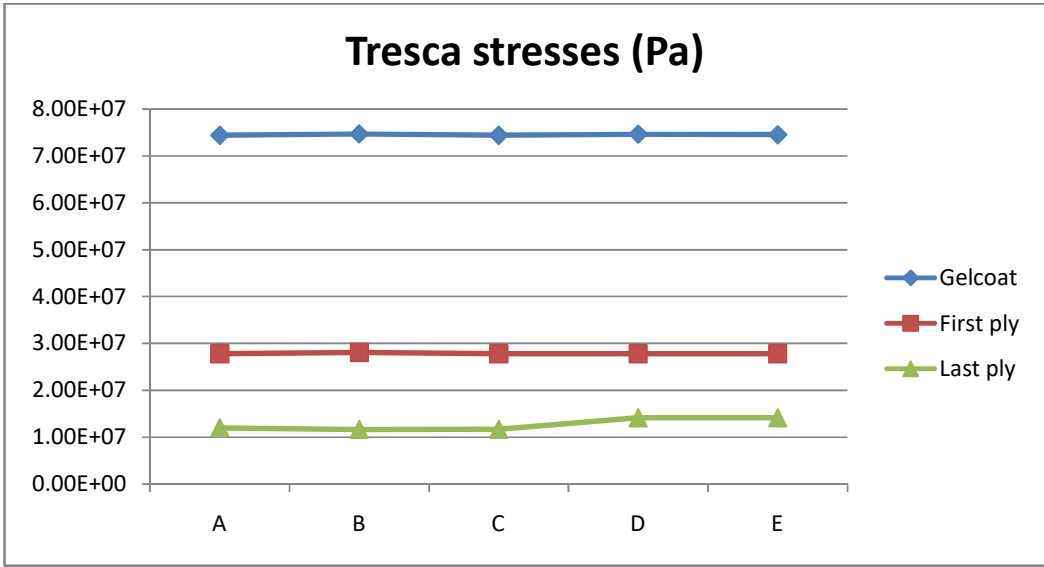

Figure 63: Maximum effective Von-Mises stresses

Figure 64: Maximum Tresca stresses

The kinetic energy across the different layers does not present any significant changes. The next figure represents the z-displacement of the different layers. The 4th case shows a different behavior since it has more degrees of freedom as it was anticipated.
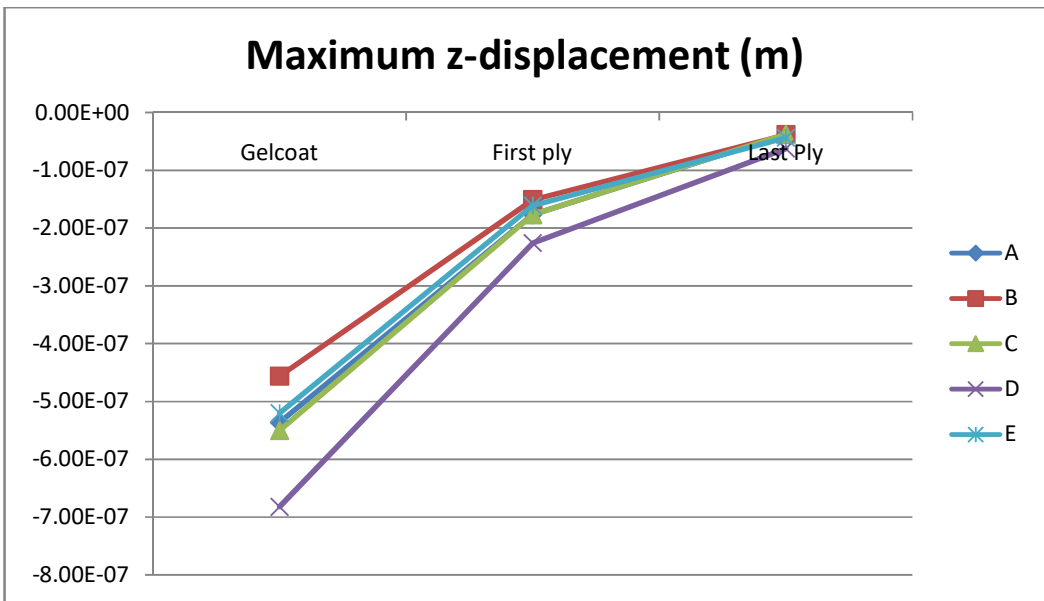
Figure 65: Maximum z-displacement across the layers

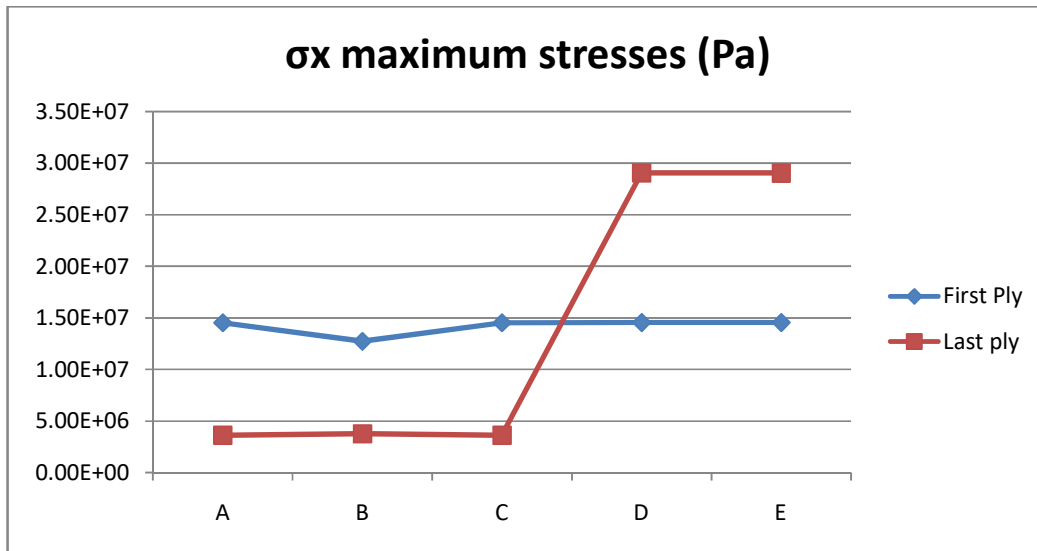The distribution of both maximum nominal and the shear stresses will be presented in the following figures.

σx maximum stresses (Pa)

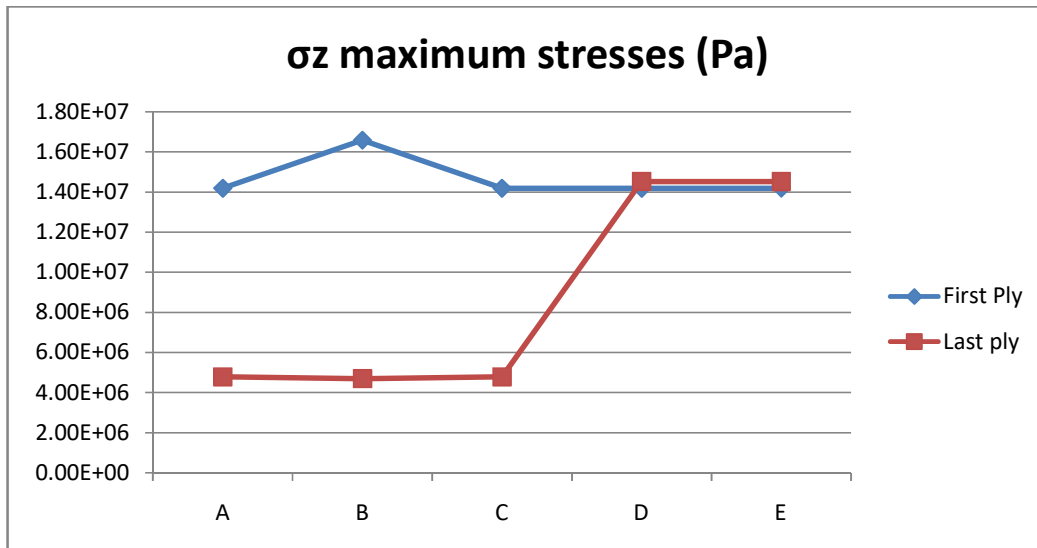

Figure 66: Maximum σ_x stresses

σz maximum stresses (Pa)

Figure 67: Maximum σ_z stresses

The σx and σz show a remarkable behavior in the last ply in the cases 4 and 5. Instead of gradual decrease in the stress field they present an increase, which can be explained by the next graph representing the distance from the center of impact.
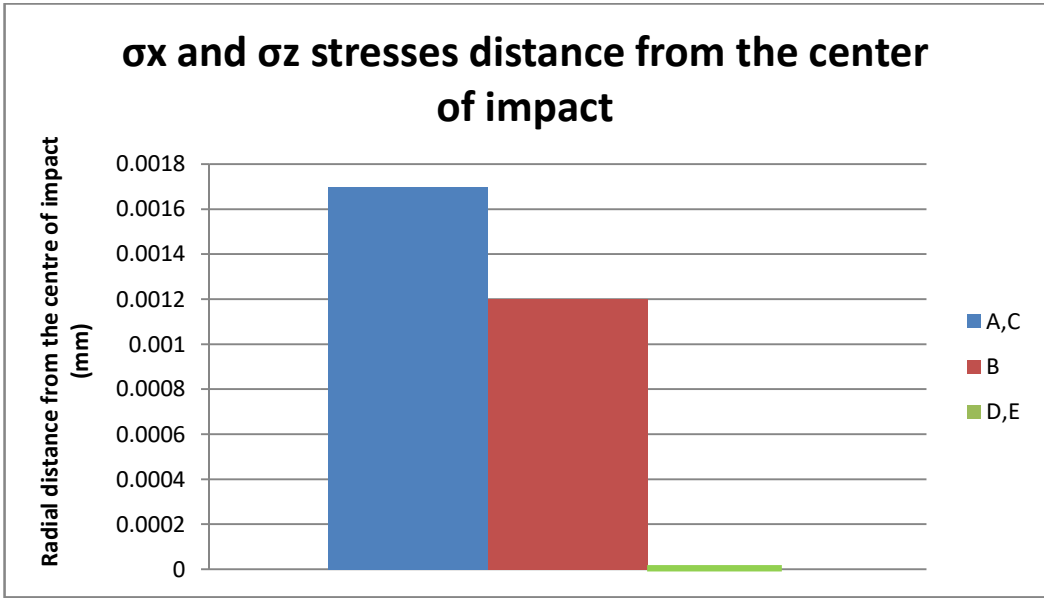
Figure 68: Distance from the centre of impact for nominal stresses

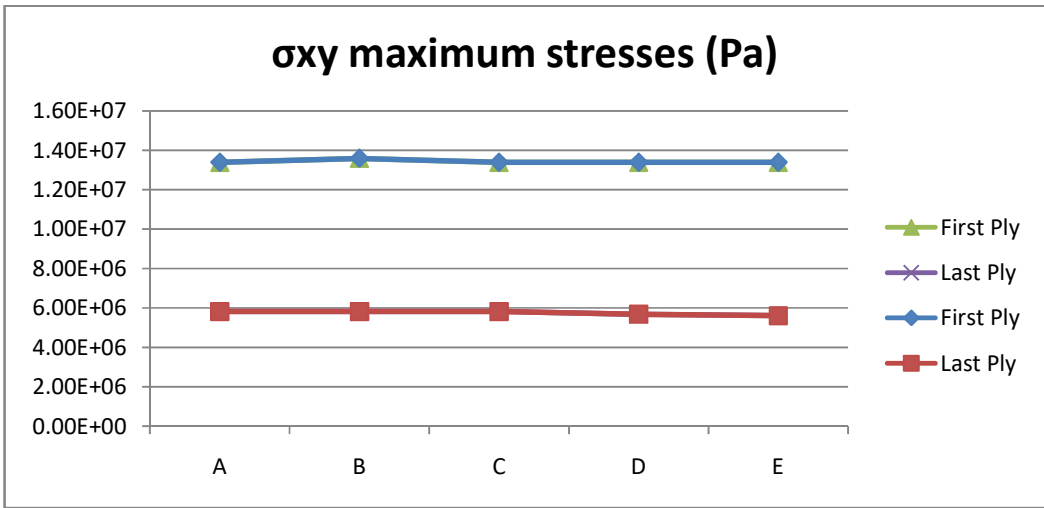This behavior does not seem to occur in the case of shear stresses.

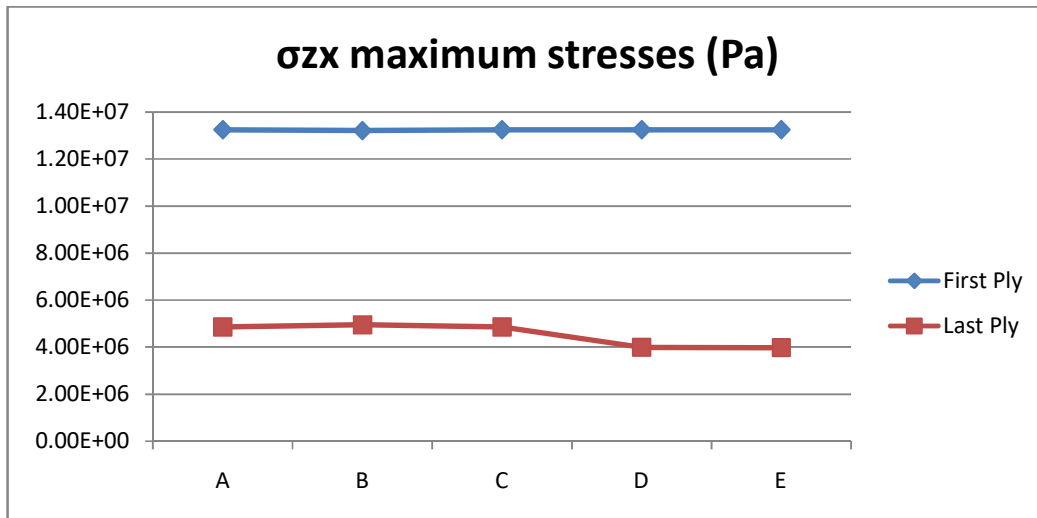**Figure 69:** Maximum σ_{xy} stresses

Figure 70: Maximum σ_{zx} stresses

In general, there are three individual groups according to the results acquired in this sub-chapter:

- Group 1: Case B
- Group 2: Case A and case C
- Group 3: case D and case E

The z-displacement response of the different layers along with some other figures is placed in Appendix 2.

As far as the damage threshold velocity concerns it was found that it was steady at 61 m/s regardless of the changes in the gelcoat thicknesses or the boundary conditions. The value was double-checked through equations (21) and (22). First of all the Rayleigh wave velocity had to be calculated via the use of material properties of the coating epoxy material, as being described in chapter 4. The result of equation (22) showed a Rayleigh wave velocity of 830 m/s. With this value and by changing the fracture toughness between 0.5, 1 and 1.5 MPa $\sqrt{m}$ and water's speed of sound at 1427 m/s at 5°C, the damage threshold velocities were determined and are presented in the following diagram. Through the following diagram and the result of the

simulations, the fracture toughness of Epoxy Epon E 862 is determined at 0.77 MPa$\sqrt{m}$, designated with red color.
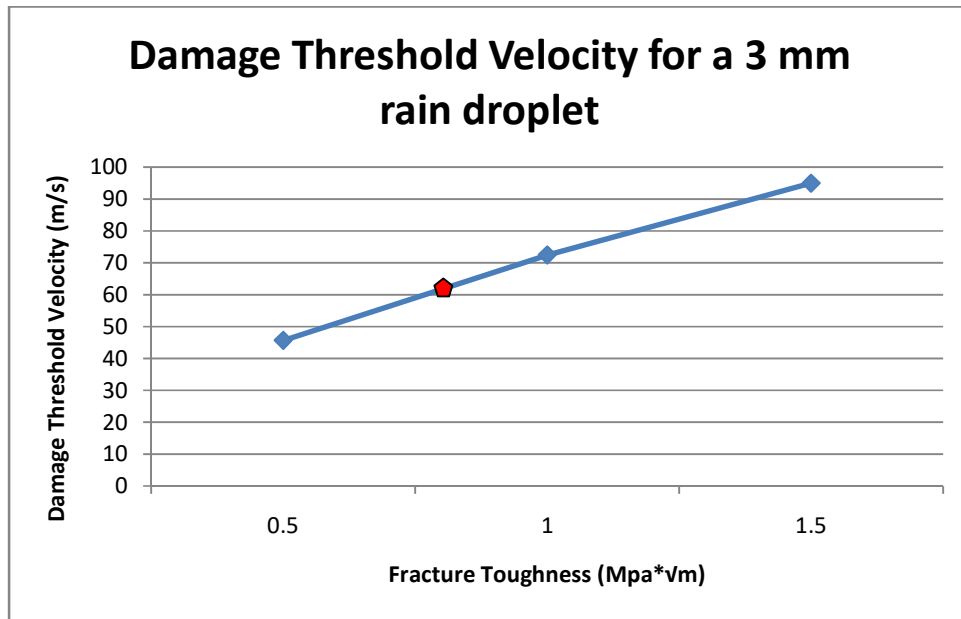

Figure 71: Damage Threshold Velocity Diagram

6. Concluding remarks

This chapter of the dissertation intends to present in a condensed form the conclusions and observations throughout this work. A part of this chapter will be dedicated to the discussion points concerning the results and the procedure. Also, the challenges that have been faced and the assumptions being made will be summarized. Moreover, further work points that have been considered interesting will be discussed along with the final conclusions.

6.1 Discussion

The intention of this research study concerned the investigation of erosion of offshore wind turbine blades. In an attempt to investigate on erosion which has been reported as a vital issue in wind turbine blades, rain as an aspect of erosion has been found to be severe for the following reasons. Firstly, UK is a country which experiences severe levels of precipitation every year; nonetheless it is a country that attains the highest numbers in installed capacity offshore. Also, rain is a factor that can be simulated via proper software and thus can be investigated in depth and tackled.

Worst case scenarios for both rain droplet sizes and impact velocities have been chosen for simulation. The variables of this thesis have been selected to be the variable gelcoat thicknesses with values being below, within and above the standard DNV-OS-J102 (Der Norske Veritas, 2010). Therefore, the cases of over excess and lack of gelcoat protection have been investigated. The effects of changing boundary conditions were examined with respect to periodical relaxation levels.

A validation model was created in an isotropic material so as to validate the results, which will allow the study to progress with the use of a composite structure. A correlation between the analytical expressions and the results of the software was attempted in accordance with the kinetic energy, the waterhammer pressure and the impact force.

The first common observation of the complex model concerned the damage threshold velocity which remained steady at 61 m/s independently of gelcoat thicknesses and changing boundary conditions. Based on equation (21) the damage threshold velocity has a value of 61 m/s indicating that the target's fracture toughness is 0.77 MPa $\sqrt{m}$ according to figure 66. This property was not assigned to the software since it was not reported by Littel, et al. (2008).

As far as the first approach concerned, the plastic strain occurs after 1μs in the cases of 0.4 mm, 0.6 mm and 0.8 mm compared to the case of 0.2 mm. This means that erosion takes place earlier in the case of 0.2 mm compared to the other cases. Also, for the case of 0.2 mm the waterhammer pressure elevates at the same levels not only during the onset of lateral jetting but also before and after. For the case of 0.8 mm effective plastic strain happens after the onset of lateral jetting.

As far as the stresses concerned the cases of 0.6 mm and 0.8 mm seem to have the lowest stress field and similar values. Nominal stresses for the case of 0.6 mm show a steadier and smoother response in the stress distribution. The case of 0.6 mm shows the best behavior in the last layer of the composite, whereas the case of 0.8 mm shows the best performance in the first layer. As far as the shear stresses concerned, the behavior in the last ply is the same for all the cases. Also, for the cases of 0.2 mm and 0.4 mm the divergence from the center of impact is lower compared to the 0.6 mm and 0.8 mm cases, which means that the damage is localized. The stresses created in the x and y directions seem to be the ones that are mostly affected by the changing gelcoat thickness resulting in higher values compared to the stresses in the z-direction.

The second part of the investigation study presented some interesting results in the case of stresses. The structure seemed to have some differences in the nominal stresses σ_x and σ_z but this was not the case in the shear stresses. The dominating stresses are the nominal ones with the shear ones being almost the same. Apart from this key finding the case of changing boundary conditions did not seem to change significantly the results.

In general the cases of 0.4 mm, 0.6 mm and 0.8 mm had a better behavior against the impact. As a result, for the materials being used in this study and the layup of the structure the cases of 0.4 mm and 0.6 mm seem to be the best, while the case of 0.8 mm is out of standards and induces on top extra costs and weight. Moreover, in the case of boundary conditions, the degrees of freedom should not exceed the threshold of two, in order to minimise the effect of nominal stresses and not exceed the order of magnitude. However, in such structures considering the rotation of the blades, the cases D and E seem to be more realistic, since out of plane movements or rotations are not allowed, which describes the engineering function of a sandwich structure.

This work presented an aspect of weakness of offshore wind turbines with the ambition to describe rain erosion which takes place. The specific materials used for this study confirmed the DNV Standard DNV-OS-J102 (Der Norske Veritas, 2010), concerning the gelcoat thickness to be between 0.3 mm and 0.6 mm. Also, the simplified model attempted to simulate the complex one, by applying different levels of relaxation in the boundary conditions. Moreover, the damage threshold velocity and the fracture toughness were identified with the assistance of both the software and the analytical expressions for epoxy EPON E 862.

6.2 Limitations

The challenges of this dissertation are located mainly in the lack of available information. Gelcoat epoxy materials used for coating protection are not commercially available. Therefore, the epoxy gelcoat material which has been used for the simulations may not be the exact case for offshore wind turbine protection. The lack of industry gelcoat materials made the search of epoxy properties a challenging issue itself.

Apart from the epoxy properties the next challenge was the determination of the structure layup. The layup differs between manufacturers, in an attempt for them to provide safety and reliability to the structure, different protection systems can be used for further reinforcement. Similarly, in this case the deficiency of manufacturing

materials data is a challenge and a meticulous investigation in the literature is required.

The time of simulations was another factor that affected significantly the escalation of this study. Each simulation required in average 1 hour and 20 minutes and thus some aspects were not altered or examined in depth if they could have modified the results. Therefore, the computational cost was found to be one important aspect in such engineering problems.

6.3 Future recommendations

This study is a preliminary investigation on rain erosion phenomena in offshore wind turbines. More study is needed in the field of the interface zone between the different layers of the structure. For instance, the interlaminar failure stresses have not been defined due to lack of information. Moreover, a study on the viscous damping between the different layers of the structure in needed in order to define more accurately the failure mechanisms. Also, the substrate was steady and not rotating which might induced some simplifications to the model. Furthermore, a study on the effect of the different integration methods and the fluctuation of the results can be another case. An experimental validation of the results is required to recognise any non-linearities and factors that drive the problem and have not been identified via the software. Last but not least, a financial analysis is always a good practice depending on the material properties and the boundary conditions of the structure, in order to determine the cost-effective solution taking into account the lifetime of such projects in hostile environments.

6.4 Conclusions

The goals and ambitions of this dissertation have been the investigation of erosion in depth in the case of offshore wind turbines. By choosing the blades of the structure for further analysis and rain as a wear mechanism capable for erosion initiation, some important remarks derived from various simulations. First of all, the damage threshold velocity has the same value independently of the boundary conditions or the changing

coating protection thickness. Also, nominal stresses seem to be more susceptible to changes in the boundary conditions of such engineering structures. Furthermore, the effective Von-Mises stresses have higher values compared to the Tresca criterion for both approaches in the first two layers of the structure; nonetheless this situation changes in the last ply of the structure, where shear stresses dominate over the nominal. Moreover, the value of fracture toughness was calculated with the use of both the software and the mathematical equations. The changing boundary conditions shed some light in the response of the structure, revealing the dominance of nominal stresses over the shear ones. A comparison between the different cases was attempted in order to simulate the realistic response in the best possible way, revealing that cases D and E are most appropriate as boundary conditions to be applied. The thickness of 0.2 mm should be avoided in the case of such structure with the simulated material properties, since plasticity is created before, during and after the onset of lateral jetting. This in turn creates a higher stress field worsening the condition of the structure. The cases of 0.6 mm and 0.8 mm have the best behavior concerning the nominal and shear stresses. The case of 0.4 mm presents some weaknesses mainly in the first ply of the composite, but with a different layup this behavior may change. However, the addition of gelcoat material leads to higher costs and weight to the structure which in turns indicate the importance of a financial analysis for a reliable conclusion on that choice.

7. References

Achenbach, J.D., 1973. *Wave Propagation In Elastic Solids.* Amsterdam: Elsevier Science Publishers B.V.

ACT Blade, 2015. *Eradicating erosion*. [online] Available at: http://actblade.com/eradicating-erosion/ [Accessed at 7 August 2017]

Adler, W.F., 1995. Waterdrop impact modeling. *Wear*, Elsevier Ltd, 186-187 (1995), pp.341-351

Ahmad, M., Casey, M. & Sürken, N., 2009, Experimental assessment of droplet impact erosion resistance of steam turbine blade materials. *Wear*, [e-journal] 267 (2009), pp.1605-1618. 10.1016/j.wear.2009.06.012

Amirzadeh, B., Louhghalam, A., Raessi, M. & Tootkaboni, M., 2017, A computational framework for the analysis of rain-induced erosion in wind turbine blades, part I: Stochastic rain texture model and drop impact simulations. *Journal of Wind Engineering & Industrial Aerodynamics*, [e-journal] 163 (2017), pp.33-43 http://dx.doi.org/10.1016/j.jweia.2016.12.006

Amirzadeh, B., Louhghalam, A., Raessi, M. & Tootkaboni, M., 2017, A computational framework for the analysis of rain-induced erosion in wind turbine blades, part II: Drop impact-induced stresses and blade coating fatigue life. *Journal of Wind Engineering & Industrial Aerodynamics*, [e-journal] 163 (2017), pp.44-54 http://dx.doi.org/10.1016/j.jweia.2016.12.007

ANSYS Inc., 2017, *LS-DYNA*. [online] Available at:http://www.ANSYS.com/products/structures/ANSYS-LS-DYNA [Accessed 12 July 2017]

Griffith D.T. and Ashwill, T.D., 2011. The Sandia 100 meter All glass baseline wind turbine blade: SNL 100-00, SAND 2011-3779. [pdf]. California:Sandia National Laboratories.Available at: http://energy.sandia.gov/wp-content/gallery/uploads/SAND2011-3779.pdf [Accessed at 22 August 2017]

ASM Aerospace Specification Metals Inc., 2000. *Aluminum Standards and Data*. [online] Available at: http://asm.matweb.com/search/SpecificMaterial.asp?bassnum=ma6061t6 [Accessed 20 Jul. 2017]

ASTM, 2010. *ASTM G73-10 Standard test method for liquid impingement erosion using rotating apparatus*. [online] Available at: https://www.astm.org/Standards/G73.htm [Accessed 17 August 2017]

Aymerich, F., 2012. Composite materials forwind turbine blades: issues and challenges. SYSWIND Summer School. [pdf] University of Patras and University of Cagliari . Available at: http://people.unica.it/francescoaymerich/files/2013/11/Composite-Materials-for-Wind-Turbine-Blades.pdf [Accessed at 22 August 2017]

Azevedo, C.R.F. & Sinátora, A., 2009. Erosion-fatigue of steam turbine blades. *Engineering Failure Analysis*, [e-journal] 16 (2009), pp.2290-303. 10.1016/j.engfailanal.2009.03.007

Best , A.C., 1950. The size distribution of raindrops. *Royal Meteorological Society*, [e-journal] 76(327), pp.16-36. 10.1002/qj.49707632704

Bir, G. and Migliore, P., 2004. Preliminary Structural Design of composite blades for two and three-blade rotors NREL/TP-500-31486. [pdf]. Colorado:National Renewable Energy Laboratory. Available at: https://www.nrel.gov/docs/fy04osti/31486.pdf [Accessed at 22 August 2017]

Bower, A.F., 2008. Constitutive Models- Relations between stress and strain, *Applied Mechanics of Solids,* [online] Avalable at: http://solidmechanics.org/text/Chapter3_2/Chapter3_2.htm [Accessed at 20 July 2017]

British Standards, 2005. BS EN 61400-1:2005 Wind turbines — Part 1: Design requirements. [pdf] London: University College London. Available at: http://www.homepages.ucl.ac.uk/~uceseug/Fluids2/Wind_Turbines/Codes_and_Manuals/BS_EN_61400-1_2005.pdf [Accessed at 22 August 2017]

British Standards, 2009. BS EN 61400-3:2009 Wind Turbines-Part 3:Design requirements for offshore wind turbines. [pdf] London: University College London. Available at: http://www.homepages.ucl.ac.uk/~uceseug/Fluids2/Wind_Turbines/Codes_and_Manuals/BS_EN_61400-3_2009.pdf [Accessed at 22 August 2017]

Bureau lesswatts, 2015. *Je suis (ausis) contre*, [online] Avalable at: http://bureaulesswatts.nl/2015/11/29/je-suis-aussi-contre/ [Accessed at 5 August 2017]

BVG Associates, 2011. Offshore wind: Opportunities for the composites industry, [pdf] Crown Estate, Siemens. Available at: https://www.thecrownestate.co.uk/media/5448/ei-km-in-sc-supply-062011-offshore-wind-opportunities-for-the-composites-industry.pdf [Accessed at 22 August 2017]

Cao, W., Xie Y. & Tan Z., 2012. *Wind turbine generator technologies*. Advances in Wind Power. [online] Avalable at: https://www.intechopen.com/books/advances-in-wind-power/wind-turbine-generator-technologies [Accessed at 5 August 2017]

Castorrini, A., Corsini, A., Rispoli, F., Venturini, P., Takizawa, K. and Tezduyar, T.E., 2016. Computational analysis of wind-turbine blade rain erosion, *Computers and Fluids*, [e-journal] 141 (2016), pp.175-183 http://dx.doi.org/10.1016/j.compfluid.2016.08.013

Catapult Offshore Renewable Energy, 2015. *Catapult launches joint industry project to tackle turbine blade erosion*. [online] Available at: https://ore.catapult.org.uk/press-release/catapult-launches-joint-industry-project-to-tackle-turbine-blade-erosion/ [Accessed at 7 August 2017]

Clark, J. and Kelly, N., 2016. *Wind Energy*, ME909/ME922/ME927: Energy Resources and Policy, University of Strathclyde. Available at: http://www.esru.strath.ac.uk/Courseware/Class-ME909-ME922-ME927/Presentations/wind.pdf [Accessed 24 August 2017]

Comission Directive 2009/28/EC of the European Parliament and of the Council of 23 April 2009, *Official Journal of the European Union*

Cortés, E., Sánchez, F., Domenech, L., Olivares, A., Young, T.M., O'Caroll A. and Chinesta, F., 2017. Manufacturing issues which affect coating erosion performance in wind turbine blades. [online], Available at: https://www.researchgate.net/publication/313768435_Manufacturing_issues_which_affect_coating_erosion_performance_in_wind_turbine_blades [Accessed at 22 August 2017]

Dalili, N., Edrisy, A. & Carriveau R., 2009. A review of surface engineering issues critical to wind turbine performance. *Renewable and Sustainable Energy Reviews*, [e-journal] 13 (2009), pp.428-438. 10.1016/j.rser.2007.11.009

Dear, J.P. and Field, J.E. 1988. High-speed photography of surface geometry effects in liquid/solid impact. *Journal of Applied Physics 63*, [e-journal] 1015 (1998). 10.1063/1.340000

Der Norske Veritas, 2010. Offshore Standard DNV-OS-J102.Design and manufacture of wind turbine blades, offshore and onshore wind turbines. [pdf] Der Norske Veritas. Available at: https://rules.dnvgl.com/docs/pdf/DNV/codes/docs/2010-11/DS-J102.pdf [Accessed at 22 August 2017]

Der Norske Veritas, 2014. DNV-OS-J101 Design of Offshore Wind Turbine Structures. [pdf] Der Norske Veritas. Available at: https://rules.dnvgl.com/docs/pdf/DNV/codes/docs/2014-05/Os-J101.pdf [Accessed at 22 August 2017]

EITobgy, M.S., Ng, E. and Elbestawi, M.A, 2005. Finite element modeling of erosive wear. *Machine tools and manufactures*, [e-journal] 45 (2005), pp.1337-1346. 10.1016/j.ijmachtools.2005.01.007

Environmental and Energy Study Institute, 2010. Offshore Wind Energy.[pdf] Environmental and Energy Study Institute. Available at: http://www.eesi.org/files/offshore_wind_101310.pdf [Accessed at 22 August 2017]

Evans, A.G., Gulden, M.E. & Rosenblatt M., 1976. Impact damage in brittle materials in the elastic-plastic response regime. *Rockwell International Science Center,* [e-journal] 361, pp. 343-365. 10.1098/rspa.1978.0106

Global Wind Energy Council, 2016. Offshore Wind.[pdf] GWEC. Available at: http://www.gwec.net/wp-content/uploads/2017/05/Global-Offshore-2016-and-Beyond.pdf [Accessed at 22 August 2017]

Gohardani, O., 2011. *The influence of erosion and wear on the accretion and adhesion of ice for nano reinforced polymeric composites used in aeronautics*, Ph.D. Cranfield University, Cranfield

Gohardani, O., 2011. Impact of erosion testing aspects on current and future flight conditions. *Progress in Aerospace Sciences*, [e-journal] 47 (2011), pp.280-303. 10.1016/j.paerosci.2011.04.001

Greaves, P., 2016. Design of offshore wind turbine blades, *Offshore Wind Farms*, [e-journal] 2016, pp. 105-135, Ch.6 http://dx.doi.org/10.1016/B978-0-08-100779-2.00006-4

Green Investment Bank, Renewable UK, The Crown Estate & UKTI's Offshore wind team, 2015. UK Offshore Wind: Opportunities for trade and investment.[pdf] Crown. Available at:

https://www.gov.uk/government/uploads/system/uploads/attachment_data/file/437077/Offshore_Wind.pdf [Accessed at 22 August 2017]

Hassan, G., 2013. A Guide to UK Offshore Wind Operations and Maintenance.[pdf]. Scottish Enterprise and the Crown Estate. Available at: https://www.thecrownestate.co.uk/media/5419/ei-km-in-om-om-062013-guide-to-uk-offshore-wind-operations-and-maintenance.pdf [Accessed at 22 August 2017]

Hetcel, S. 2014. *Reliability Centered Maintenance: For wind turbine blades*. North Americal Clean Energy. [online] Available at:
http://www.nacleanenergy.com/articles/17870/reliability-centered-maintenance-for-wind-turbine-blades [Accessed at 5 August 2017]

Hu, W., Choi, K.K., Zhupanska, O. and Buchholz J.H.J., 2015. Integrating Variable Wind load, aerodynamic and structural analyses towards accurate fatigue life prediction in composite wind turbine blades. *Structural and Multidisciplinary Optimization,* Springer, 53 (3), pp.375-394

Imeson, A.C., Vis, R. & de Water, E., 1981. The measurement of water-drop impact forces with a piezo-electric transducer. *Catena*, [e-journal] 8 (1981), pp.83-96. 10.1016/S0341-8162(81)80006-9

Ingenia, 2017. *Futureproofing the next generation of wind turbine blades*. Wealth Creation. [online] Available at:
http://www.ingenia.org.uk/Content/ingenia/issues/issue70/futureproofing-the-next-generation-of-wind-turbines-blades.pdf [Accessed at 7 August 2017]

International Renewable Energy Agency,2016. Innovation Outlook: Offshore Wind. [pdf] Irena. Available at: https://www.irena.org/DocumentDownloads/Publications/IRENA_Innovation_Outlook_Offshore_Wind_2016.pdf [Accessed at 22 August 2017]

Jonkman J., Butterfield, S., Musial, W. and Scott, G., 2009. Definition of a 5MW-reference wind turbine for offshore system development, NREL/TP-500-38060.[pdf]. National Renewable Energy Laboratory. Available at: https://www.nrel.gov/docs/fy09osti/38060.pdf [Accessed at 22 August 2017]

Karmouch, R. and Ross G.G., 2010. Superhydrophobic wind turbine bladesurfaces obtained by a simple deposition of silica nanoparticles embedded in epoxy, *Applied Surface Science*, [e-journal] 257 (2010), pp.665-669. 10.1016/j.apsusc.2010.07.041

Kaw, A.K., 2006. *Mechanics of Composite Materials*, Boca Raton: Taylor & Francis Group, 473

Keegan, M.H., 2014. *Wind Turbine Blade Leading Edge Erosion: An investigation of rain droplet and hailstone impact induced damage mechanisms*, Ph.D, University of Strathclyde, Glasgow

Keegan, M.H., Nash, D.H. & Stack, M., 2012. MODELLING RAIN DROP IMPACT OF OFFSHORE WIND TURBINE BLADES. ASME. Paper presented at TURBO EXPO 2012 GT2012-69175, Copenhagen, Denmark, 11/05/2012-15/05/2012

Keegan, M.H., Nash, D.H. & Stack, M., 2013. On erosion issues associated with the leading edge of wind turbine blades. *Journal of Physics D: Applied Physics.*[e-journal] 46 (383001), vol.38. https://doi.org/10.1088/0022-3727/46/38/383001

Keegan, M.H., Nash, D.H. & Stack, M., 2013. Numerical modelling of hailstone impact on the leading edge of a wind turbine blade. Paper presented at EWEA Annual Event 2013, Vienna, Austria, 04/02/2013-07/02/2013

Khlystov, N., Lizardo, D., Matsushita, K. and Zheng, J., 2013. Uniaxial Tension and Compression Testing of Materials, 3.032 Lab Report. [pdf]. Available at: file:///D:/downloads/UniaxialTestingLabReportV6%20(1).pdf [Accessed at 22 August 2017]

Kjærside Storm, B., 2013. Surface protection and coatings for wind turbine rotor blades. *Advances in Wind Turbine Blade Design and Materials*, Ch.12. https://doi.org/10.1533/9780857097286.3.387

Kubilay, A., Derome, D., Blocken, B. & Carmeliet, J., 2013. CFD simulation and validation of wind-driven rain on a building facade with an Eulerian multiphase model. Building and Environment, [e-journal] 61 (2013), pp.69-81. http://dx.doi.org/10.1016/j.buildenv.2012.12.005

Li, R., Ninokata, H. and Mori, M., 2011. A numerical study of impact force caused by liquid droplet impingement onto a rigid wall. *Progress in Nuclear Energy*, [e-journal] 53 (2011), pp.881-885 doi:10.1016/j.pnucene.2011.03.002

Littel, J.D., Ruggeri, C.R., Goldberg, R.K., Roberts, G.D., Arnold, W.A. and Binienda, W.K., 2008. Measurement of epoxy resin tension, compression and shear stress-strain curves over a wide range of strain rates using small test specimens. *Journal of Aerospace Engineering*, [e-journal] 21 (2008), pp.162-173 10.1061/_ASCE_0893-1321_2008_21:3_162_

Liu, M.B. and Liu, G.R., 2010. Smoother particle hydrodynamics (SPH):an overview and recent developments. *Arch Comput Methods Eng*, [e-journal] 17 (2010), pp.25-76. 10.1007/s11831-010-9040-7

Livermore Software Technology Corporation, 2012. *About LS-PrePost*. [online] Available at: http://www.lstc.com/lspp/ [Accessed 08/07/2017]

Livermore Software Technology Corporation, 2014. LS-DYNA Keyword User's Manual Volume I. California: Livermore Software Technology Corporation, rev.5471

Livermore Software Technology Corporation, 2014. LS-DYNA Keyword User's Manual Volume II Material Models. California: Livermore Software Technology Corporation, rev.5442

Megavind, 2016. Strategy for Extending the Useful Lifetime of a Wind Turbine. [pdf] Secretariat : Danish Wind Industry Association. Available at: https://ens.dk/sites/ens.dk/files/Forskning_og_udvikling/strategy_for_extending_the_useful_lifetime_of_a_wind_turbine_2016.pdf [Accessed at 22 August 2017]

Menna, C., Asprone, D., Caprino, G., Lopresto, V. and Prota A., 2011. Numerical Simulation of Impact tests on GFRP composite laminates. *International Journal of Impact Engineering*, [e-journal] 38 (2011), pp.677-685. 10.1016/j.ijimpeng.2011.03.003

Met Office, 2015. *How much does it rain in the UK?*. Crown Copyright. [online] Available at: http://www.metoffice.gov.uk/learning/rain/how-much-does-it-rain-in-the-uk [Accessed at 5 August 2017]

Nayfeh, A.H., 1995. *Wave propagation in layered anisotropic media*, Amsterdam: Elsevier Science Publishers B.V.

Nearing, M.A., Bradford, J.M. & Holtz R.D., 1986. Measurement of force vs. Time relations for waterdrop impact. *Soil Science Society of America Journal.* [e-journal] 50(6). 10.2136/sssaj1986.03615995005000060030x

Nijssen, R.P.L. & Brøndsted, P., 2013. Fatigue as a design driver for composite wind turbine blades. *Advances in Wind Turbine Blade Design and Materials*, [e-journal] 6 (2013), pp.175-209. 10.1533/9780857097286.2.175

Nijssen, R. & De Winkel, G.D., 2016. Developments in materials for offshore wind turbine blades. *Offshore Wind Farms*, [e-journal] 5 (2016), pp.85-104. http://dx.doi.org/10.1016/B978-0-08-100779-2.00005-2

Nijssen, R.,de Vinkel, G.D. and Peeringa, J.M., 2007. UPWIND WMC5MW laminate lay-out of reference blade for WP 3. [pdf] Netherlands:Upwind and European Commission. Available at: https://www.wmc.eu/pdf/UPWIND%20ref%20blade%20laminate%20layout_revision%201.pdf [Accessed at 22 August 2017]

Predictive Engineering, 2017. LS-DYNA Analysis for Structural Mechanics. [pdf] Predictive Engineering. Available at: http://www.predictiveengineering.com/sites/default/files/LS-DYNA-Analysis-for-Structural-Mechanics-2017-Example-Note-Set-(Partial-Set-for-Interested-Students).pdf [Accessed at 22 August 2017]

Rempel, L., 2012. Rotor blade leading edge erosion-real life experiences, Wind Systems Magazine. [online] Available at: http://www.windsystemsmag.com/article/detail/426/rotor-blade-leading--edge-erosion--real--life-experiences [Accessed at 24 August 2017]

Rosato, D., Gamesa Corporation Technology and Sandia National Laboratories, n.d. *Fast moving material advances in wind energy*, [online] Available at: http://www.multibriefs.com/briefs/exclusive/plastics_wind_energy_2.html#.WYYKx4g19Pa [Accessed at 5 August 2017]

Salman, H.A. & Yıldırım, R.O., 2011. Investigation of rain erosion on a brittle material by means of numerical simulation. *Journal of Defense Modeling and Simulation: Applications*, [e-journal] 9(4), pp.327-34. 10.1177/1548512911411330

Sareen, A., Sapre, C.A. & Selig, M.S., 2013. Effects of leading edge erosion on wind turbine blade performance. *Wind Energy*, [e-journal] 17 (2013), pp.1531-1542 10.1002/we.1649

Sayer, F., Bürkner, F., Buchholz, B., Strobel, M., van Wingerde, A.M., Busmann, H.D. and Seifert H., 2013. Influence of a wind turbine service life on the mechanical properties of the material and the blade. *Wind Energy*, [e-journal] 16 (2013), pp.163-174. 10.1002/we.536

Shadloo, M.S., Oger, G. & Le Touze D., 2016. Smoothed particle hydrodynamics method for fluid flows, towards industrial applications: motivations, current state and challenge. *Computers and Fluids*, [e-journal] 136 (2016), pp. 11-34. http://dx.doi.org/10.1016/j.compfluid.2016.05.029

Siddons, C., Macleod, C., Yang, L. & Stack, M., 2015. An experimental approach to analysing rain droplet impingement on wind turbine blade materials, Paper presented at EWEA 2015 Annual Event, Paris, France, 17/11/2015-20/11/2015

Slot, H.M., Gelinck, E.R.M., Rentrop, C. & Van der Heide E., 2015. Leading edge erosion of coated wind turbine blades:Review of coated wind turbine life models. *Renewable Energy*, [e-journal] 80 (2015),pp. 837-848. http://dx.doi.org/10.1016/j.renene.2015.02.036

Sykes, B., 2016. The roadmap to 2020 and beyond: is offshore wind on track to drive costs down, local content up and cut carbon?. [pdf] Glasgow: All Energy 2016. Available at: https://www.all-energy.co.uk/RXUK/RXUK_All-Energy/2016/Presentations%202016/Offshore%20Wind%201/Benj%20Sykes%20UPDATED.pdf?v=635993526284380223 [Accessed at 22 August 2017]

Tavner, P., 2012. Offshore Wind Turbines Reliability, availability and maintenance. London:The Institution of Engineering and Technology. IET Renewable Energy Series 13

The Scottish Government, 2017. Scottish Energy Strategy: The future of energy in Scotland. . [pdf] Edinburgh:APS Group Scotland. Available at: http://www.gov.scot/Resource/0051/00513466.pdf [Accessed at 22 August 2017]

The Crown Estate, 2016. Offshore wind operational report.[pdf] London:Crown. Available at: https://www.thecrownestate.co.uk/media/1050888/operationalwindreport2017_final.pdf [Accessed at 22 August 2017]

The Crown Estate, 2012. Offshore wind cost reduction pathways study. [pdf] London:The Institution of engineering and technology. Available at: https://www.thecrownestate.co.uk/media/5493/ei-offshore-wind-cost-reduction-pathways-study.pdf [Accessed at 22 August 2017]

The Mathworks Inc., 2017. *Matlab*. [online] Available at: https://www.mathworks.com/products/matlab.html [Accessed at 24 August 2017]

The Scottish Government, 2011. 2020 Routemap for Renewable Energy in Scotland. [pdf] Edinburgh:APS Group Scotland. Available at: http://www.hi-energy.org.uk/Downloads/General%20Documents/2020%20Routemap%20for%20Renewable%20Energy%20in%20Scotland%20110630.pdf [Accessed at 22 August 2017]

The Scottish Government, 2009. Climate Change (Scotland) Act 2009 (asp 12).Crown

Thomson, R.C. & Harrison, G.P., 2015. Life Cycle Costs and Carbon Emissions of Offshore Wind Power.[pdf] University of Edinburgh. Available at: http://www.climatexchange.org.uk/files/4014/3325/2377/Main_Report_-_Life_Cycle_Costs_and_Carbon_Emissions_of_Offshore_Wind_Power.pdf [Accessed at 22 August 2017]

Troedsson, M., n.d. Blade inspection Maintenance regime offshore. [pdf]. PES Wind. Available at: http://cdn.pes.eu.com/assets/misc_dec/macteen-consulting-edpdf-811218578346.pdf [Accessed at 22 August 2017]

Unfccc, 2015. ADOPTION OF THE PARIS AGREEMENT, [online] Available at: https://unfccc.int/resource/docs/2015/cop21/eng/l09r01.pdf [Accessed at 22 August 2017]

Unfcc, 1998. Kyoto Protocol to the United Nations Framework convention on climate change, [online] Available at: https://unfccc.int/resource/docs/convkp/kpeng.pdf [Accessed at 22 August 2017]

University of Cambridge, 2002. *Specific stiffness-specific strength*. [online] Available at: http://www-materials.eng.cam.ac.uk/mpsite/interactive_charts/spec-spec/basic.html [Accessed at 5 August 2017]

U.S. Department of energy, 2014. 2014 Wind energy technology.[pdf] Wind and Water Power Technologies Office. Available at: https://www.energy.gov/sites/prod/files/2014/06/f16/eere_wpp_2014_peer_review_DistributedWind.pdf [Accessed at 22 August 2017]

Valaker, E.A., Armada, S. & Wilson, S., 2015. Droplet erosion protection coatings for offshore wind turbine blades. *In Energy Procedia*, [e-journal] 80 (2015), pp.263-275 10.1016/j.egypro.2015.11.430

Yarraparedy, E. and Kovacevic, R., 2007. Numerical Simulation and characterization of slurry erosion of laser chadded surfaces by using failure analysis approach. Journal of *Failure analysis and Prevention,* [e-journal] 7 (2007), pp. 467-474. 10.1007/s11668-007-9083-8

Zahavi, J., Nadiv, S. & Schmitt Jr., G.F., 1981. Indirect damage in composite materials due to raindrop impact. *Wear*, Lausanne:Elsevier Sequoia S.A., 72 (1981), pp.305-313

Zhang, S., Dam-Johansen, K., Nørkjær, S., Bernad Jr., P.L. and Kiil S., 2015. Erosion of wind turbine blade coatings - Design and analysis of jet-based laboratory equipment for performance evaluation. *Progress in Organic Coatings*, [e-journal] 78 (2015), pp.103-115. http://dx.doi.org/10.1016/j.porgcoat.2014.09.016

Zhang, S., Kiil, S., Dam-Johansen, K. and Bernad Jr., P.L., 2014. Accelerated rain erosion of wind turbine blade coatings, Ph.D, Dannmarks Tekniske Universitet, Lyngby

Wind Trust, 2013. Designing the wind turbine of the future. [pdf] Wind Trust. Available   at: http://www.greenovate-europe.eu/sites/default/files/publications/Windtrust_booklet_Final_web.pdf [Accessed at 22 August 2017]

Wood, K., 2011. *Blade repair: Closing the maintenance gap*. [online] Available at: http://www.compositesworld.com/articles/blade-repair-closing-the-maintenance-gap [Accessed 7 Jul. 2017]

3M ™, 2016. Building in productivity.From the ground up. [pdf] USA:Renewable Energy Division. Available at: http://multimedia.3m.com/mws/media/1226740O/3m-wind-full-line-brochure.pdf [Accessed at 22 August 2017]
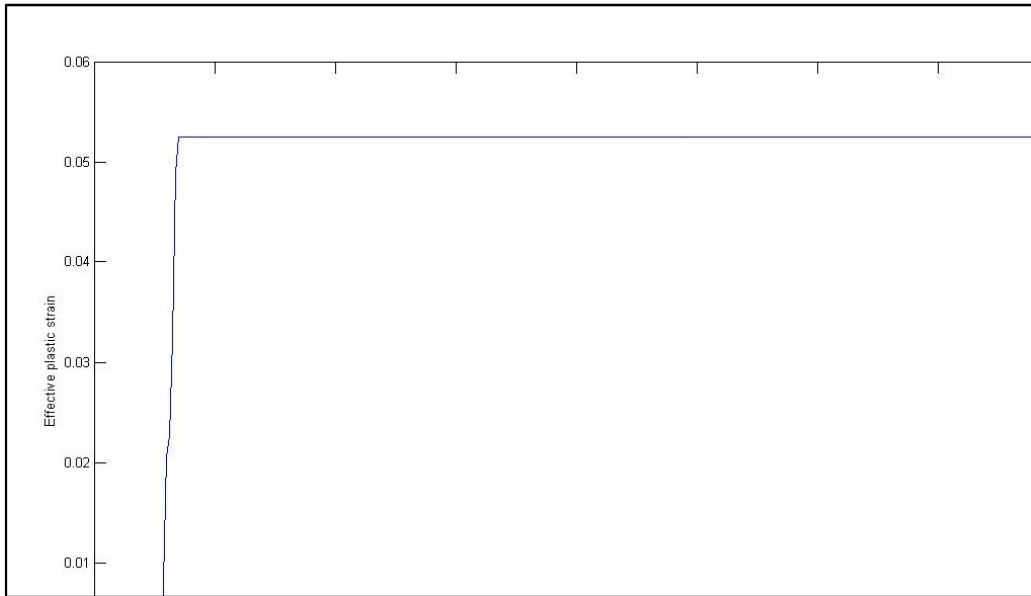
Figure 72: Effective Plastic Strain at 0.2 mm
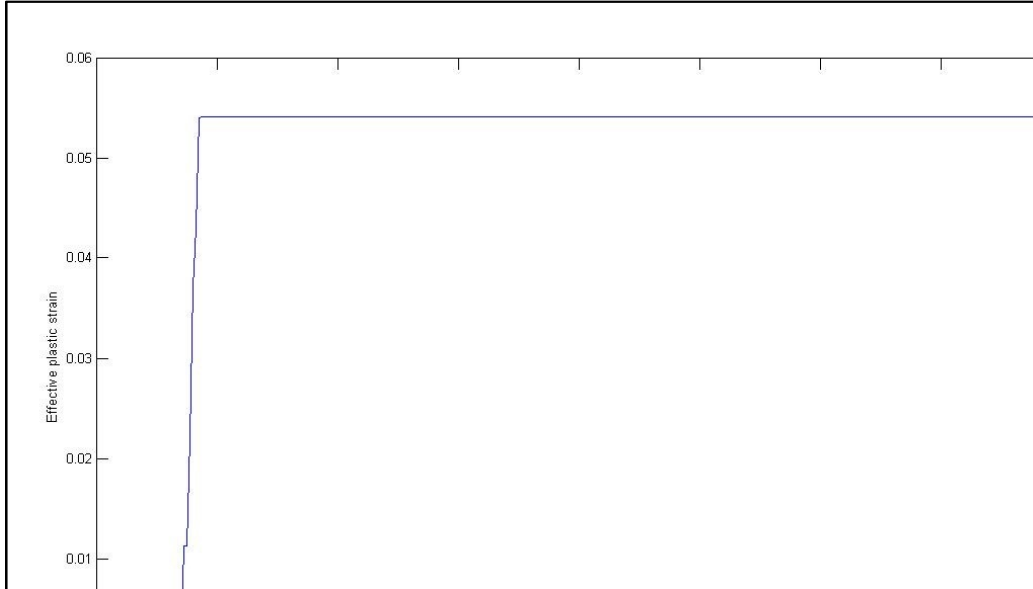
Figure 73: Effective Plastic Strain at 0.4 mm
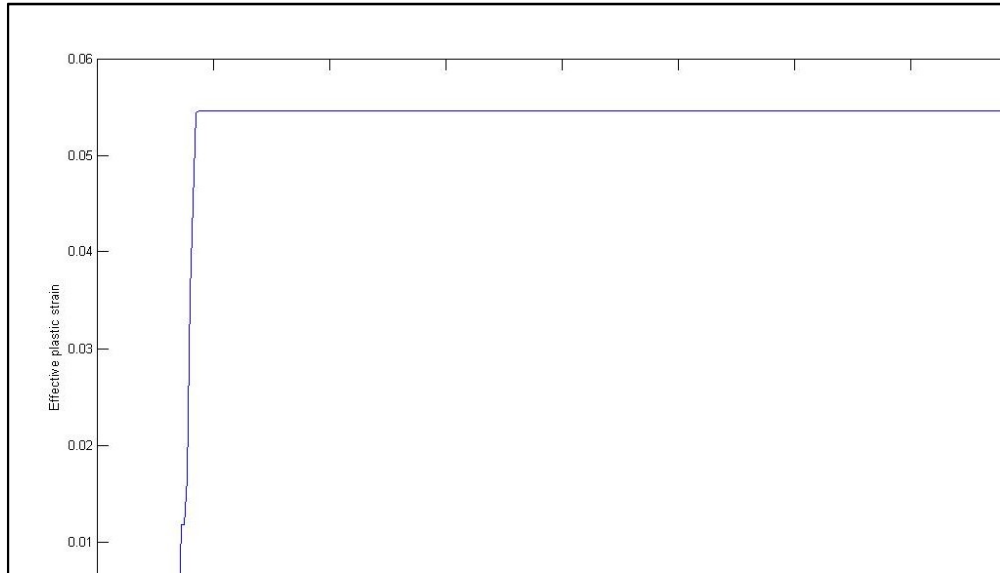
Figure 74: Effective Plastic Strain at 0.6 mm
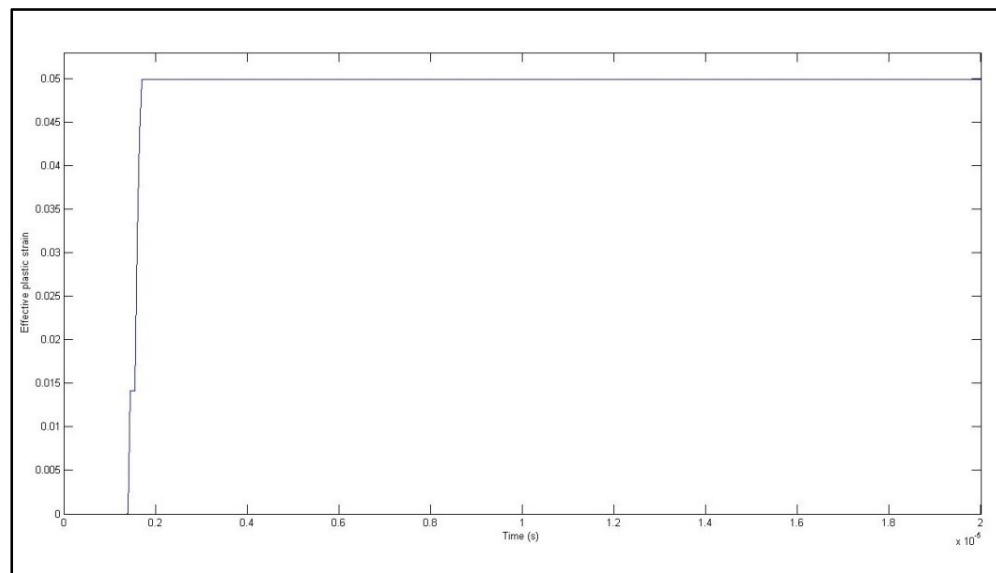
Figure 75: Effective Plastic Strain at 0.8 mm
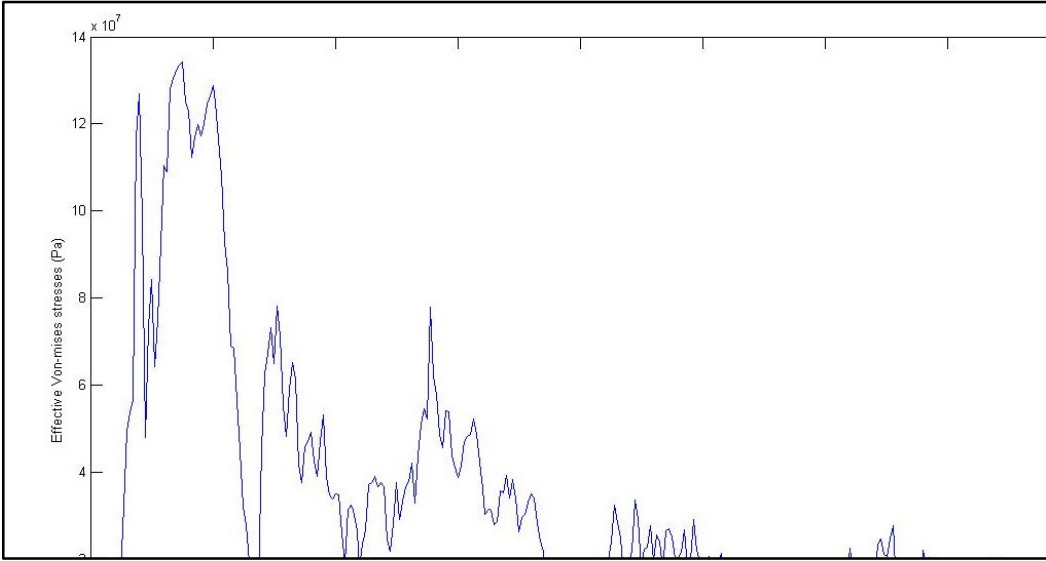
Figure 76: Effective Von-Mises stress at 0.2 mm
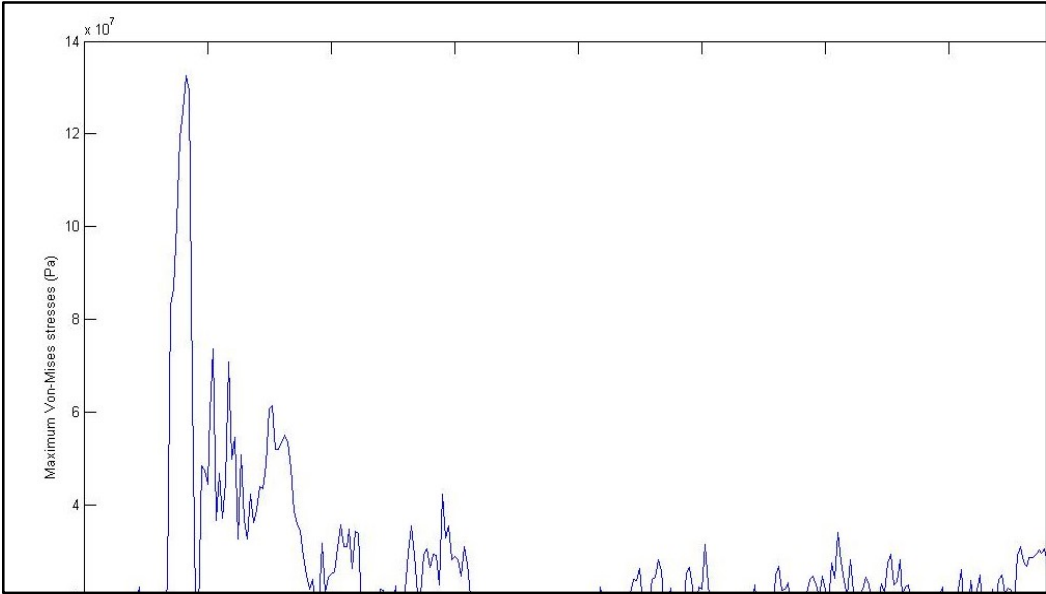
Figure 77: Effective Von-Mises stress at 0.4 mm

99
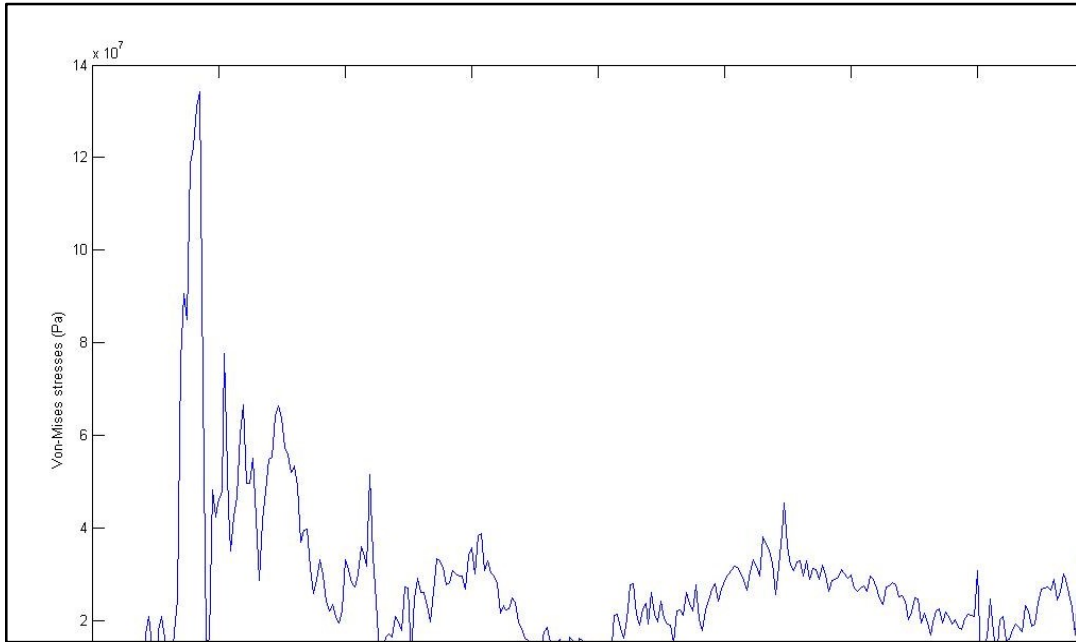
Figure 78: Effective Von-Mises stress at 0.6 mm
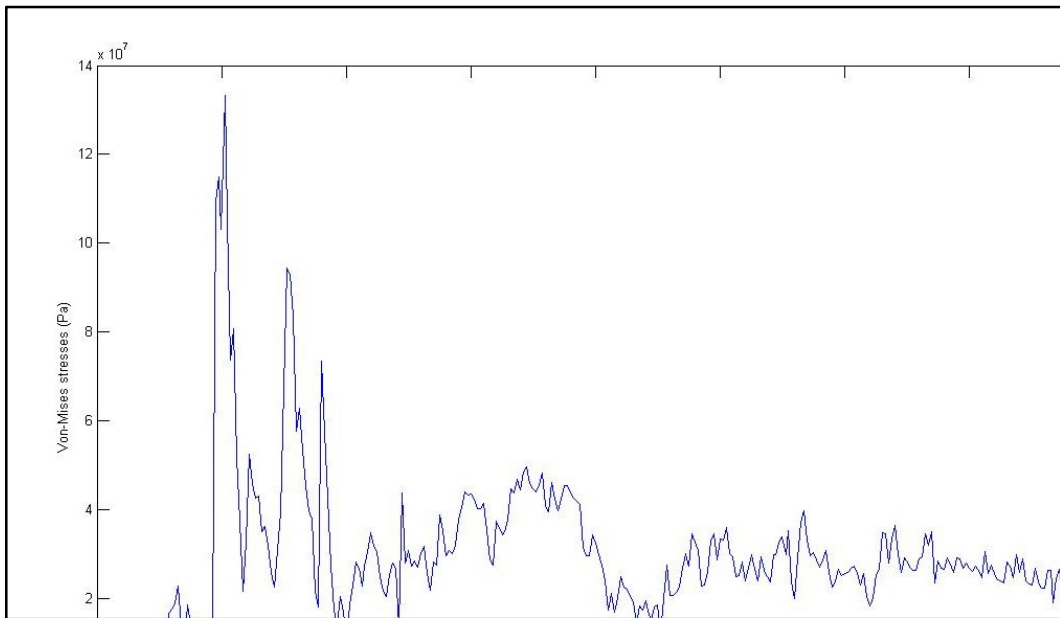
Figure 79: Effective Von-Mises stress at 0.8 mm
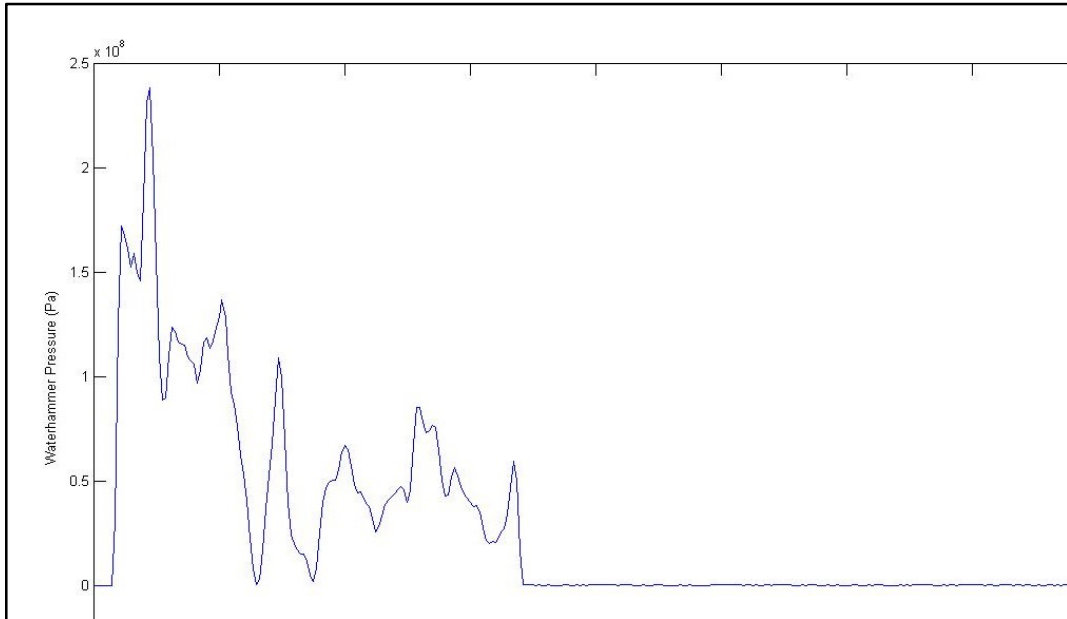
Figure 80: Waterhammer pressure at 0.2 mm
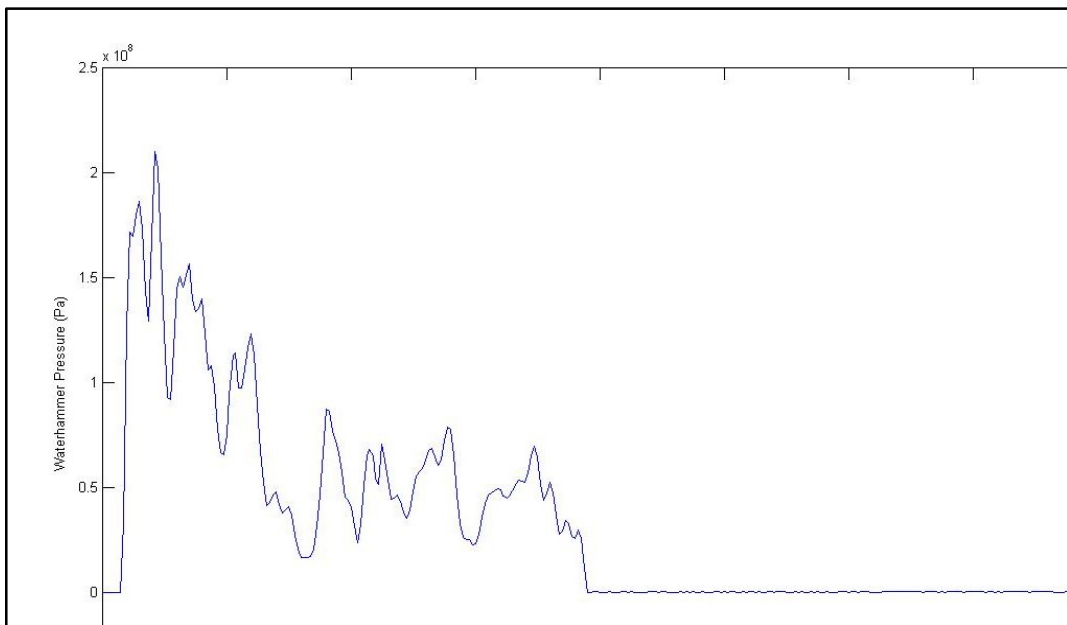
Figure 81: Waterhammer pressure at 0.4 mm
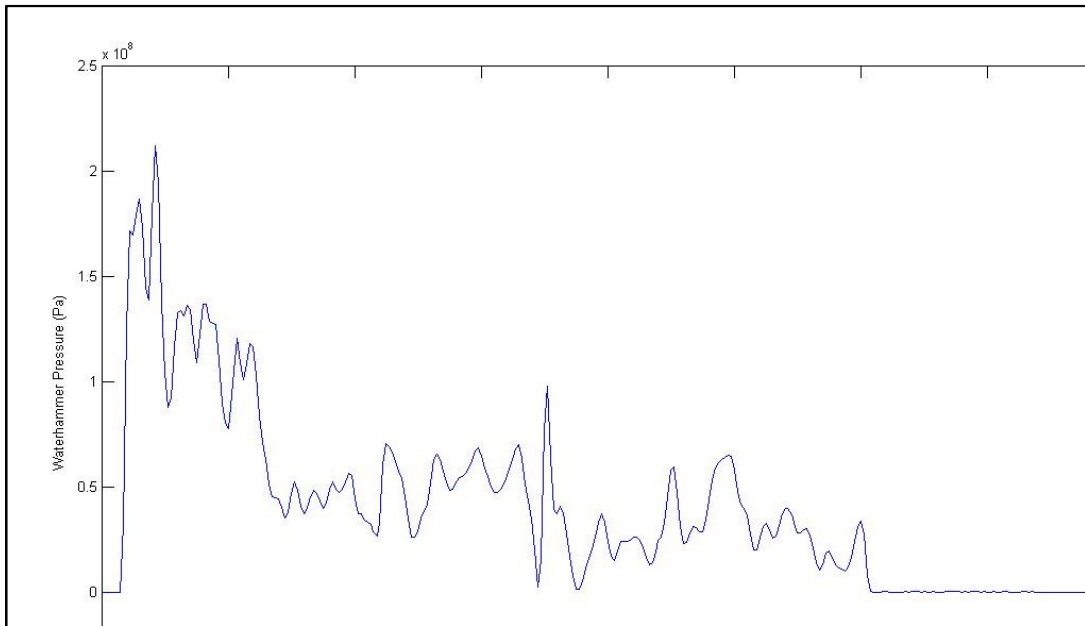
Figure 82: Waterhammer pressure at 0.6 mm
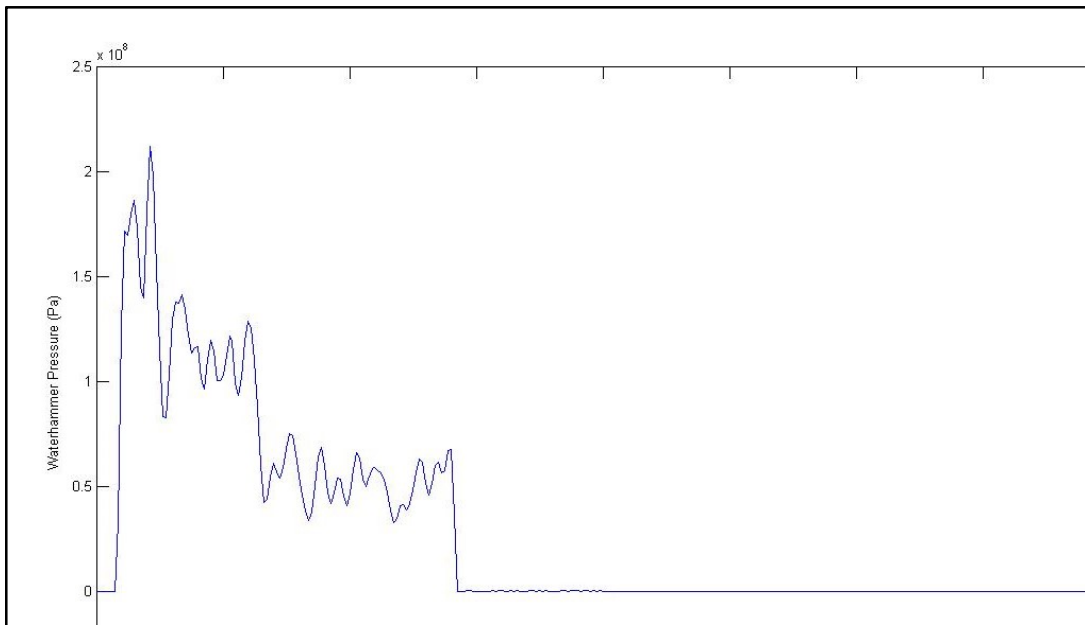
Figure 83: Waterhammer pressure at 0.8 mm
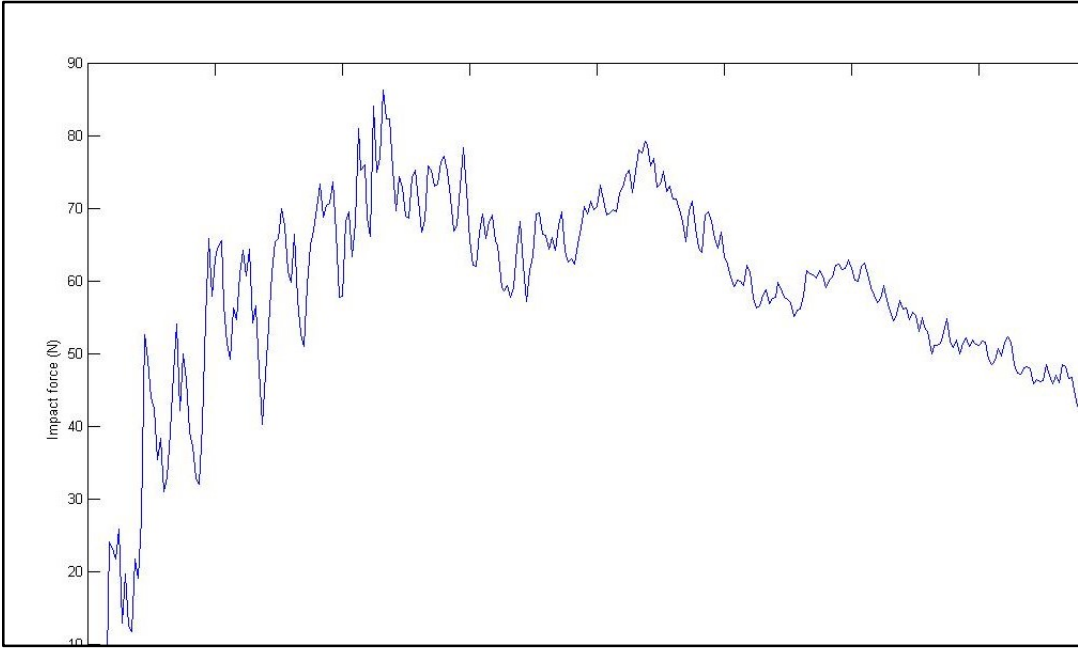
Figure 84: Impact Force at 0.2 mm
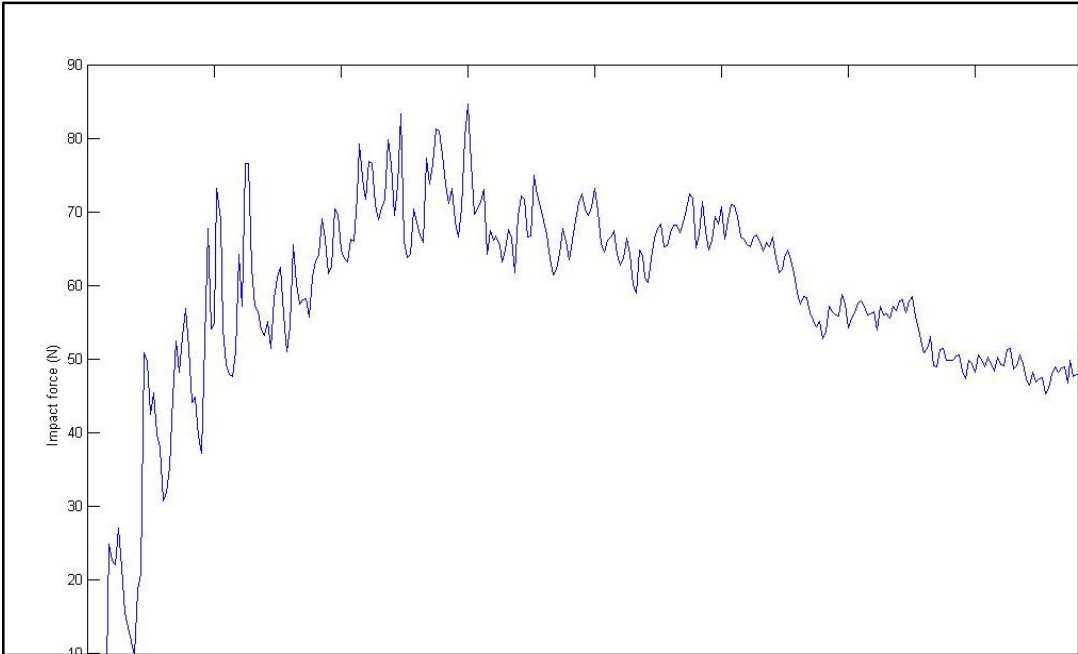
Figure 85: Impact Force at 0.4 mm
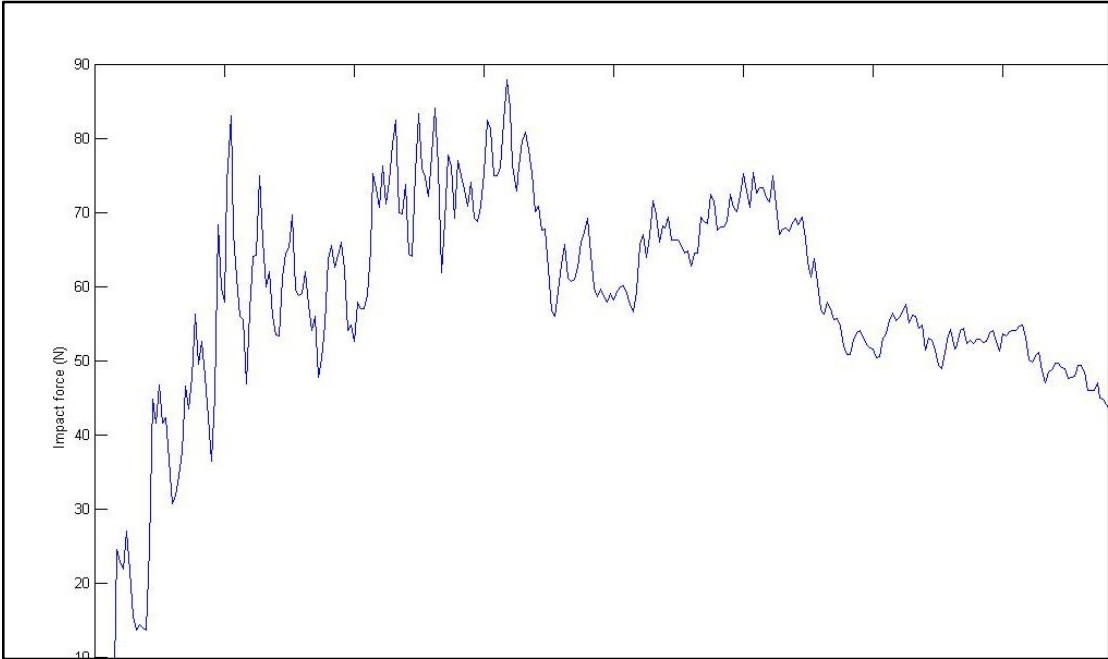
Figure 86: Impact Force at 0.6 mm
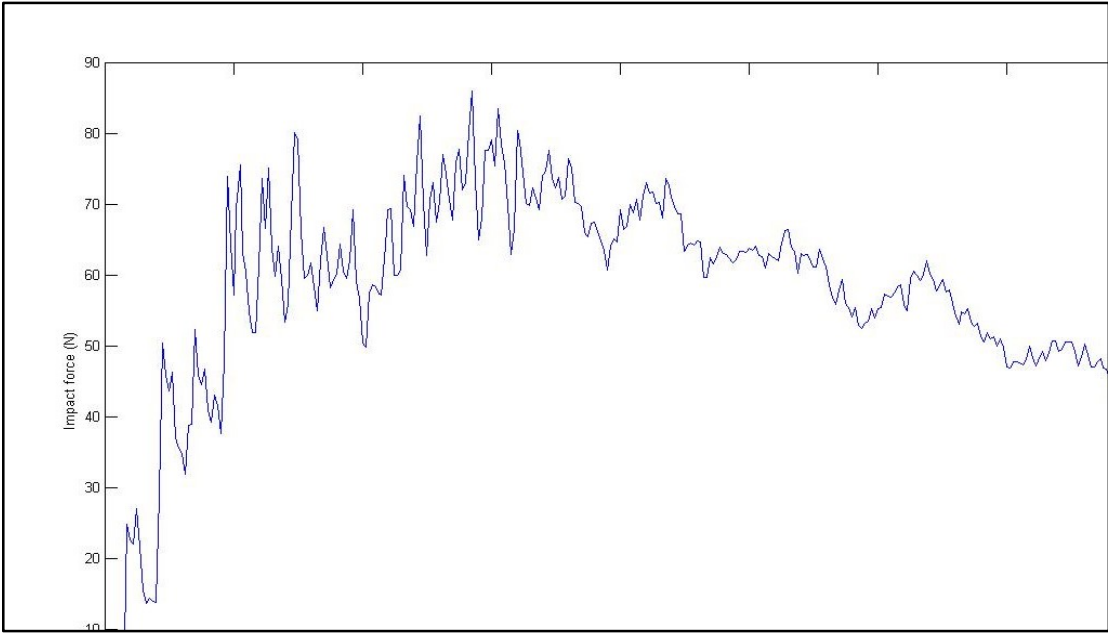
Figure 87: Impact Force at 0.8 mm
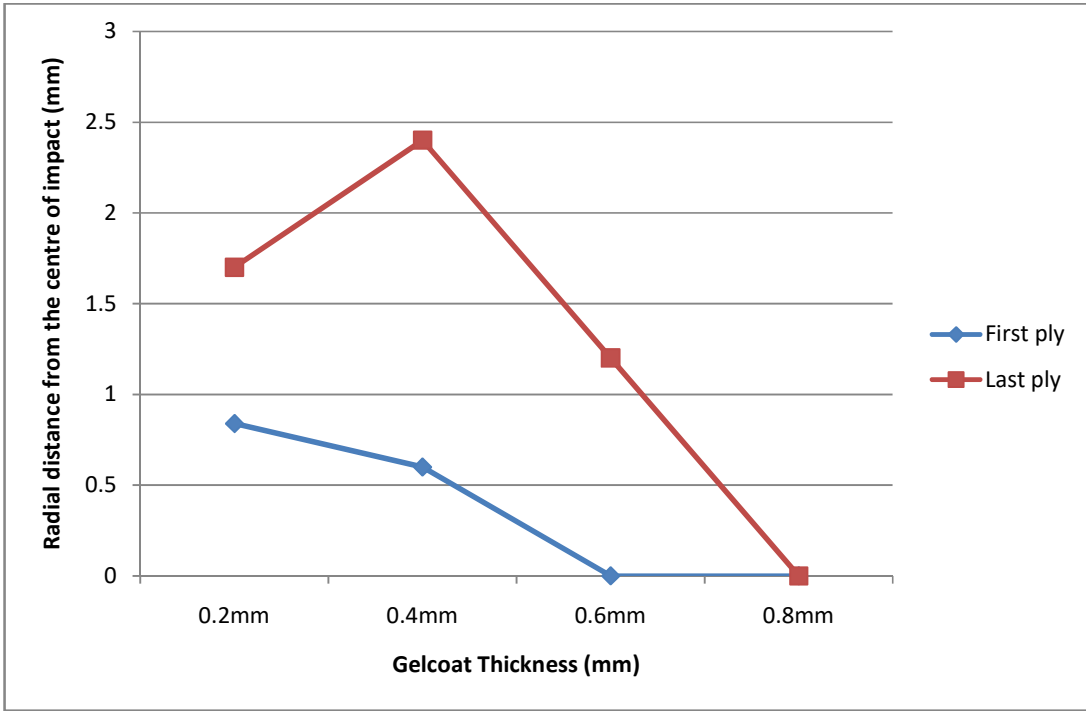
Figure 88: Distance from the centre of impact for σ_x stresses
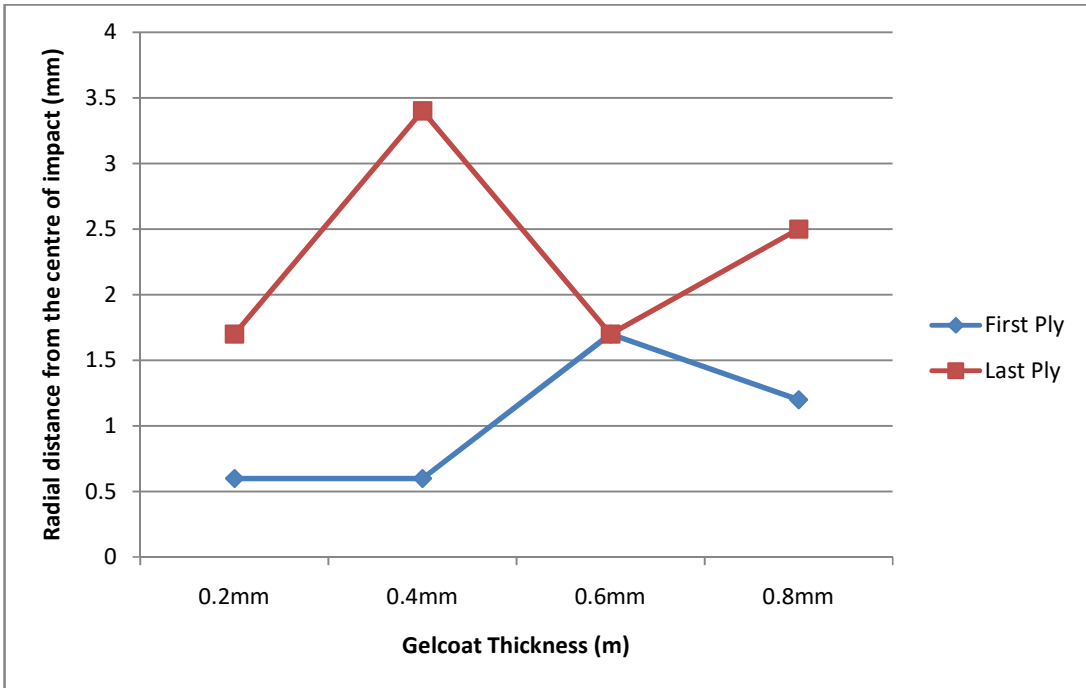
Figure 89: Distance from the centre of impact for σ_z stresses

105
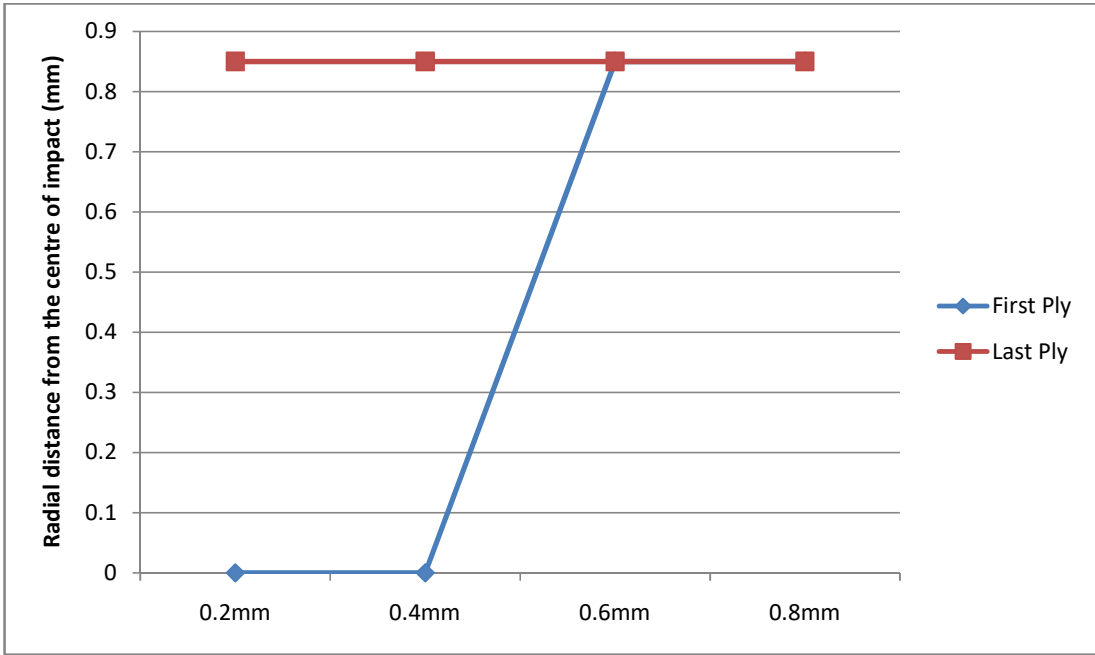
Figure 90: Distance from the centre of impact for σ_{xy} stresses
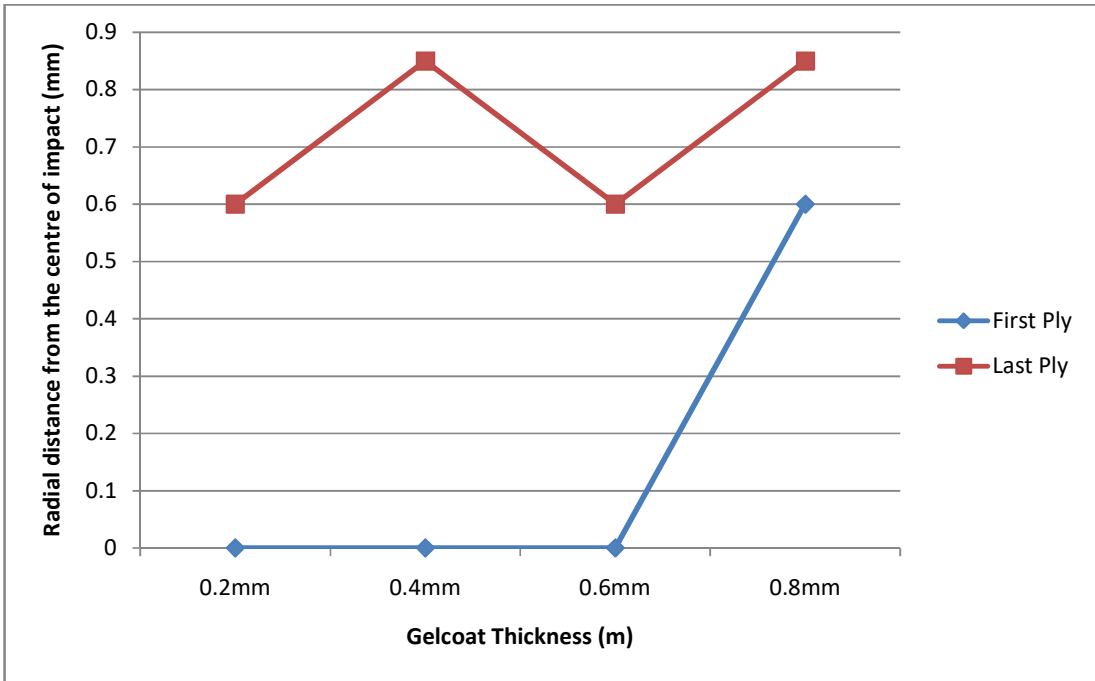
Figure 91: Distance from the centre of impact for σ_{zx} stresses

Case of 0.2 mm stresses between composite plies
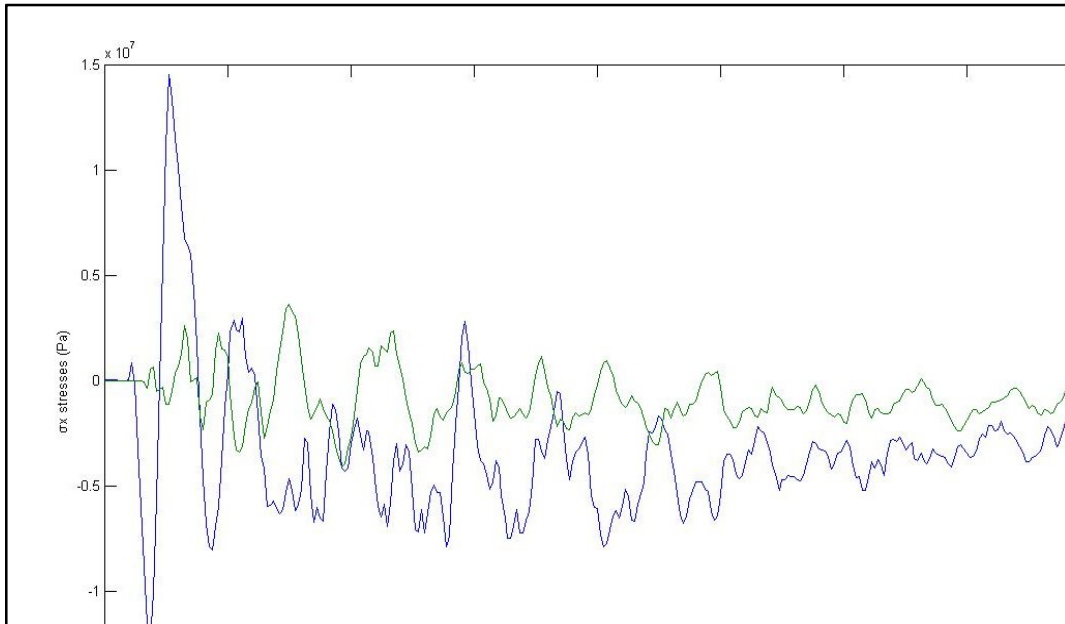
Figure 92: Stresses σ_x
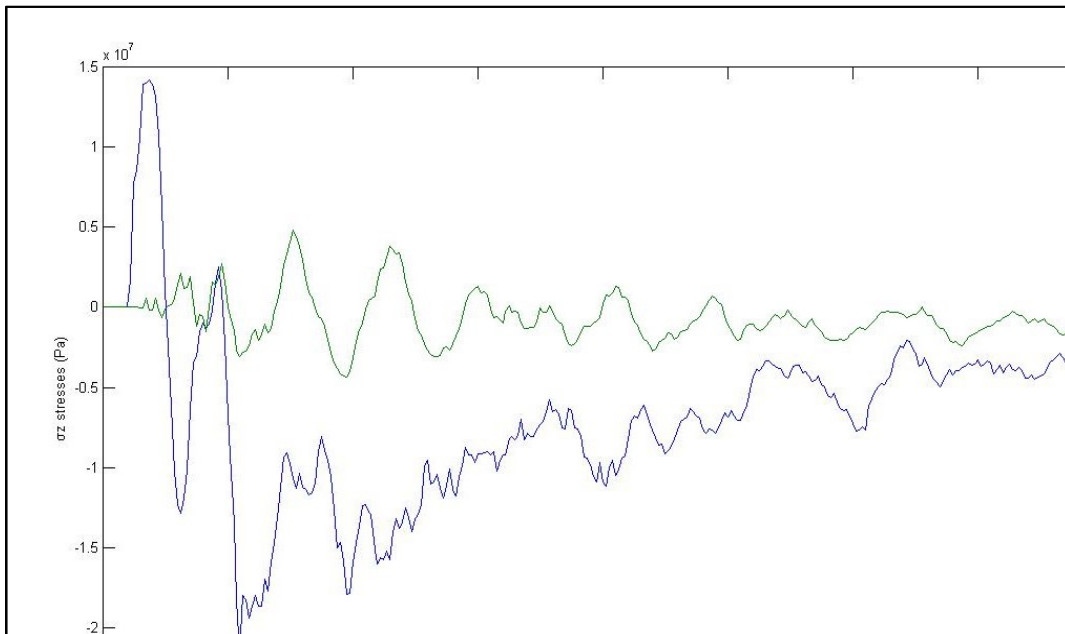
Figure 93: Stresses σ_z

107
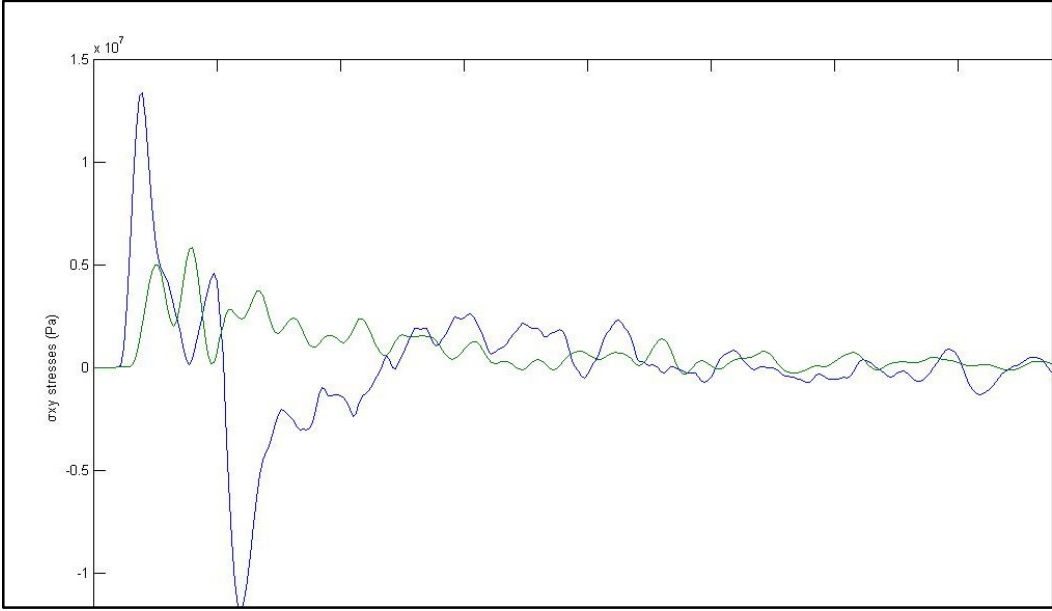
Figure 94: Stresses σ_{xy}
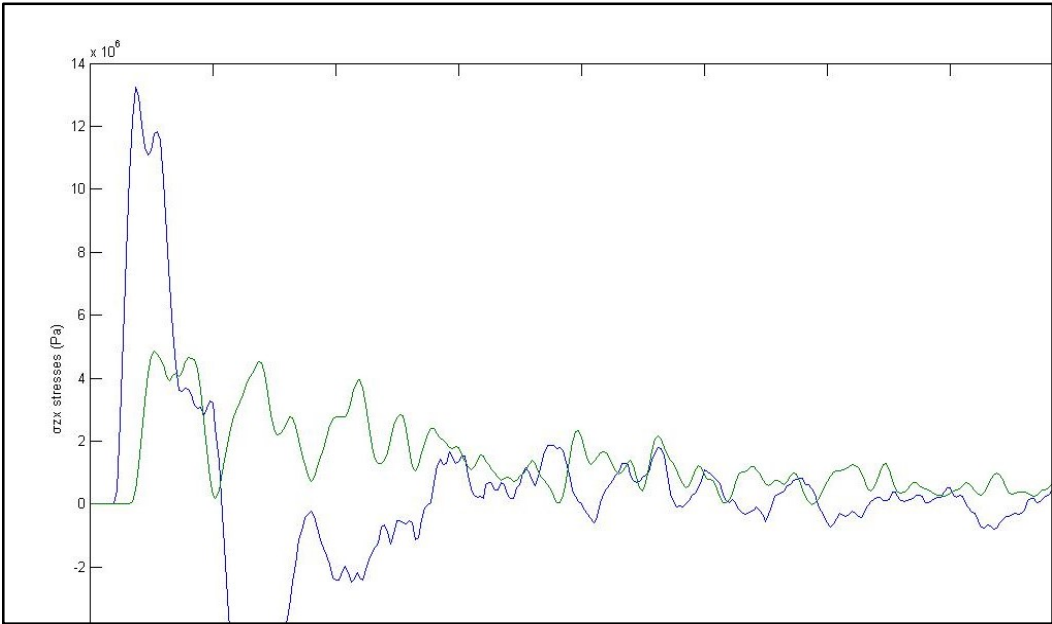
Figure 95: Stresses σ_{zx}

Case of 0.4 mm stresses between composite plies
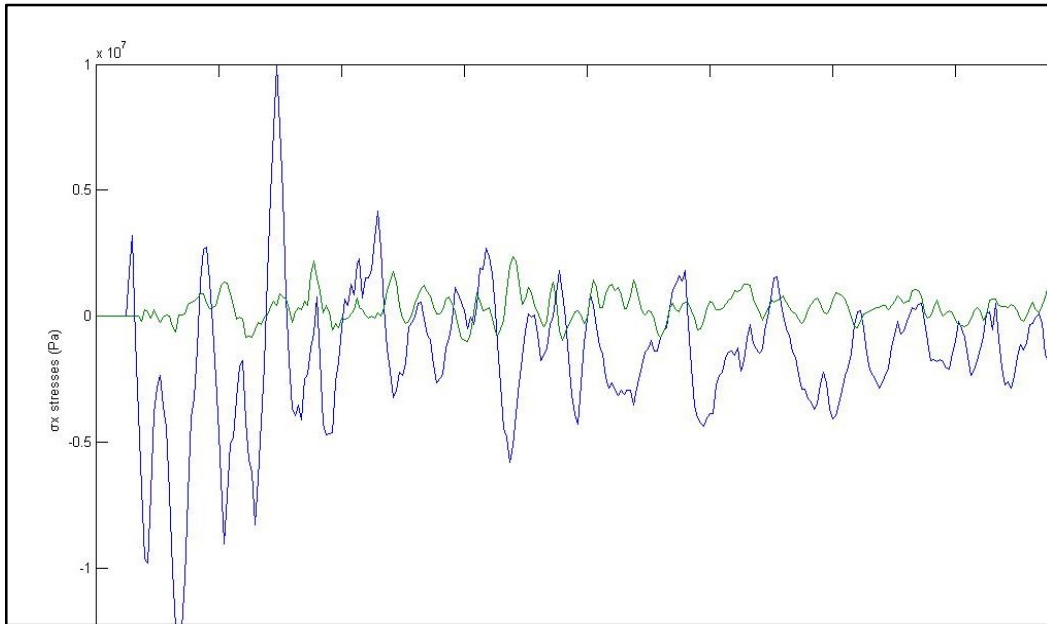
Figure 96: Stresses σ_x
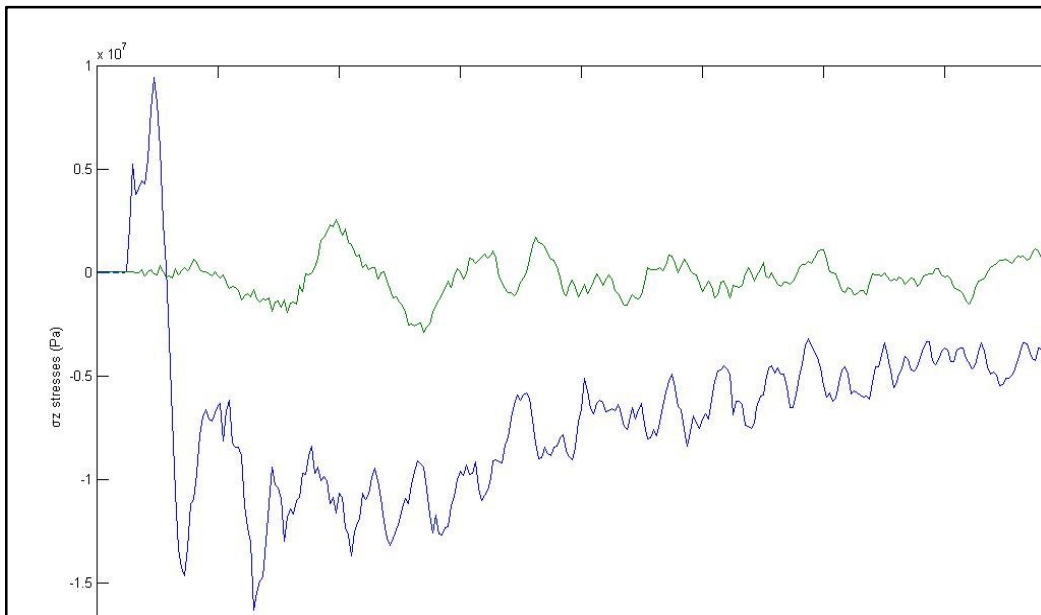
Figure 97: Stresses σ_z

109
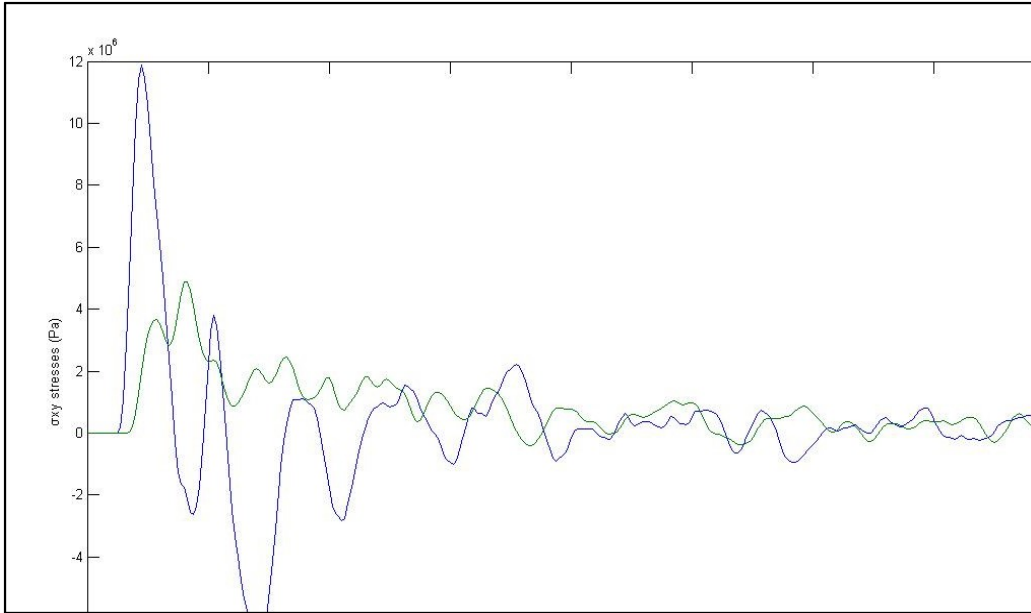
Figure 98: Stresses σ_{xy}
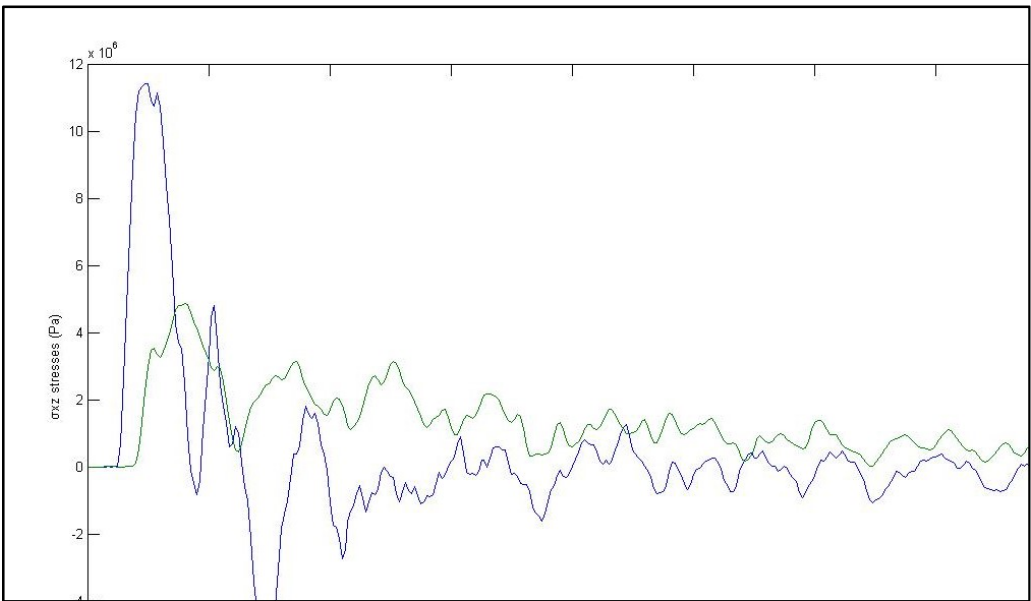
Figure 99: Stresses σ_{zx}

110

Case of 0.6 mm stresses between composite plies
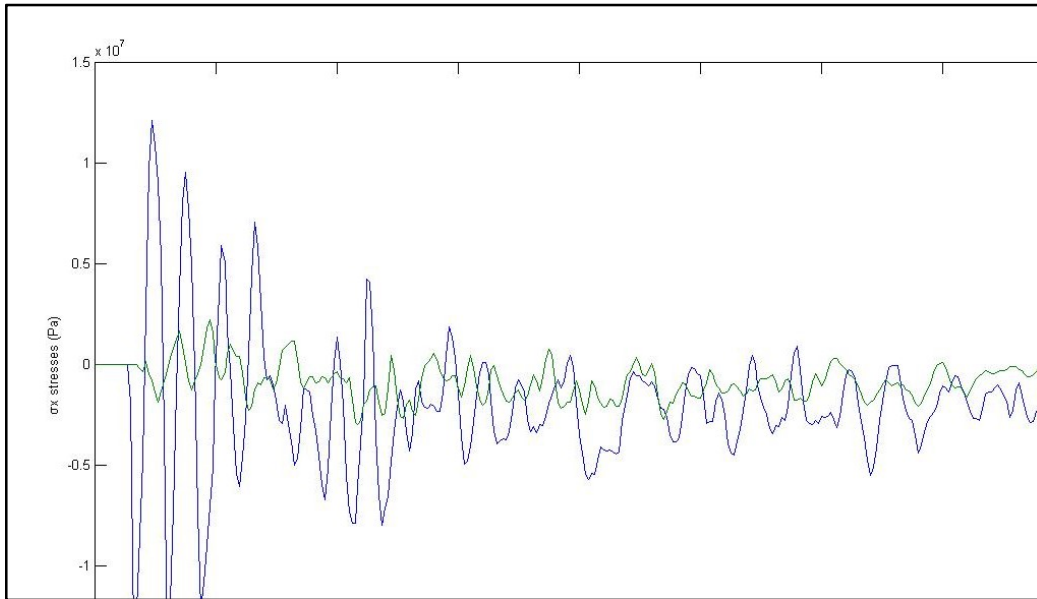
Figure 100: Stresses σ_x
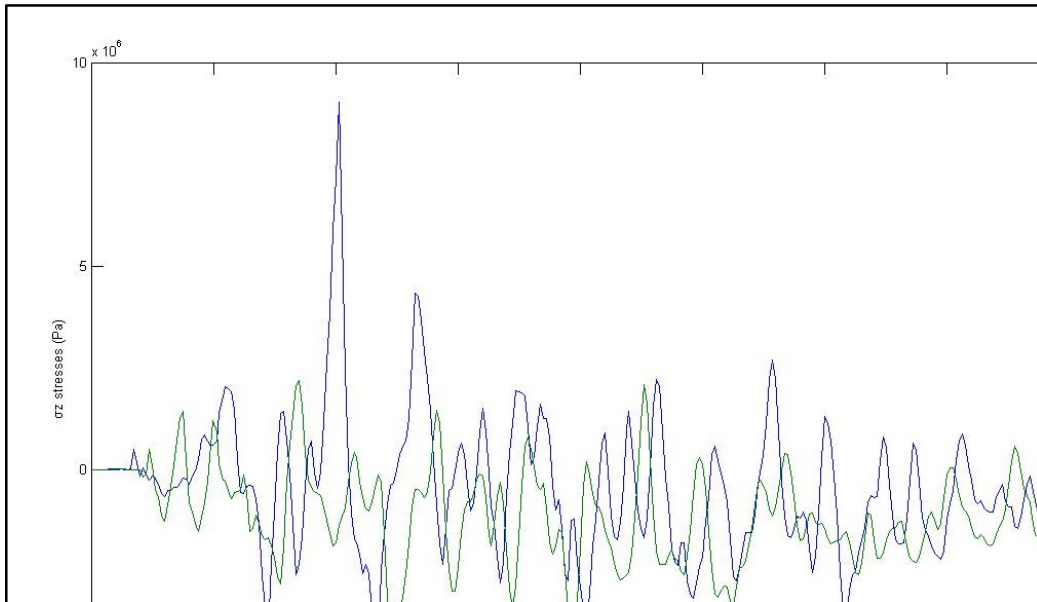
Figure 101: Stresses σ_z
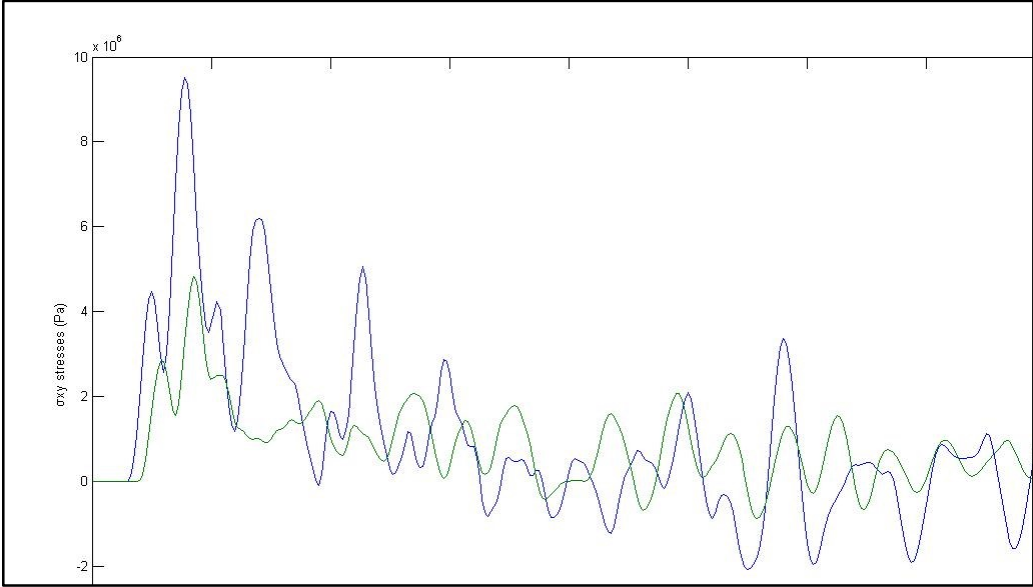
Figure 102: Stresses σ_{xy}
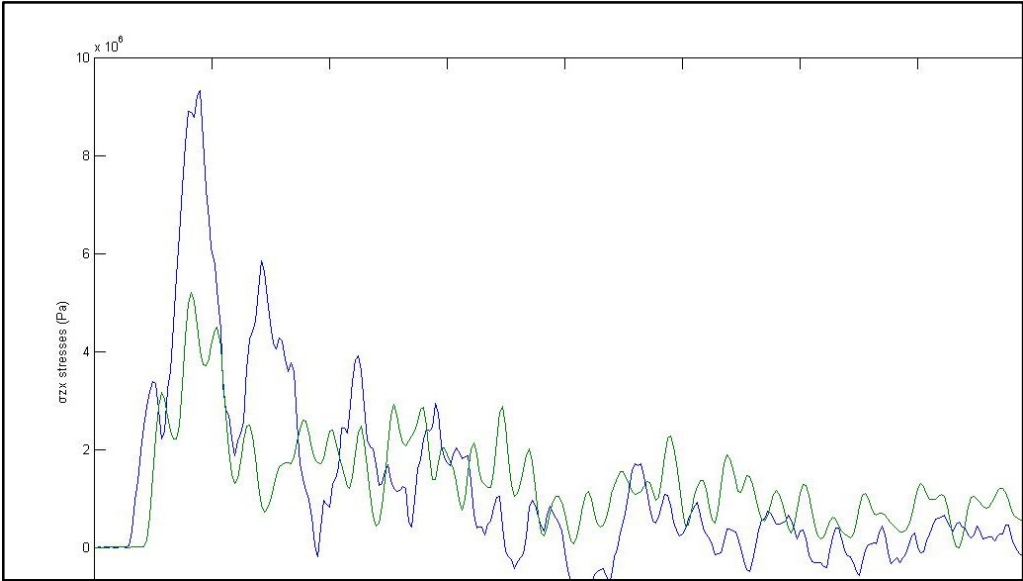
Figure 103: Stresses σ_{zx}

112

Case of 0.8 mm stresses between composite plies
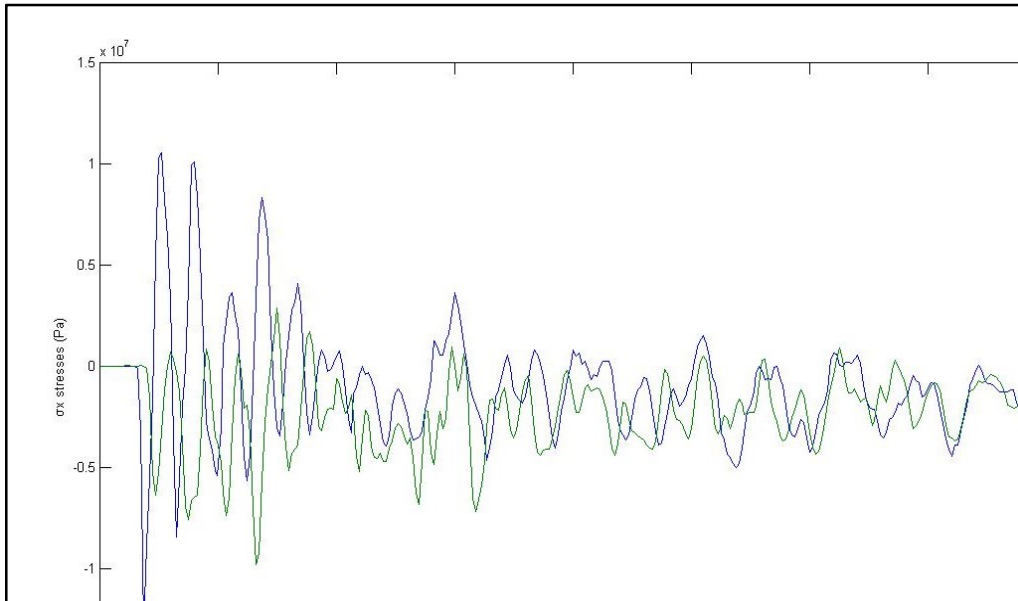
Figure 104: Stresses σ$_x$
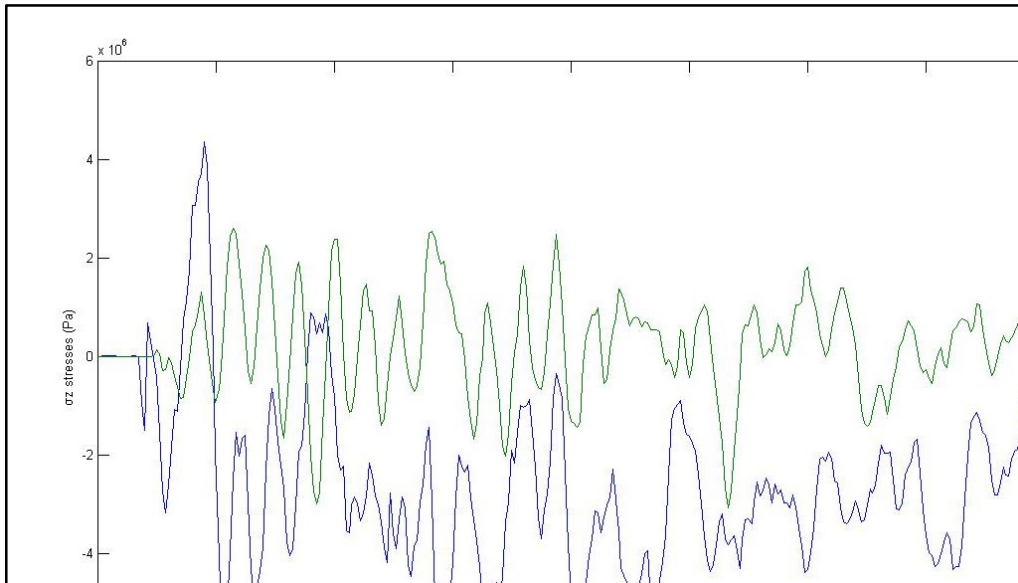
Figure 105: Stresses σ$_z$

113
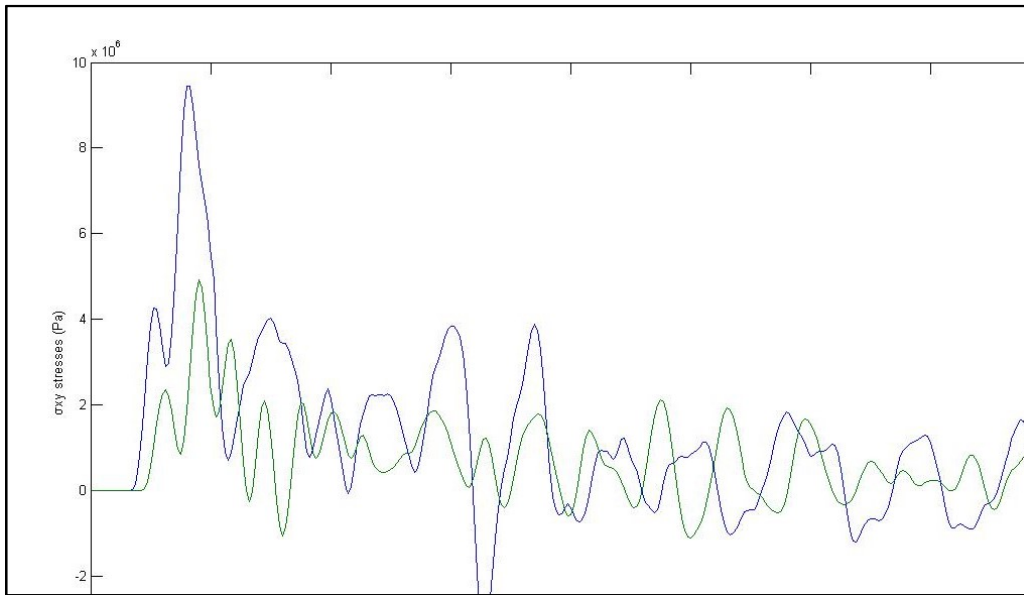
Figure 106: Stresses σ$_{xy}$
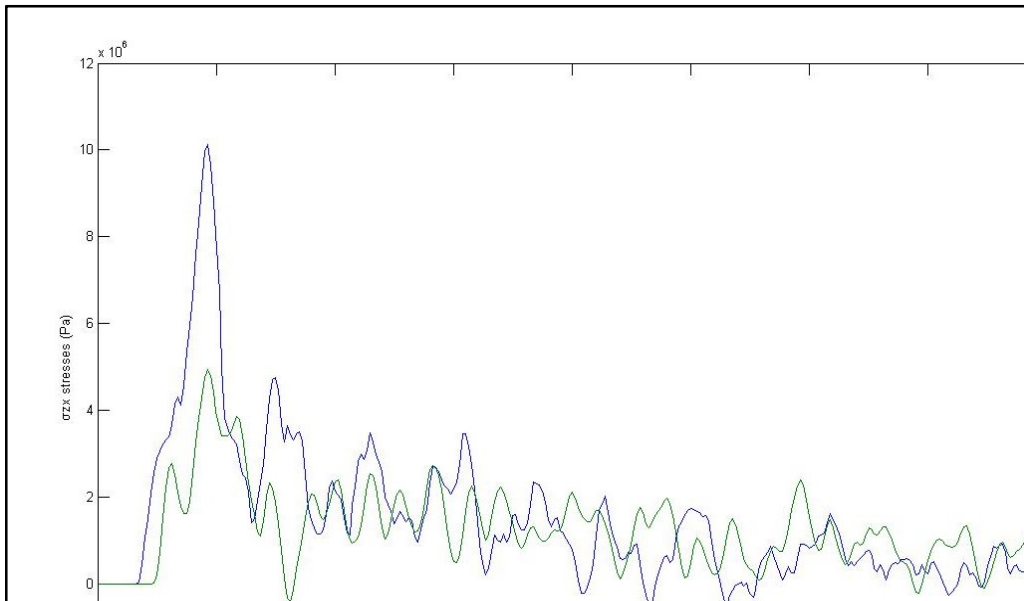
Figure 107: Stresses σ$_{zx}$

114

APPENDIX 2
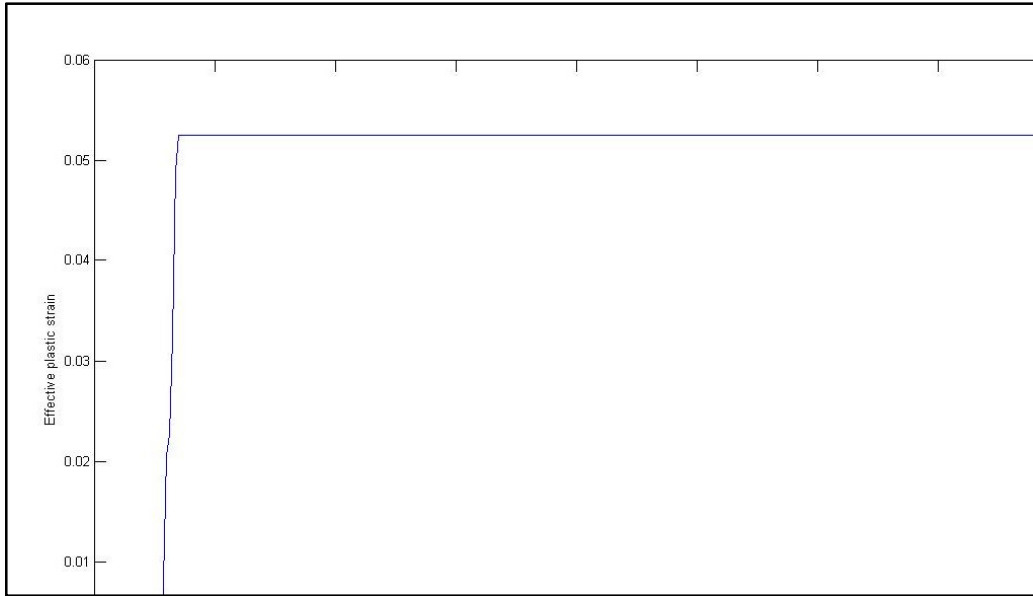
Figure 108: Effective plastic strain for case A
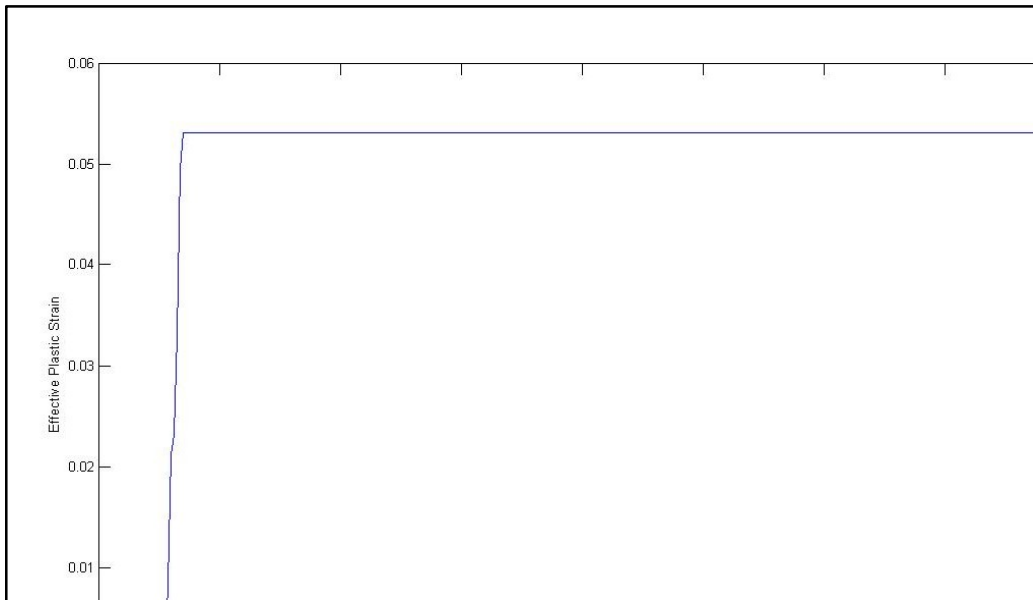
Figure 109: Effective plastic strain for case B
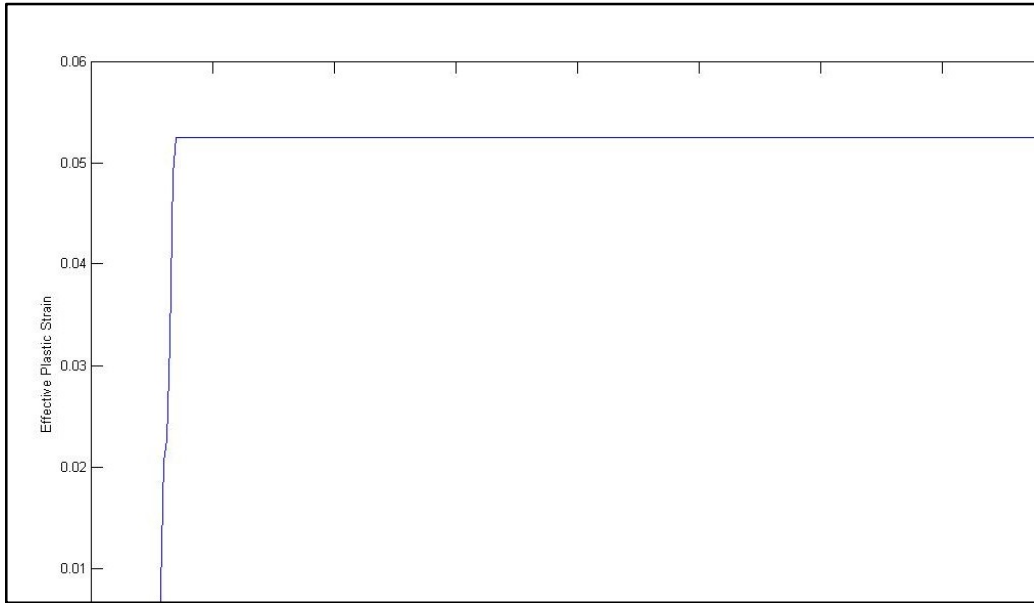
Figure 110: Effective plastic strain for case C
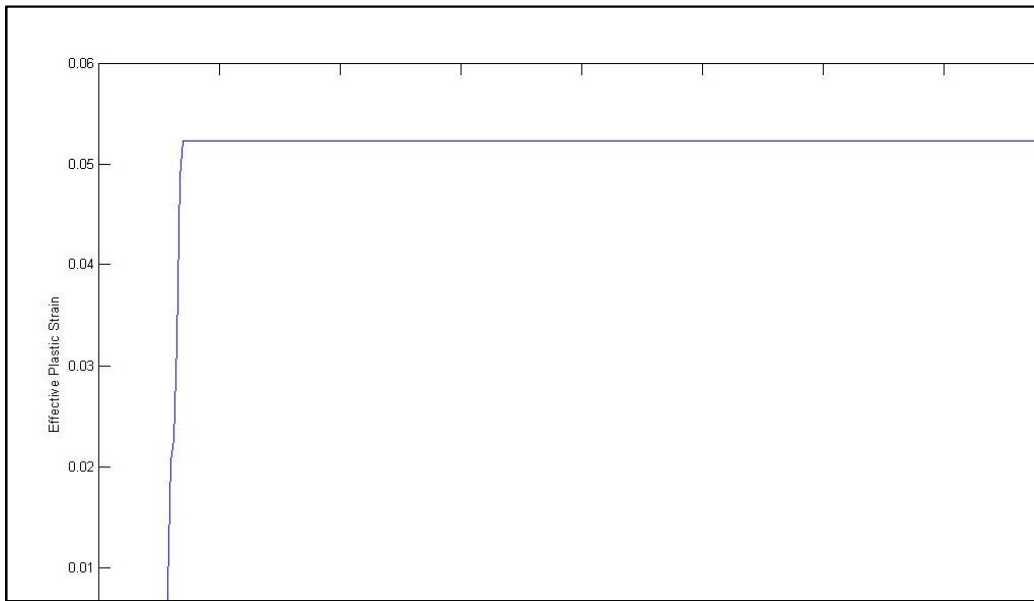
Figure 111: Effective plastic strain for case D
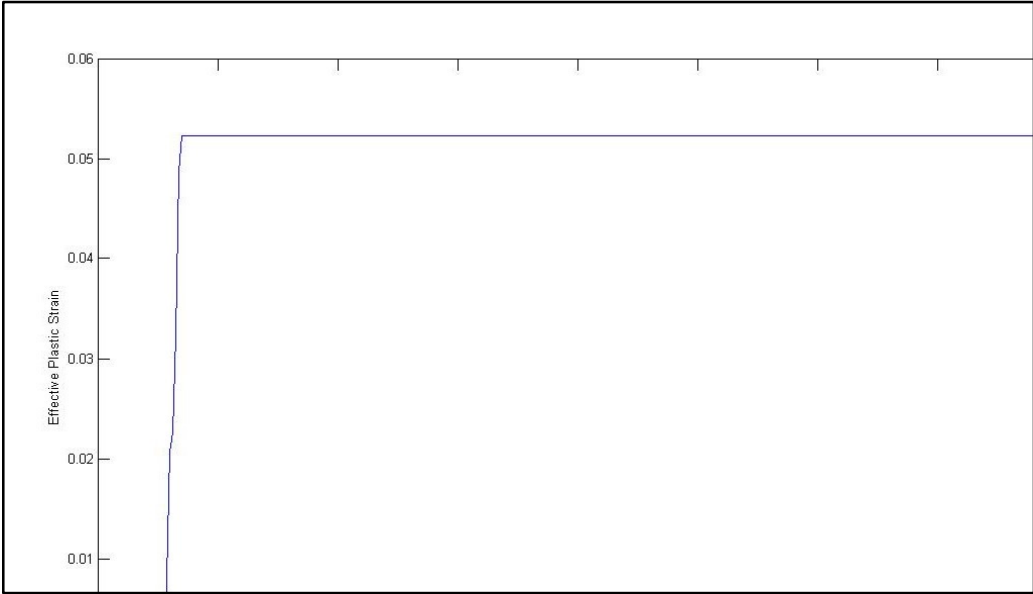
Figure 112: Effective plastic strain for case E
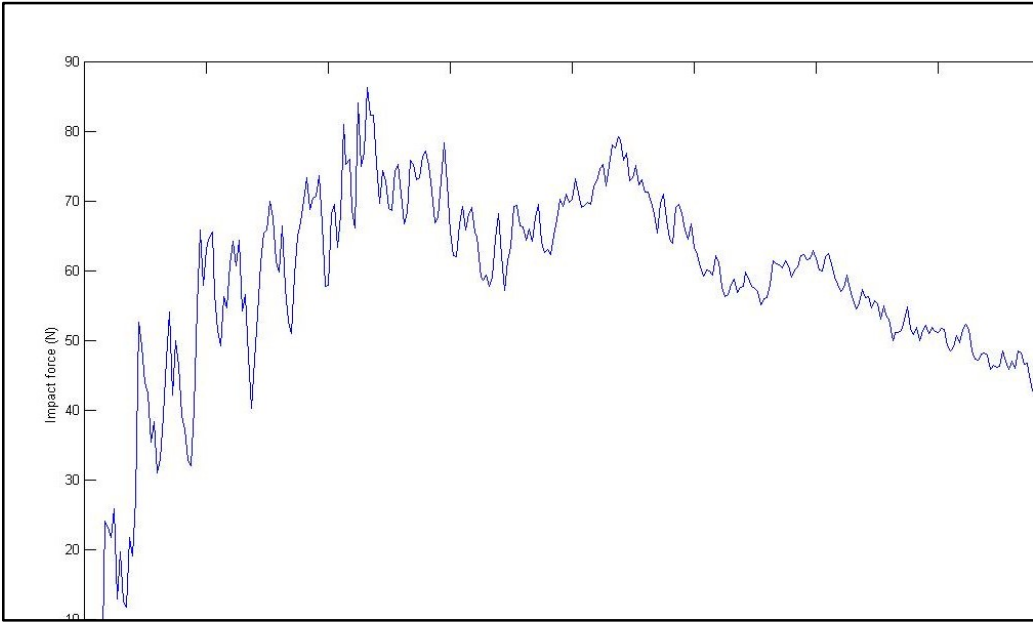
Figure 113: Impact force for case A

117
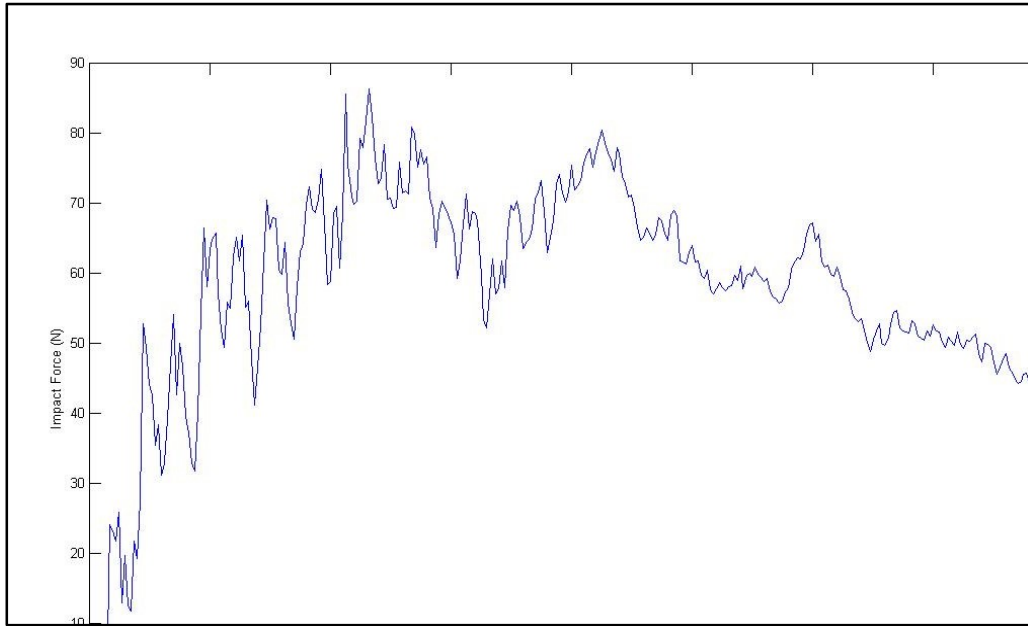
Figure 114: Impact force for case B
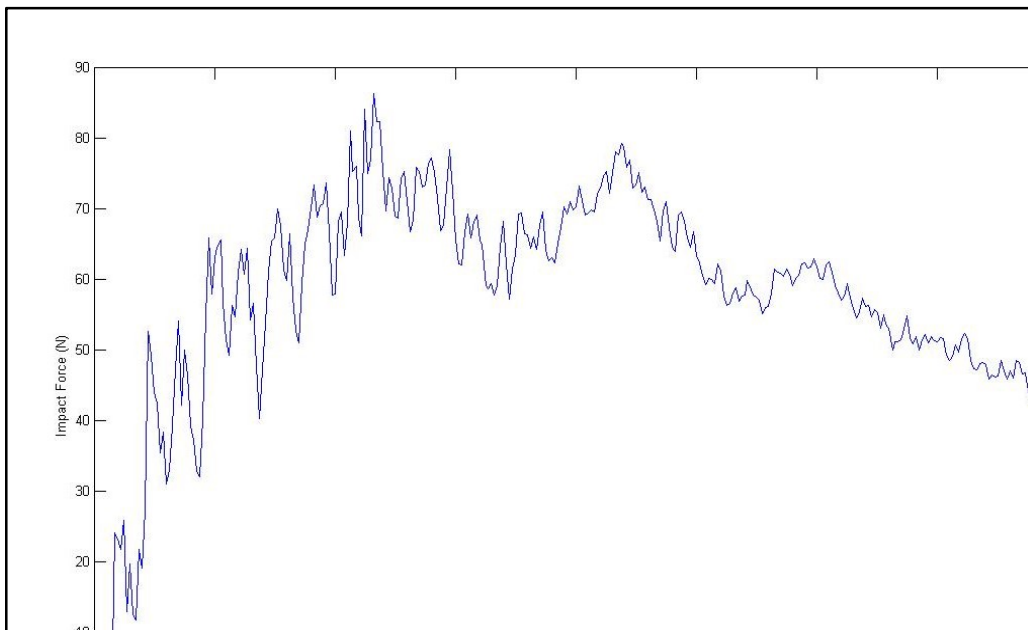
Figure 115: Impact force for case C
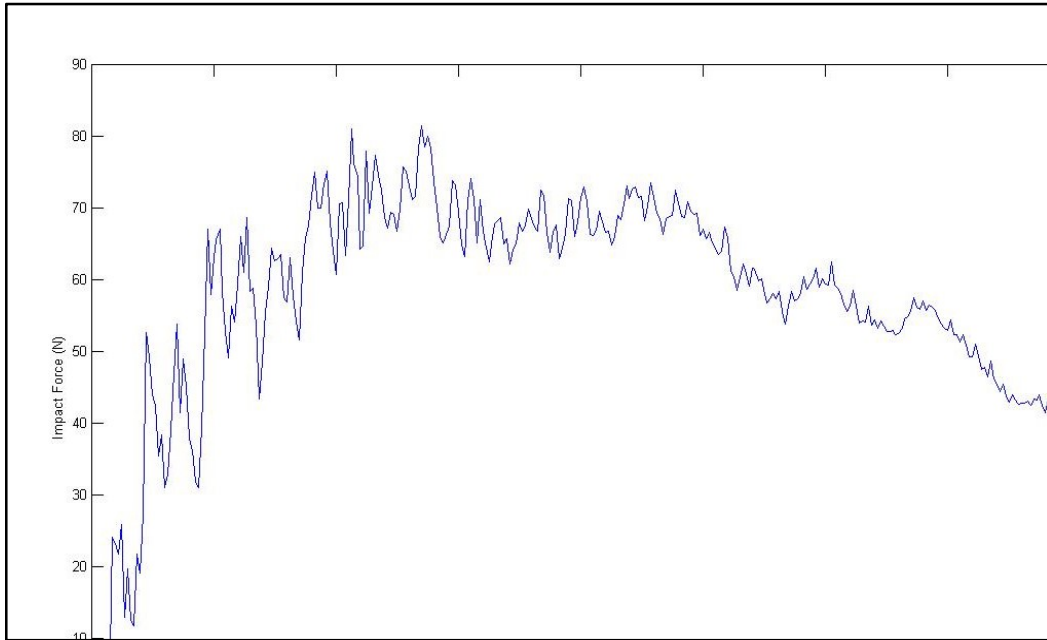
Figure 116: Impact force for case D
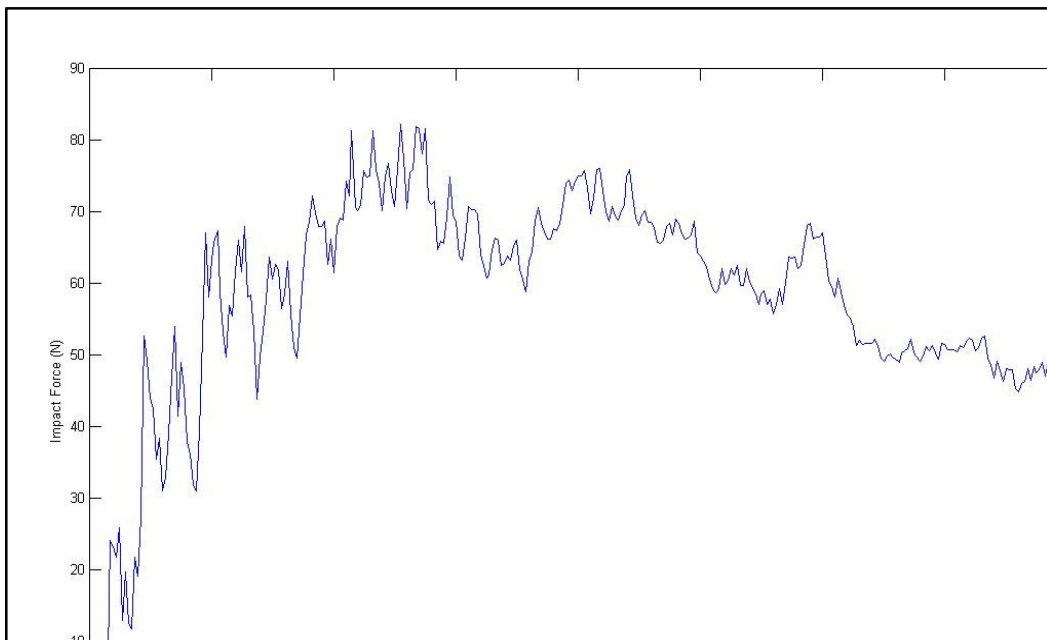
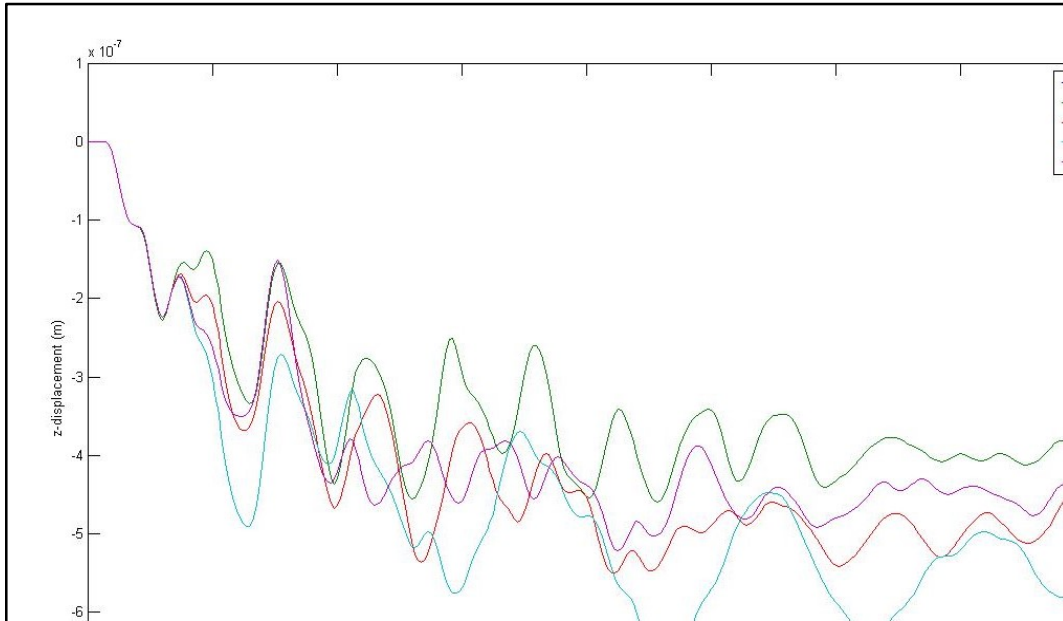**Figure 117:** Impact force for case E

119

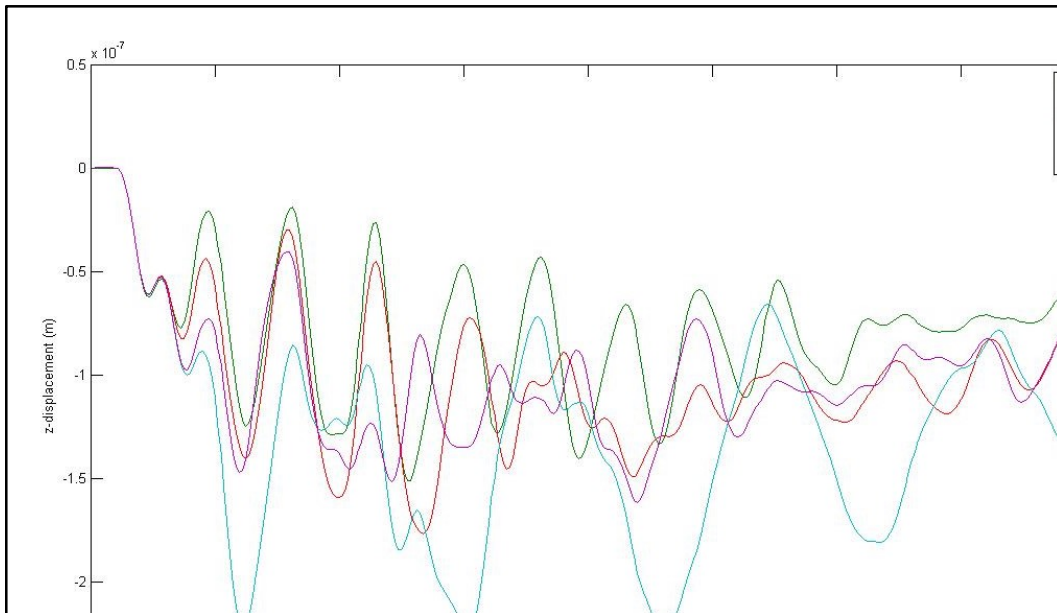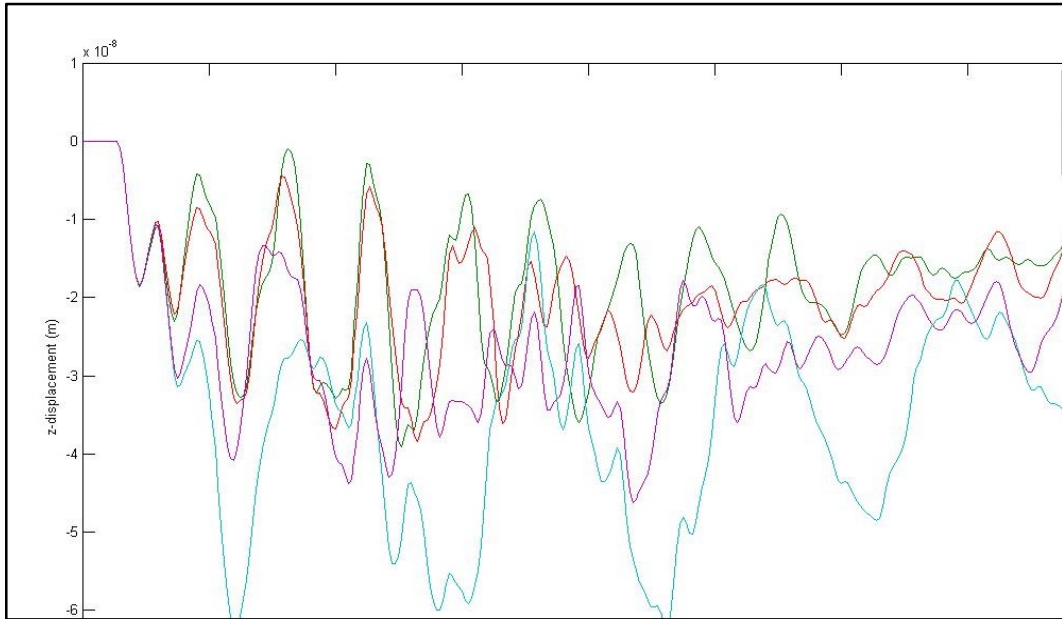**Figure 118:** z-displacement gelcoat layer

Figure 119: z-displacement first ply of composite

Figure 120: z-displacement last ply of composite